

AD-A157 059

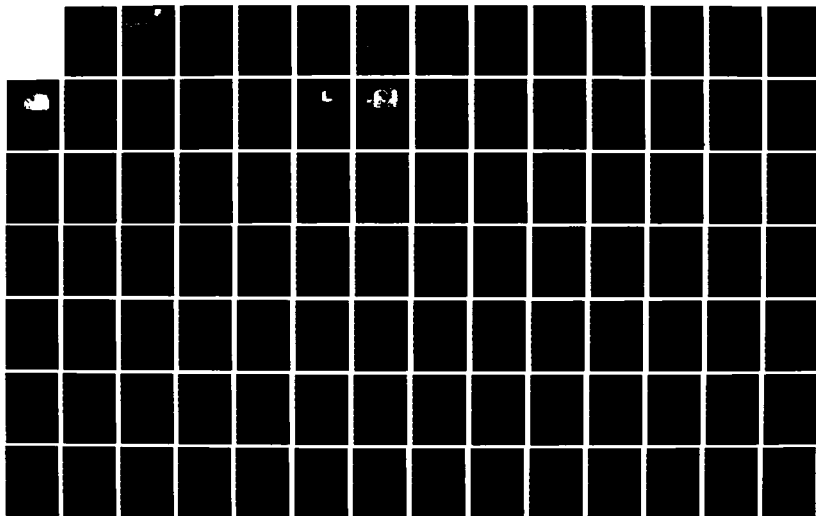
MICROENVIRONMENTAL MOISTURE RESEARCH(U) UNIVERSITY OF
SOUTH FLORIDA TAMPA DEPT OF ELECTRICAL ENGINEERING
J H AMMONS ET AL. APR 85 RADC-TR-85-58 F30602-80-C-0169

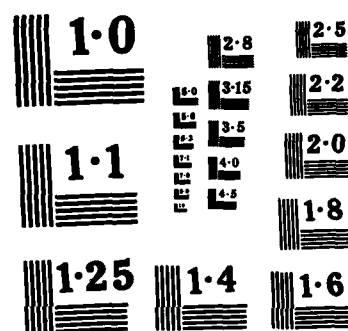
1/2

UNCLASSIFIED

F/G 9/5

NL





NATIONAL BUREAU OF STANDARDS
MICROCOPY RESOLUTION TEST CHART

AD-A 157 059

2

RADC-TR-85-58
Final Technical Report
April 1985

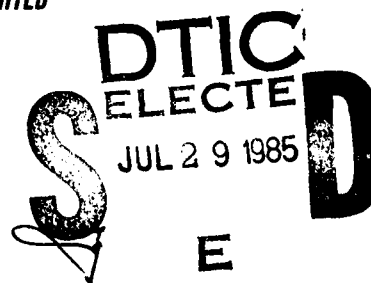


MICROENVIRONMENTAL MOISTURE RESEARCH

University of South Florida

J. M. Ammons, J. H. Linn, M. G. Kovac and W. E. Swartz

APPROVED FOR PUBLIC RELEASE; DISTRIBUTION UNLIMITED



ROME AIR DEVELOPMENT CENTER
Air Force Systems Command
Griffiss Air Force Base, NY 13441-5700

DTIC FILE COPY

This report has been reviewed by the RADC Public Affairs Office (PA) and is releasable to the National Technical Information Service (NTIS). At NTIS it will be releasable to the general public, including foreign nations.

RADC-TR-85-58 has been reviewed and is approved for publication.

APPROVED:



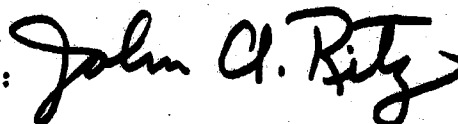
ROBERT W. THOMAS
Project Engineer

APPROVED:



W. S. TUTHILL, Colonel, USAF
Chief, Reliability & Compatibility Division

FOR THE COMMANDER:



JOHN A. RITZ
Acting Chief, Plans Office

If your address has changed or if you wish to be removed from the RADC mailing list, or if the addressee is no longer employed by your organization, please notify RADC (RBRE) Griffiss AFB NY 13441-5700. This will assist us in maintaining a current mailing list.

Do not return copies of this report unless contractual obligations or notices on a specific document requires that it be returned.

UNCLASSIFIED

SECURITY CLASSIFICATION OF THIS PAGE

REPORT DOCUMENTATION PAGE

1a. REPORT SECURITY CLASSIFICATION UNCLASSIFIED			1b. RESTRICTIVE MARKINGS N/A		
2a. SECURITY CLASSIFICATION AUTHORITY N/A			3. DISTRIBUTION/AVAILABILITY OF REPORT Approved for public release; distribution unlimited.		
2b. DECLASSIFICATION/DOWNGRADING SCHEDULE N/A					
4. PERFORMING ORGANIZATION REPORT NUMBER(S) N/A			5. MONITORING ORGANIZATION REPORT NUMBER(S) RADC-TR-85-58		
6a. NAME OF PERFORMING ORGANIZATION University of South Florida		6b. OFFICE SYMBOL (If applicable)	7a. NAME OF MONITORING ORGANIZATION Rome Air Development Center (RBRE)		
6c. ADDRESS (City, State and ZIP Code) Department of Electrical Engineering Tampa FL 33620			7b. ADDRESS (City, State and ZIP Code) Griffiss AFB NY 13441-5700		
8a. NAME OF FUNDING/SPONSORING ORGANIZATION Air Force Office of Scientific Research		8b. OFFICE SYMBOL (If applicable)	9. PROCUREMENT INSTRUMENT IDENTIFICATION NUMBER F30602-80-C-0169		
8c. ADDRESS (City, State and ZIP Code) Bolling AFB DC 20332			10. SOURCE OF FUNDING NOS.		
			PROGRAM ELEMENT NO. 61102F	PROJECT NO. 2306	TASK NO. J4
					WORK UNIT NO. 09
11. TITLE (Include Security Classification) MICROENVIRONMENTAL MOISTURE RESEARCH					
12. PERSONAL AUTHOR(S) J. M. Ammons, J. H. Linn, M. G. Kovac, W. E. Swartz					
13a. TYPE OF REPORT Final		13b. TIME COVERED FROM Jun 80 to Jun 83		14. DATE OF REPORT (Yr., Mo., Day) April 1985	
15. PAGE COUNT 126					
16. SUPPLEMENTARY NOTATION N/A					
17. COSATI CODES			18. SUBJECT TERMS (Continue on reverse if necessary and identify by block number)		
FIELD	GROUP	SUB. GR.			
14	04		Moisture Failure Threshold Failure Mechanisms		
20	12		Moisture Adsorption Mechanisms Moisture Measurement and Control		
19. ABSTRACT (Continue on reverse if necessary and identify by block number) The advancement of the science of reliability physics is the foundation for increased microelectronic circuit reliability. A common denominator for many types of failure mechanisms in integrated circuits is water trapped within the package cavity. Because of the nature of water in all types of circuits, an understanding of the fundamental interaction of water with package materials is essential. The research reported here was aimed at elucidating the nature of its sources, its dynamics of interaction, and ultimately its role in failure mechanisms. The nature and past history of surfaces is well known to influence its adsorption/desorption properties particularly with respect to water. It is necessary, therefore, to establish the chemical composition and morphology of the surface under investigation. All test structures and their treatment should closely approximate those found in production run packages in order to infer parallel response characteristics. The preparation and treatment of test samples for use in the work reported herein was done so as to simulate various stages of manufacturing. Comparison to production samples was done where possible.					
20. DISTRIBUTION/AVAILABILITY OF ABSTRACT UNCLASSIFIED/UNLIMITED <input checked="" type="checkbox"/> SAME AS RPT. <input type="checkbox"/> OTIC USERS <input type="checkbox"/>			21. ABSTRACT SECURITY CLASSIFICATION UNCLASSIFIED		
22a. NAME OF RESPONSIBLE INDIVIDUAL Robert W. Thomas			22b. TELEPHONE NUMBER (Include Area Code) (315) 330-3730		22c. OFFICE SYMBOL RADC (RBRE)

DD FORM 1473, 83 APR

EDITION OF 1 JAN 73 IS OBSOLETE.

UNCLASSIFIED
SECURITY CLASSIFICATION OF THIS PAGE

TABLE OF CONTENTS

I.	Introduction	3
II.	Metal Ion Transport Within Packages	4
III.	Diffusion of Transition Metals through Gold Films	34
IV.	Physisorption of Water on Surfaces	55
V.	Chemisorption of Water on Surfaces	72
VI.	Moisture Failure Thresholds	84
VII.	Effects of Hydrogen on Metal Wall Surfaces as Determined by XPS	92
VIII.	Effects of Plasma Cleaning on Surfaces	102
IX.	Bibliography	118

Appendix A - Publications and Presentations resulting from this contract.

Accession For	
NTIS GRA&I	<input checked="" type="checkbox"/>
DTIC TAB	<input type="checkbox"/>
Unannounced	<input type="checkbox"/>
Justification	
By	
Distribution/	
Availability Codes	
Dist	Avail and/or Special
A-1	




EVALUATION

The contractor was assigned a number of tough problems associated with the way in which moisture interacts with an integrated circuit chip and packaging materials. Many previous studies on moisture related failure mechanisms have produced negative or ambiguous results. This was an effort to answer some of the basic questions concerning moisture so that more effective accelerated life tests for moisture could be designed. The results of the contract have many other applications ranging from improving moisture sensor design and stability to establishing the rationale for changing the current Mil Std ambient in which burn-in is accomplished.

Not all goals of the contract were met, but this is not unusual considering the basic research nature of the effort. Still unresolved is a test to determine the moisture failure threshold for a particular device. The establishment of failure thresholds for moisture would be valuable in setting general moisture limits such as now exist in MIL-STD-883, Method 1018, Method 5004 and Method 5008. The lack of success in this experiment could well mean that moisture related failures are much more random in nature and depend on loss of hermeticity, pinholes and small but concentrated amounts of surface contamination.

This effort is one of a continuing research program at Rome Air Development Center to further the understanding moisture adsorption mechanisms, transfer mechanisms, and failure mechanisms. It directly supports our activities in moisture measurement and control as specified in MIL-M-38510 and MIL-STD-883, Method 1016.2.


ROBERT W. THOMAS
Project Engineer

1.0 INTRODUCTION

The advancement of the science of reliability physics is the foundation for increased microelectronic circuit reliability. A common denominator for many types of failure mechanisms in integrated circuits is water trapped within the package cavity. Because of the ubiquitous nature of water in all types of circuits, an understanding of the fundamental interaction of water with package materials is essential. The research reported here was aimed at elucidating the nature of its sources, its dynamics of interaction, and ultimately its role in failure mechanisms.

The nature and past history of a surface is well known to influence its adsorption/desorption properties particularly with respect to water. It is necessary, therefore, to establish the chemical composition and morphology of the surface under investigation. All test structures and their treatment should closely approximate those found in production run packages in order to infer parallel response characteristics. The preparation and treatment of test samples for use in the work reported herein was done so as to simulate various stages of manufacturing. Comparison to production samples was done where possible.

2.0 METAL ION TRANSPORT WITHIN PACKAGES

The objective of this series of experiments was to determine the validity of the "metal ion transport via water pump" theory. This theory holds that it is possible to transport metal ions around the interior of an integrated circuit (IC) package by the pumping of water as it goes from the liquid to vapor state and back again as a function of temperature cycling. Since sodium (Na) is an apparently ubiquitous metallic contaminant in IC packages, studies were initiated to investigate the plausibility of transporting sodium (as Na^+) from one surface to another in the IC package.

2.1 QUANTITATIVE ANALYSIS VIA XPS

Samples were to be analyzed via X-ray photoelectron spectroscopy (XPS). Therefore, initial experiments were performed in which the sodium signal intensity was determined as a function of surface concentration. These experiments had a two fold purpose: (1) to determine if microgram quantities of sodium encountered in IC packages could be detected with XPS and (2) to obtain representative signal intensities such that a semi-quantitative estimate of the amount of sodium present on a surface could be established.

The theoretical XPS peak signal strength (I_A) due to electrons photo-ejected elastically from atoms of type A with energy ϵ_A is determined from an equation of the form

$$I_A = fn_A \sigma_A \lambda(\epsilon_A) T(\epsilon_A) \quad (2.1)$$

where f is the X-ray flux, n_A is the density of atoms of type A, σ_A is the photo-ionization cross section, $\lambda(\epsilon_A)$ is the mean free path (escape depth)

of an excited electron having energy ϵ_A and $T(\epsilon_A)$ is the fraction of electrons detected by the analyzer (the transmission efficiency) (1). At constant X-ray flux on a given instrument, the variables are n_A , σ_A , and $\lambda(\epsilon_A)$. To perform a quantitative analysis via comparison to a standard calibration curve, the density and thickness of the atomic layers are important. The thickness of the effective sample must be identical for the calibration standards and the unknown. With this in mind, attempts were made to generate a series of NaCl standards suitable for the quantitative analysis of IC package lids. The lids employed were either Kovar or gold plated Kovar (Au/Kovar) which met military specifications.

Known microgram quantities of NaCl in aqueous solution were delivered to Kovar or Au/Kovar lids via a microliter syringe. The lid was then dried in an oven. When dry, the lids were analyzed via XPS. Since the ESCA 36 employed in these studies analyzes an area of 2mm^2 , it is extremely important that the NaCl deposit be uniform over the sampled area. This uniformity was found impossible to achieve with an aqueous solution because of the extremely poor wettability of the metallic lid. The solution invariably formed droplets over the surface rather than a uniform film. Therefore, the NaCl solutions were prepared in mixed solvents of varying water/alcohol ratio. Even up to approximately 50% alcohol, a uniform film could not be formed over the surface of the package lid. Thus, it appeared that the preparation of standards which were similar to the lids was impossible.

It was still necessary to determine if XPS could detect the trace amounts of sodium found in IC packages. Therefore, another set of "standards" was prepared in which the substrate was a glass filter. This is not the optimum substrate since the solution would obviously be adsorbed

into the pores of the filter. Since XPS is a surface sensitive technique with a probing depth of 0 - 50 Å, the adsorbed material would not contribute to the signal intensity. Nevertheless, the data obtained would provide an upper estimate of the detection limit of XPS. The samples were prepared as described above. Since the most intense line in the XPS spectrum for sodium chloride is the X-ray excited $KL_{23}L_{23}$ Auger line at approximately 990 eV, its intensity was monitored as a function of the weight of sodium chloride added to the filter. Figure 2.1 is a plot of the data from 0 to 200 ng of sodium. The sodium content indicated in the figure has been corrected for the fact that the ESCA 36 photoelectron spectrometer samples only 2 mm² of the 0.5 cm² sample. Homogeneous distribution of the sodium over the surface has been assumed. No correction has been made for the loss of sodium into the interior of the glass fibers. Note that the fibers themselves contain detectable amounts of sodium as the curve does not go through the origin. As 200 ng of sodium is approached, the curve plateaus because the thickness of the deposited layer has surpassed the escape depth of the $Na(KL_{23}L_{23})$ electrons. The data also suggest that the detection limit of sodium via XPS is < 2.5 ng/mm². Thus, XPS is able to detect the amounts of sodium routinely encountered in the IC package environment.

2.2 TRANSPORT OF NaCl

The purpose of this series of experiments was to demonstrate whether transport of metal ions can occur from one surface to another within a micropackage under various conditions of contamination and moisture. The

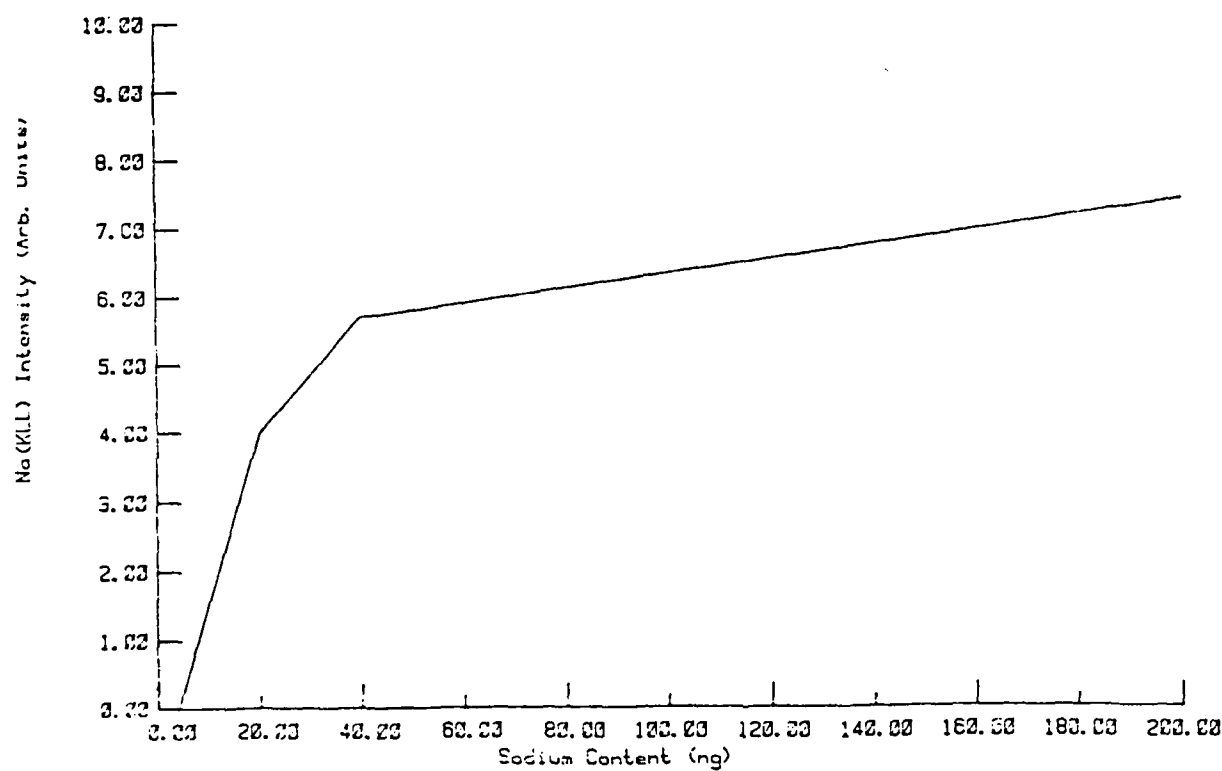


Figure 2.1. Na(KLL) intensity as a function of sodium content.

transport in question is transport which occurs via a "through space" mechanism rather than that of surface migration.

2.2.1 Microchamber. To provide maximum flexibility, a demountable pseudo-micropackage was fabricated as shown in Figure 2.2. A stainless steel VCO (registered trademark, Cajon) coupling with a blank gland serves as the package. The internal volume of the chamber is approximately 1 mL (1 cc). The gland is adapted such that a standard 0.5" x 0.5" package lid can be attached via a threaded stud which has been soldered to the underside of the lid. An hermetic seal is provided by an aluminum compression gasket as shown. The microchamber as received from the vendor contained a silver lubricant on the threads. As it was found that this silver could migrate to the lid surface during temperature cycling, it was necessary to remove the silver with a nitric acid rinse prior to use. The microchamber was then cleaned via the following procedure:

- a) wash with dilute HCl
- b) wash with deionized water
- c) ultrasonic clean in ethanol
- d) ultrasonic clean in trichloroethylene
- e) bake at 150°C for 15-30 minutes
- f) ultrasonic clean in trichloroethylene
- g) bake at 150°C for 15-30 minutes

2.2.2 Lid Preparation. In order to minimize any contamination via surface migration, the package lid should be suspended inside the microchamber with minimal contact. This was accomplished by mounting a solid solder screw to the underside of the lid as shown in Figure 2.3. The screw was then threaded into the microchamber so that the lid made no appreciable contact

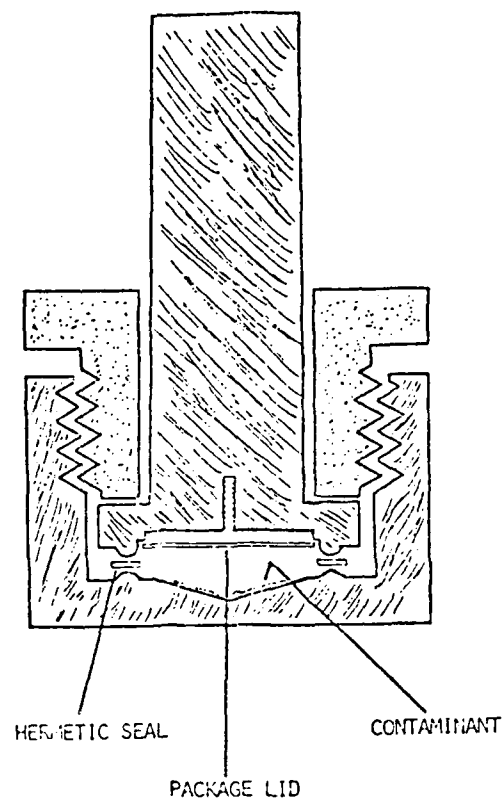


Figure 2.2. Microchamber employed in transport studies.

Table 2.3. Na(KLL) and Cl(2p) Intensities for
Cycled Kovar Lids With Varying
NaCl Contamination

<u>Lid #</u>	<u>NaCl (μg)</u>	<u>Moisture</u>	<u>Peak Intensities (C/20s)</u>	
			<u>Na(KLL)</u>	<u>Cl(2p)</u>
1	500	50% RH	ND*	212
2	100	"	ND	135
3	5.0	"	ND	219
4	0.5	"	ND	516
5	0.10	"	120	184
6	0	"	tr?***	180

* ND = not detected

** tr = questionable trace

Table 2.2. Na(KLL) and Cl(2p) Intensities for
Blanked Kovar Lids Without Ar⁺ Ion
Etching

<u>Lid#</u>	Peak Intensities (C/20s)	
	<u>Na(KLL)</u>	<u>Cl(2p)</u>
1	388	392
2	712	372
3	408	488
4	252	260
5	114	115
6	236	36

The initial data were accumulated on a series of Kovar lids that were cleaned via the following procedure:

- 1) burnish with 4/0 steel wool
- 2) ultrasonic clean in trichloroethylene
- 3) dry at 150°C
- 4) wipe with trichloroethylene

The XPS data for Na(KLL) and Cl(2p) electrons for these blanks are shown in Table 2.2. Note that in all cases, the blanks contained easily detectable amounts of sodium and chlorine. Repeated attempts were made to chemically blank the lids with no significant improvement.

A series of packages with Kovar lids cleaned by the above procedure was prepared. Various amounts of NaCl and 50% RH were sealed in the package and the package was cycled. The data are shown in Table 2.3. The Cl(2p) intensities are essentially identical to those of the blank and no significant transport of Na^+ is seen.

Typical Na(KLL) and Cl(2p) intensities for Au/Kovar lid blanks which had been subjected to the same cleaning procedure outlined above are given in Table 2.4. These lids were then sealed with constant 50% RH and varying amounts of NaCl. The packages were then cycled from 3°C to 150°C forty (40) times over a period of 72 days. As can be seen in Table 2.5 no detectable increase in Na signal was observed. Therefore, the data do not support the transport hypothesis.

Since it is more desirable to measure a signal versus a blank rather than to determine the increase of a signal relative to a detectable blank, further attempts were made to improve the cleanliness of the lid surface. It was found that after a 30 minute exposure to a 10KeV Ar^+ ion beam, the only detectable contaminant remaining on a Kovar lid was carbon. However,

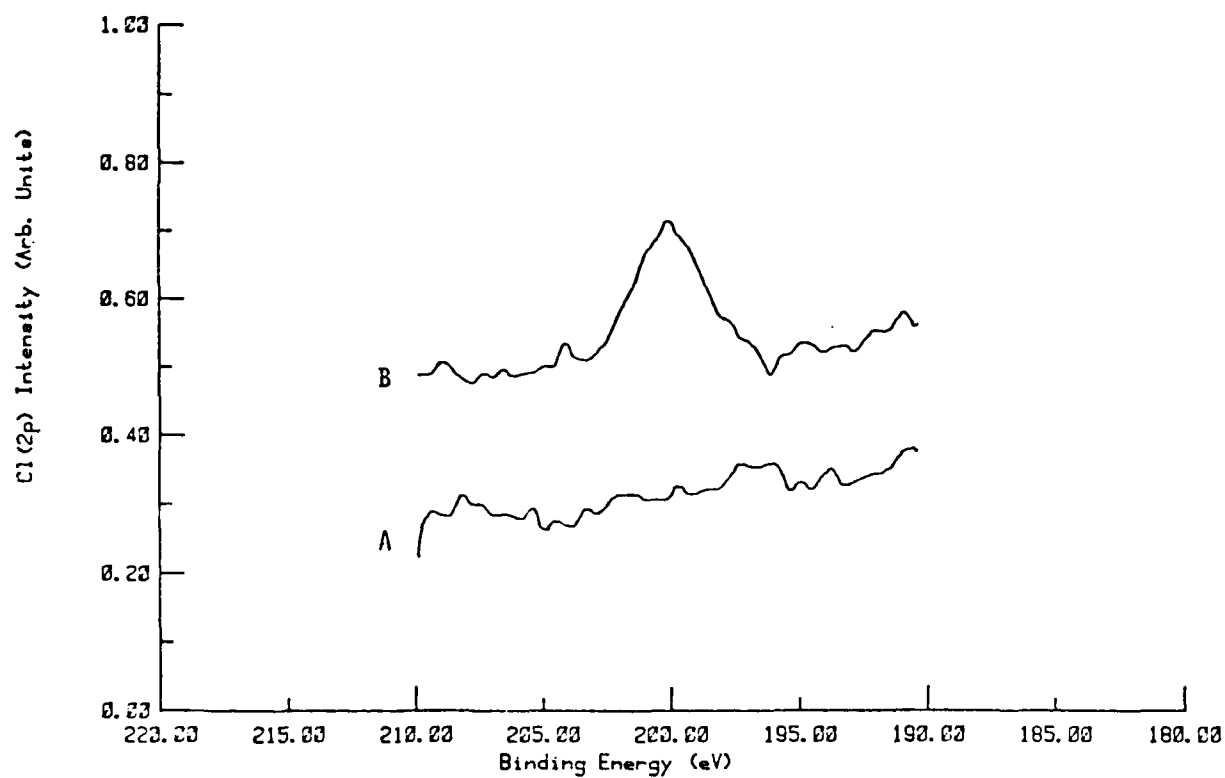


Figure 2.9. Cl(2p) spectra (A) prior to and (B) after gross contamination.

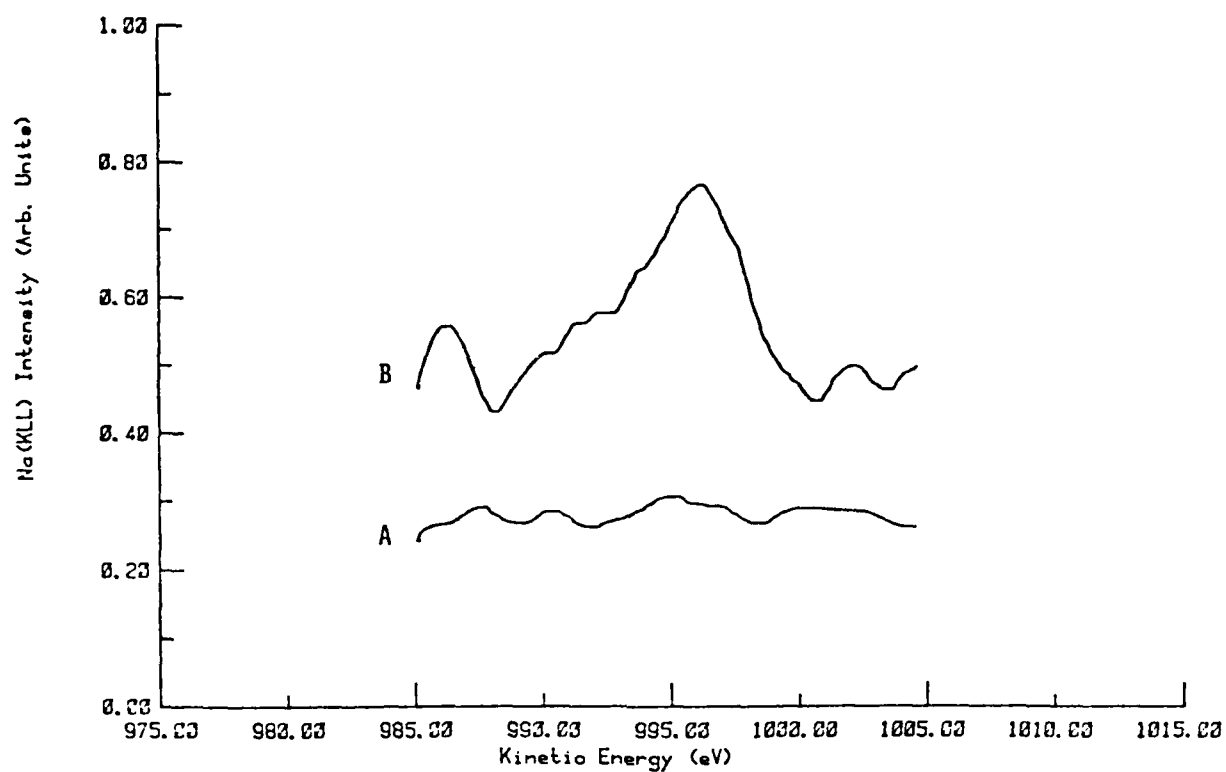


Figure 2.8. Na(KLL) spectra (A) prior to and (B) after gross contamination.

Table 2.1. Na(KLL) and Cl(2p) Intensities For
Grossly Contaminated Samples

<u>Lid #</u>	<u>Composition</u>	<u>NaCl (μg)</u>	<u>H₂O (μl)</u>	<u>#cycles</u>	<u>Na(KLL) Intensity (C/20s)</u>	<u>Cl(2p) Intensity (C/4s)</u>
1 A	Au/Kovar	500	10	18	ND*	ND
2 A	Au/Kovar	500	10	18	TR**	ND
3 A	Au/Kovar	500	10	18	ND	130
1 B	Kovar	500	10	14	336	TR
2 B	Kovar	500	10	13	3208	391

*ND = None detected

**TR = Trace

2.3.1 Gross Contamination. Initial experiments were designed to test a "worst case" hypothesis in which the microchamber was grossly contaminated. In these instances a series of chambers with either Au/Kovar or Kovar lids in place were contaminated with 500 μg of NaCl and 10 μL of water. The internal volume of the chamber is approximately 1 mL (1cc). The chambers were then cycled for 792 hours between 3 and 150°C. The data are tabulated in Table 2.1. Typical Na(KLL) and Cl(2p) spectra before and after cycling are shown in Figures 2.8 and 2.9 respectively. In all cases, the lids were visually spotted in a random fashion. Visual inspection of the chamber cavity also showed a random orientation of spots.

Since XPS analyses approximately 2mm^2 , the XPS data represent an average across a given portion of the lid. Typical Auger spectra are excited with an electron beam which can be point focused. Therefore, AES is routinely employed to analyze for surface inhomogeneity. AES data indicated that the spots were essentially pure deposits of NaCl, while the unspotted areas contained no NaCl. In lids 1A and 3A the average concentration of NaCl was apparently below the XPS detection limits.

These data strongly suggest that an aerosol is forming (due to boiling of the water) and the NaCl is transported by the aerosol. This would definitely yield the spotted, inhomogeneous distribution of NaCl on the lids.

2.3.2 Moderate Controlled Contamination. A series of experiments were performed in which either Kovar or Au/Kovar lids were placed in chambers contaminated with varying amounts of NaCl and water. The packages were cycled for varying amounts of time between 3 and 150°C after a blank XPS spectrum was determined.

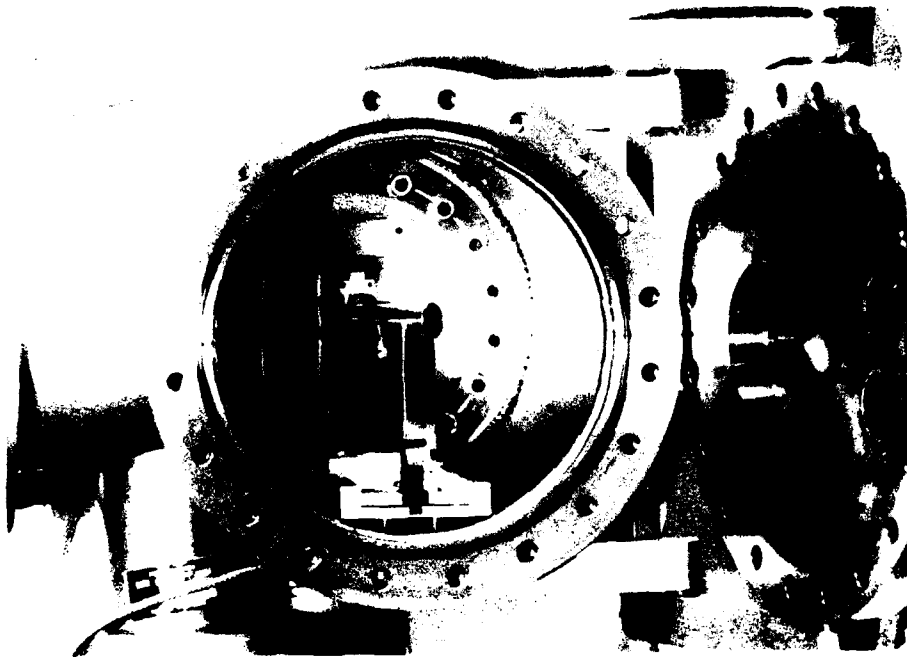


Figure 2.7. Au/Kovar lid in position for analysis.

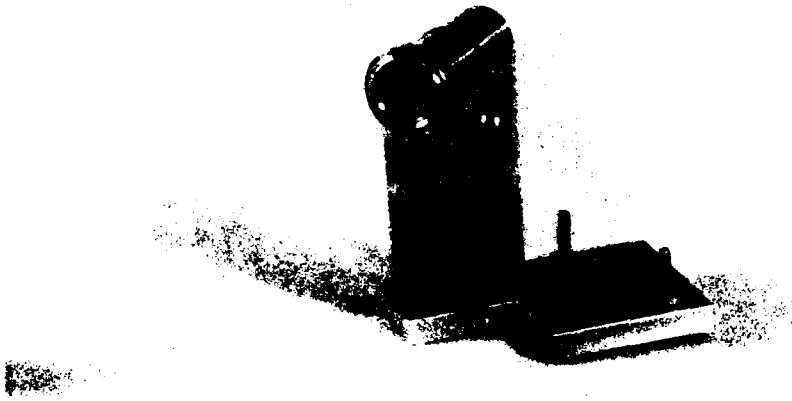


Figure 2.6. Mounted Au/Kovar lid on positioning device.

which contains 0 to 20,000 ppmV of water vapor. The moisture content is standardized against a National Bureau of Standards traceable optical dew point hygrometer (General Eastern Corporation). The microchamber is flushed with the desired atmosphere for 5 minutes prior to sealing. The hermeticity of the sealed package was verified by standard helium leak detection procedures.

Once the chamber had been contaminated, it was cycled from 3 to 150°C by alternately placing it in a refrigerator and oven for known periods of time. During the cycling steps, extreme care was taken to ensure that the chamber remained in an upright configuration so that the NaCl was not dislodged from its initial position.

Once the cycling had been completed, the chamber was opened and the lid was analyzed. Again, precautions were taken such that the lid was not inadvertently contaminated. The cycled lids were then analyzed via XPS and Auger electron spectroscopy. In the case of XPS analysis, a device was fabricated which permits the lid to be mounted in the sample chamber while still attached to the mounting gland of the microchamber. This device is shown in Figure 2.6 and as it is mounted in Figure 2.7.

AES analyses were performed at the University of Florida (UF) on standard Auger instrumentation equipped with a double pass cylindrical mirror analyzer. Contamination during transport was minimized by carefully packaging the specimens. Standard handling techniques employed in surface analytical procedures were used at UF to ensure minimum inadvertent contamination during the course of mounting the specimens in the AES vacuum chamber.

2.3 RESULTS

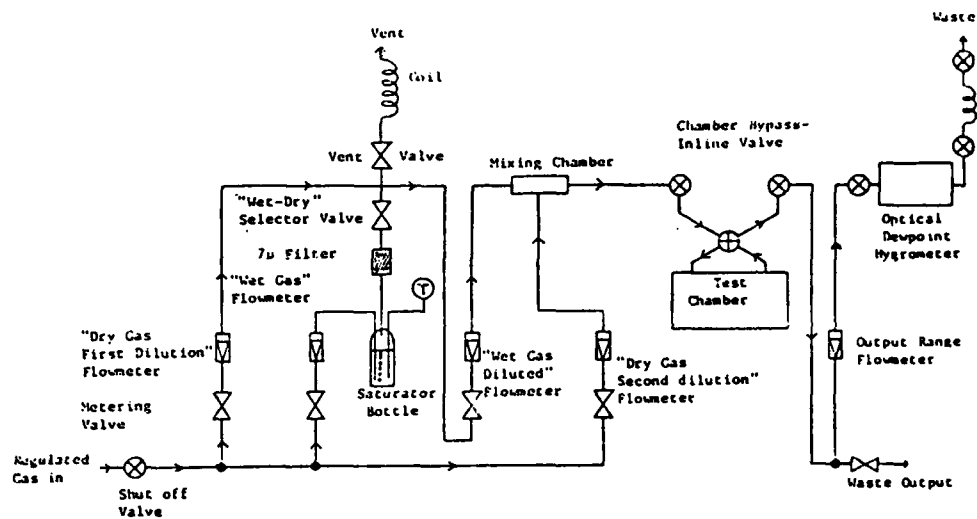


Figure 2.5. Gas dilution apparatus for controlling package moisture.

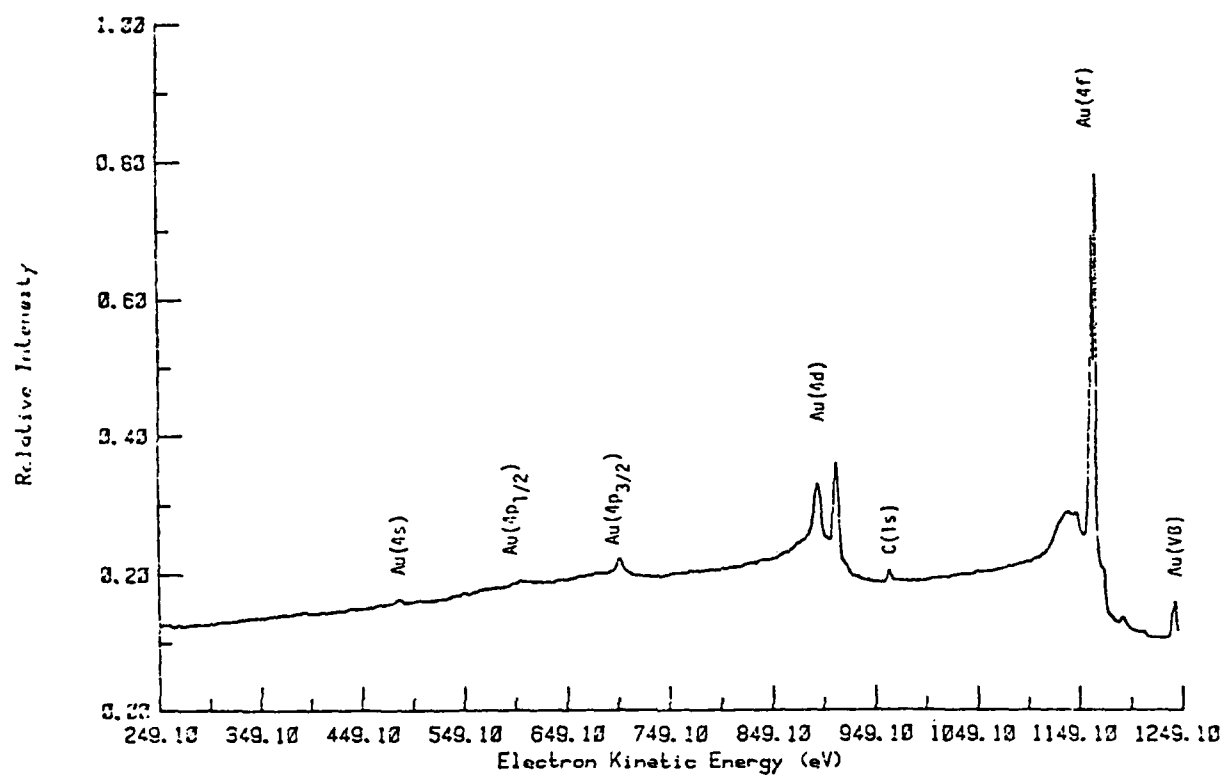


Figure 2.4. XPS survey spectrum of clean Au/Kovar lid

other than at the screw. This makes the surface migration of contaminants extremely improbable.

Prior to mounting, the lids were blanked via the following procedure:

- a) lightly burnish with 4/0 steel wool or #600 emery
- b) wash with ethanol
- c) ultrasonic clean in trichloroethylene
- d) dry at 150°C
- e) mount and rinse with trichloroethylene
- f) etch with 10KeV Ar⁺ for 30 min.

This procedure produces an acceptable blank in that the XPS spectra show no appreciable contamination. However, the procedure is extremely time consuming. It has been demonstrated that equivalent blanks are produced if the chemical cleaning (b and c) is eliminated. Therefore, the cleaning is accomplished simply by etching with 10KeV Ar⁺ ions in the XPS sample chamber for 30 minutes. The XPS survey spectrum for a typical blank gold lid is shown in Figure 2.4. The only contaminant present is a slight amount of hydrocarbon.

2.2.3 Contaminant Introduction. To investigate contaminant transport across the volume of the microchamber, known amounts of an aqueous NaCl solution were added to the base of the chamber with a microsyringe. The base was then dried in an oven at 150°C. The moisture content was adjusted by either syringing gross microliter amounts of water into the cavity prior to sealing or the chamber was simply sealed at ambient relative humidity (60%). If calibrated amounts of moisture were needed, the chamber was carefully sealed in a controlled environment provided by the gas dilution apparatus shown in Figure 2.5. The apparatus provides a nitrogen atmosphere



Figure 2.3. Au/Kovar lid with mounting screw.

Table 2.4. Na(KLL) and Cl(2p) Intensities for
Au/Kovar Lids Blanked Without Ar⁺
Etching

<u>Lid #</u>	Peak Intensity (C/20s)	
	<u>Na(KLL)</u>	<u>Cl(2p)</u>
1	ND	328
2	ND	104
3	ND	108
4	ND	100
5	tr	508
6	tr?	472
7	204	348

Table 2.5. Na(KLL) and Cl(2p) Intensities for
Au/Kovar Lids Which Have Been Cycled

<u>Lid #</u>	<u>NaCl (μg)</u>	<u>Moisture</u>	<u>Peak Intensity (C/20s)</u>	
			<u>Na(KLL)</u>	<u>Cl(2p)</u>
1	500	50% RH	ND	312
2	100	"	ND	460
3	50	"	176	392
4	5	"	tr	372
5	0.5	"	tr?	524
6	0.1	"	tr?	276
7	0	"	tr	516

on Au/Kovar lids the chlorine was ubiquitous. It is generally accepted that it is extremely difficult to obtain a gold surface that contains no chlorine (2). All further experiments were performed on lids that had been sputtered with 10KeV Ar^+ ions.

As mentioned above, the only contaminant present at detectable levels was carbon. Table 2.6 contains the data obtained on Au/Kovar lids from cycled packages which contain 500 μg NaCl while the water content was varied. Each package was cycled 42 times. Note that even though no sodium was detected, very significant amounts of chlorine were present after the cycling. To further investigate this unusual result, survey scans from 1000 eV - 0 eV binding energy were taken. The data indicated the presence of large amounts of nickel and perhaps some iron. Since each lid, including the blank, contained large surface concentrations of nickel and chlorine, the presence of the surface species appeared to be independent of the NaCl content. The nickel from the Kovar base was found to migrate through the 12000 Å of gold at 150° C (See section 3). Similar low temperature diffusion has been reported for other systems (3,4,5,6,7). It seems likely that the chlorine which is usually found in/on gold (2) moves to the surface with the nickel. Chlorine has been found to readily migrate in other metals (8,9). Figures 2.4 and 2.10 are the survey spectra of the lids before and after cycling, respectively.

A series of Kovar lids was subjected to an experiment identical to that of gold discussed in the previous paragraph with the identical result: no sodium was transported. It must be mentioned that during the course of all of the cycling experiments the C(1s) spectrum indicated the presence of an oxygen containing carbonaceous species on the surface after cycling. A

C(1s) spectrum before and after cycling is shown in Figure 2.11. The origin and exact nature of this species has not been identified.

One series of experiments was conducted in which the metal lids were replaced with silicon wafers. The wafers were obtained from Texas Instruments with a nominal $8\text{K}\text{\AA}$ thickness of thermal oxide. The wafers were diced, mounted and wiped with ethanol. They were not etched. The XPS data on the blanks indicated only Si, O and C on the surface. The spectrum is shown in Figure 2.12. The packages were contaminated with $500\text{ }\mu\text{g}$ NaCl and 50% RH. The packages were held at 3°C for 72 hours and were then placed in an oven at 150°C for 40 days. Analysis of the silicon chips after thermal treatment yielded the data shown in Figure 2.13. Obviously, no transport occurred.

All of the above data suggest that transport of soluble contaminants such as NaCl does not occur via the "water pump mechanism". In no instance was it possible to contaminate a surface by cycling the package between 3 and 150°C for extended periods of time under controlled conditions. Transport of NaCl did occur when the package was grossly contaminated. The mechanism for transport under gross conditions occurs via aerosol formation. The aerosol forms via the boiling of the macro-amounts of water in the package.

Table 2.6. Na(KLL) and Cl(2p) Intensities for
Au/Kovar Lids Cycled With Varying
Amounts of Water

<u>Lid #</u>	<u>NaCl(ug)</u>	<u>Water (ppm V)</u>	<u>Peak Intensities (C/20s)</u>	
			<u>Na(KLL)</u>	<u>Cl(2p)</u>
1	500	250	ND	91
2	500	500	ND	472
3	500	1350	ND	284
4	500	4900	ND	376
5	500	10,500	ND	256
6	500	18,000	ND	324
7	500	0	ND	288

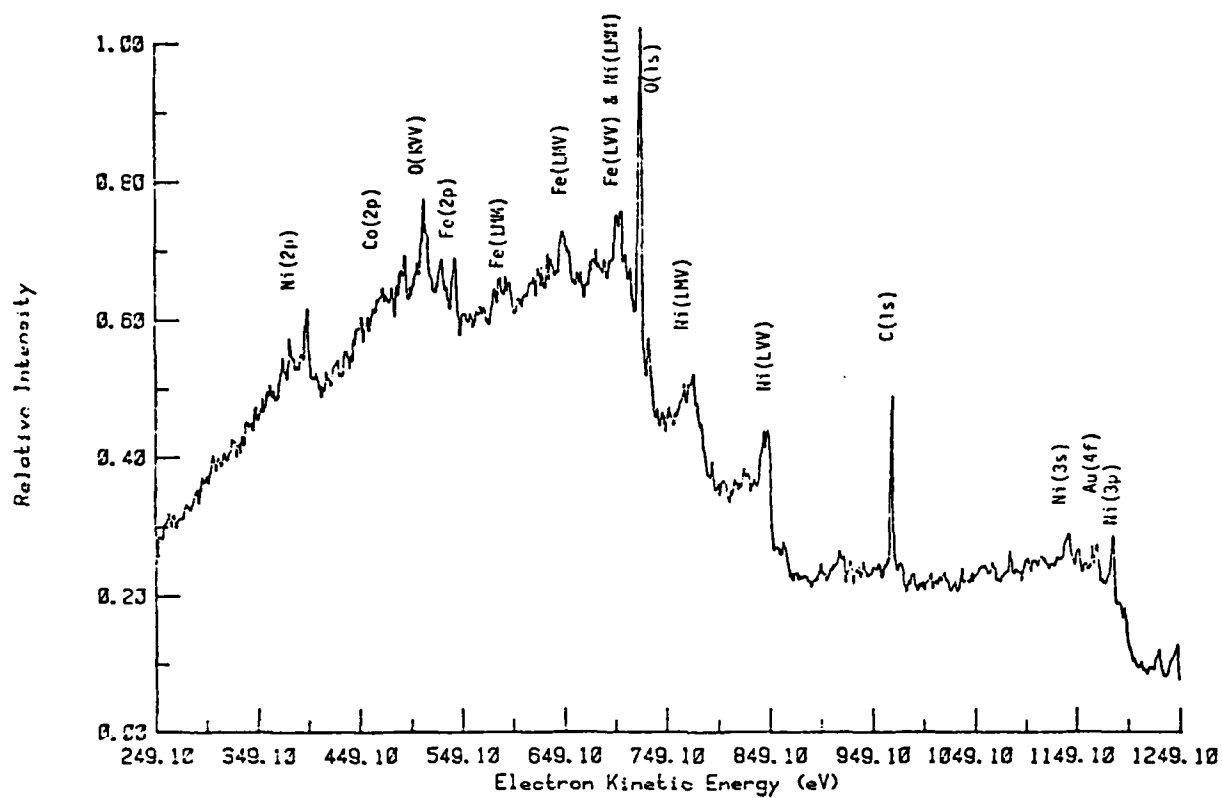


Figure 2.10. XPS survey spectrum of Au/Kovar lid heated to 360°C in air.

C(1s) spectrum before and after cycling is shown in Figure 2.11. The origin and exact nature of this species has not been identified.

One series of experiments was conducted in which the metal lids were replaced with silicon wafers. The wafers were obtained from Texas Instruments with a nominal $8\text{K}\text{\AA}$ thickness of thermal oxide. The wafers were diced, mounted and wiped with ethanol. They were not etched. The XPS data on the blanks indicated only Si, O and C on the surface. The spectrum is shown in Figure 2.12. The packages were contaminated with $500\text{ }\mu\text{g}$ NaCl and 50% RH. The packages were held at 3°C for 72 hours and were then placed in an oven at 150°C for 40 days. Analysis of the silicon chips after thermal treatment yielded the data shown in Figure 2.13. Obviously, no transport occurred.

All of the above data suggest that transport of soluble contaminants such as NaCl does not occur via the "water pump mechanism". In no instance was it possible to contaminate a surface by cycling the package between 3 and 150°C for extended periods of time under controlled conditions. Transport of NaCl did occur when the package was grossly contaminated. The mechanism for transport under gross conditions occurs via aerosol formation. The aerosol forms via the boiling of the macro-amounts of water in the package.

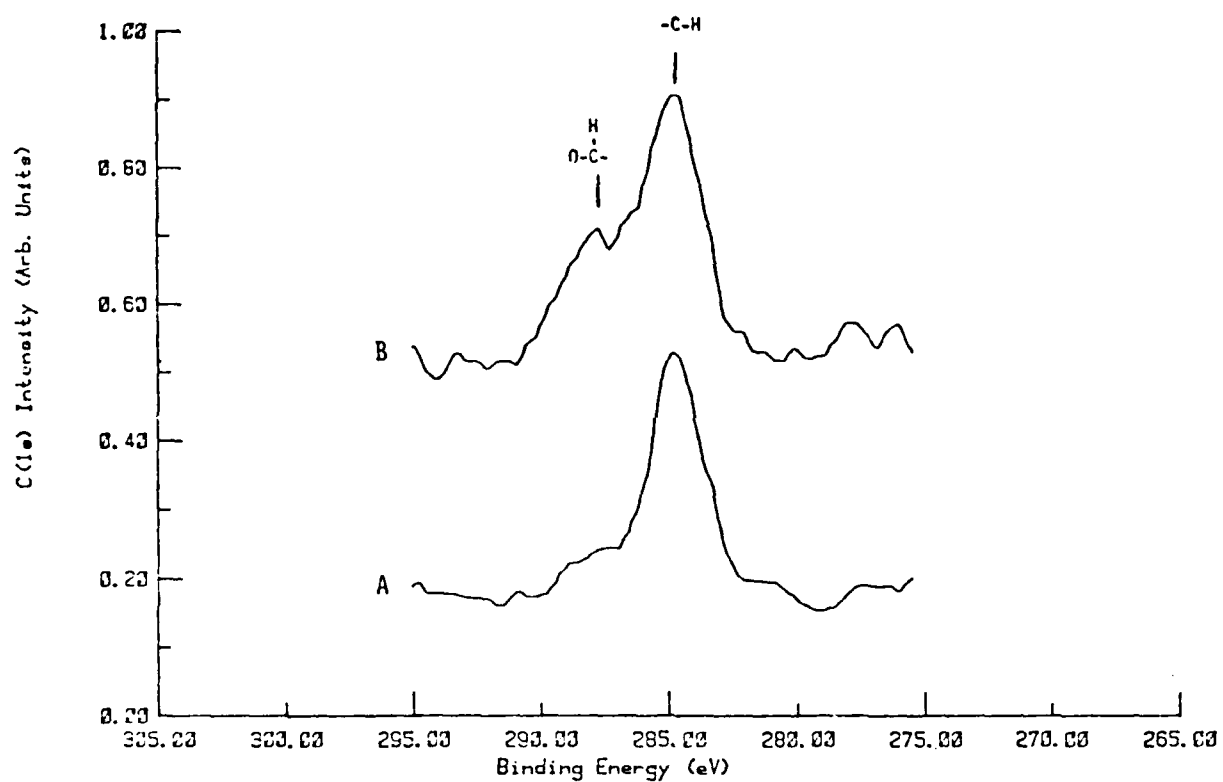


Figure 2.11. C(1s) spectra (A) before and (B) after cycling.

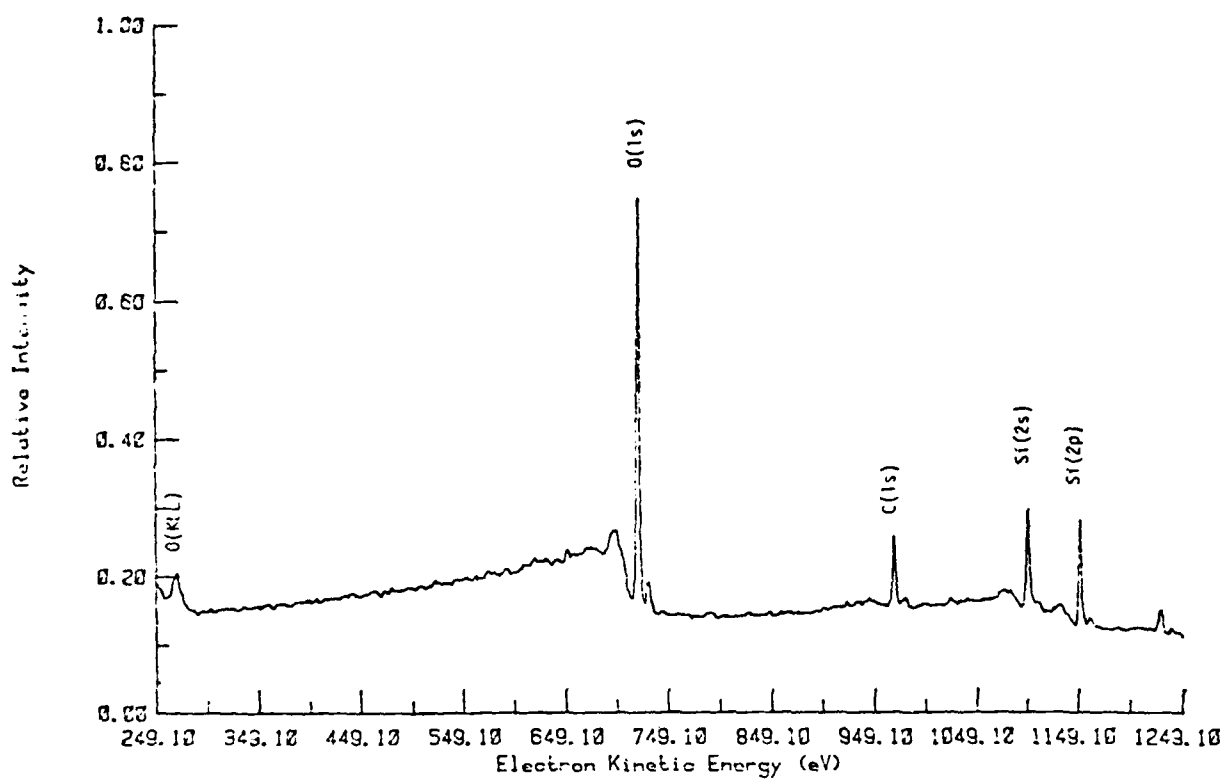


Figure 2.12. XPS survey spectrum of oxidized silicon wafer.

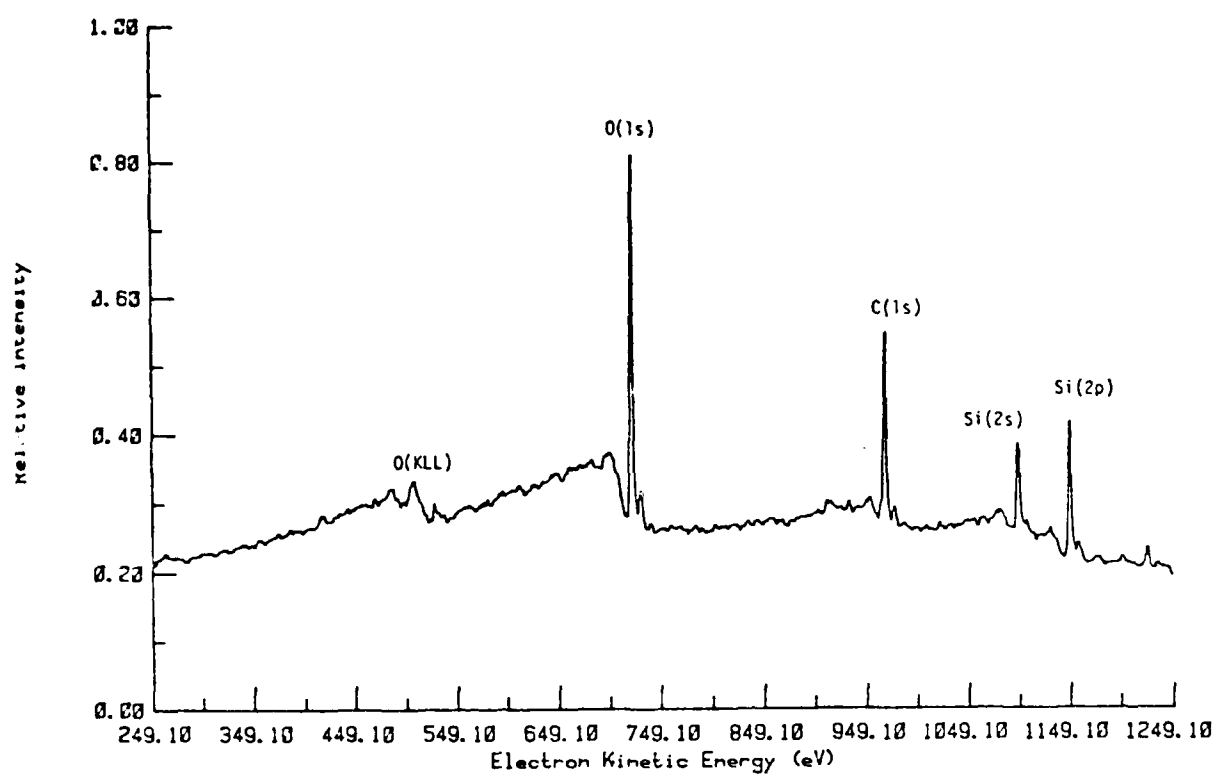


Figure 2.13. XPS survey spectrum of oxidized silicon wafer after contamination.

3.0 DIFFUSION OF TRANSITION METALS THROUGH GOLD FILMS

X-ray photoelectron spectroscopy was employed to study the thermal diffusion of iron, nickel and cobalt through gold in bilayer thin film structures under an oxidizing environment. The data suggest that the driving force for the diffusion is the oxidation of the transition metal at the surface. The activation energies are consistent with a grain boundary diffusion mechanism.

3.1 INTRODUCTION

One system routinely employed for packaging high reliability microelectronic devices consists of gold-plated Kovar, an iron, nickel and cobalt alloy. In an earlier paper (10) it has been demonstrated that, if an Au/Kovar package lid is subjected to temperatures of several hundred degrees Celsius in an oxidizing environment, the Kovar components readily diffuse through the gold to the surface. As discussed by Hall and Morabito (11) temperatures of several hundred degrees Celsius are routinely experienced during processing steps such as plastic molding, resistor stabilization and thermal screening of the devices. In addition, since power density requirements are steadily increasing, device operating temperatures are increasing. Therefore intermetallic diffusion might be expected to occur at field temperatures. Alteration of the package via intermetallic diffusion could cause problems such as loss of bond strength, loss of solderability and loss of conductivity.

More importantly, in the Au/Kovar case, the intermetallic diffusion processes tend to convert a relatively inert gold surface to a much more

chemically reactive surface which contains significant amounts of transition metal oxides. It has been shown (10) that a pure gold surface will not chemisorb or physisorb water as readily as will a surface contaminated with transition metal oxides. Since several of the major failure mechanisms (e.g. electromigration and corrosion) are known to be moisture induced, intermetallic diffusion would be expected to play a major role in moisture-induced reliability problems.

In order to understand the intermetallic diffusion processes occurring in the Au/Kovar system, a study of the kinetics of diffusion of each individual transition metal through gold was initiated. It is intended that these data can be employed to define appropriate processing temperatures, protocols and structures which will minimize the role of intermetallic diffusion in device reliability problems. X-ray photoelectron spectroscopy was the technique chosen for the study since it provides the most chemical information (e.g. oxidation states) of all the standard surface techniques (12). The rates, diffusion coefficients and activation energies for the diffusion of iron, cobalt and nickel through gold films as determined by XPS will be presented in this section.

3.2 EXPERIMENTAL DETAILS

3.2.1 Film preparation. Bilayer thin film specimens were prepared by depositing 400 Å of the transition metals (99.998% purity) onto a quartz substrate via resistive heating in a CVC deposition system at a base pressure 2.0×10^{-6} torr. Approximately 3000 Å of gold (99.99% purity) were then deposited onto the transition metal film without breaking the vacuum. Film thicknesses were monitored during deposition with a Kronos QM 311

thickness monitor equipped with an FTT 350 detector head via standard quartz crystal oscillator techniques. The films were deposited at a rate of $100 \text{ \AA} \text{ min}^{-1}$. Initial bilayer films were deposited onto borosilicate glass substrates. However, XPS analysis of these specimens indicated that, during specimen heating, sodium from the glass diffused through the bilayer structure to the surface. Therefore, quartz substrates were used in subsequent experiments. XPS analyses of the bilayer specimens indicated that the surface was pure gold with no contaminants other than the ubiquitous hydrocarbon layer normally observed in surface analytical studies.

2.2 Surface analyses. XPS spectra were obtained with a GCA-McPherson SCA 36 photoelectron spectrometer. The spectra were excited with Al $K\alpha$ X-rays ($E_x = 1486.6 \text{ eV}$) generated at a power of 320 W. The base pressure in the sample chamber was 5.0×10^{-7} torr or less.

Auger depth profiles were obtained with a Perkin-Elmer-Physical Electronics model 590 surface analysis system using 1.5kV argon ions at a beam current of 25 mA.

2.3 Sample treatment. The bilayer films were heated in a furnace at a specific temperature under ambient laboratory air as a function of time. Periodically, the heating was interrupted and the specimen was subjected to XPS analysis. This procedure allowed the surface concentration of the transition metals to be monitored as a function of time.

2.4 Data processing. The rate of diffusion was followed by monitoring the surface concentration via peak height analysis. In order to correct for

ossible instrumental and/or system changes with time, the ratio I_M/I_{Au} of the transition metal $(2p)_{3/2}$ peak height to the Au $(4f)_{7/2}$ peak height was plotted as a function of time. Further, the photoelectron signal intensities were normalized via Schofield's atomic sensitivity factors (13). The slopes of a plot of $(I_M/\alpha_M)/(I_{Au}/\alpha_{Au})$ versus time yield the rate of diffusion of the transition metal M to the surface. Arrhenius analysis of the rate data yields the activation energy and the diffusion coefficient pre-exponential factor.

3.3 RESULTS AND DISCUSSION

Figure 3.1 is a typical XPS survey spectrum for an Au/Fe bilayer film prior to heating. It should be noted that the only feature present that cannot be attributed to gold is the C (1s) signal at 285 eV. This results from the ubiquitous hydrocarbon contamination, routinely observed via surface analysis techniques. If the bilayer film is heated in air at 229°C for 1.5 h, the spectrum in Figure 3.2 results. A very intense O (1s) line, the Fe(2p) and Fe(3p) lines and the Auger features of iron are now observed. The iron has diffused through the gold to the surface. If the ratio of the Fe $(2p)_{3/2}$ intensity to that of Au $(4f)_{7/2}$ is plotted as a function of time, Figure 3.3 results. At extended times the intensity ratio saturates because the thickness of the iron deposit has exceeded the XPS sampling depth, and no further increase in Fe $(2p)_{3/2}$ intensity is noted. It should be noted that at relatively short heating times the curve is linear.

The chemical state of the diffused iron can be determined via the high resolution Fe(2p) XPS spectrum. Figure 3.4 contains the Fe(2p) spectra for an unoxidized iron film and for iron which has diffused through a gold film.

ble 3.1.

Diffusion Rates

<u>Metal</u>	<u>T C)</u>	<u>k(sec⁻¹)</u>	<u>R_{corr}*</u>
Iron	210	2.24×10^{-5}	0.992
	218	3.03×10^{-5}	0.999
	229	5.24×10^{-5}	0.996
	238	7.18×10^{-5}	0.999
Nickel	221	3.34×10^{-6}	0.999
	233	6.62×10^{-6}	0.997
	242	1.03×10^{-5}	0.994
	250	1.56×10^{-5}	0.997
Cobalt	217	8.82×10^{-7}	0.999
	225	1.45×10^{-6}	0.999
	234	2.35×10^{-6}	0.997
	239	2.83×10^{-6}	0.999

* Linear correlation coefficient

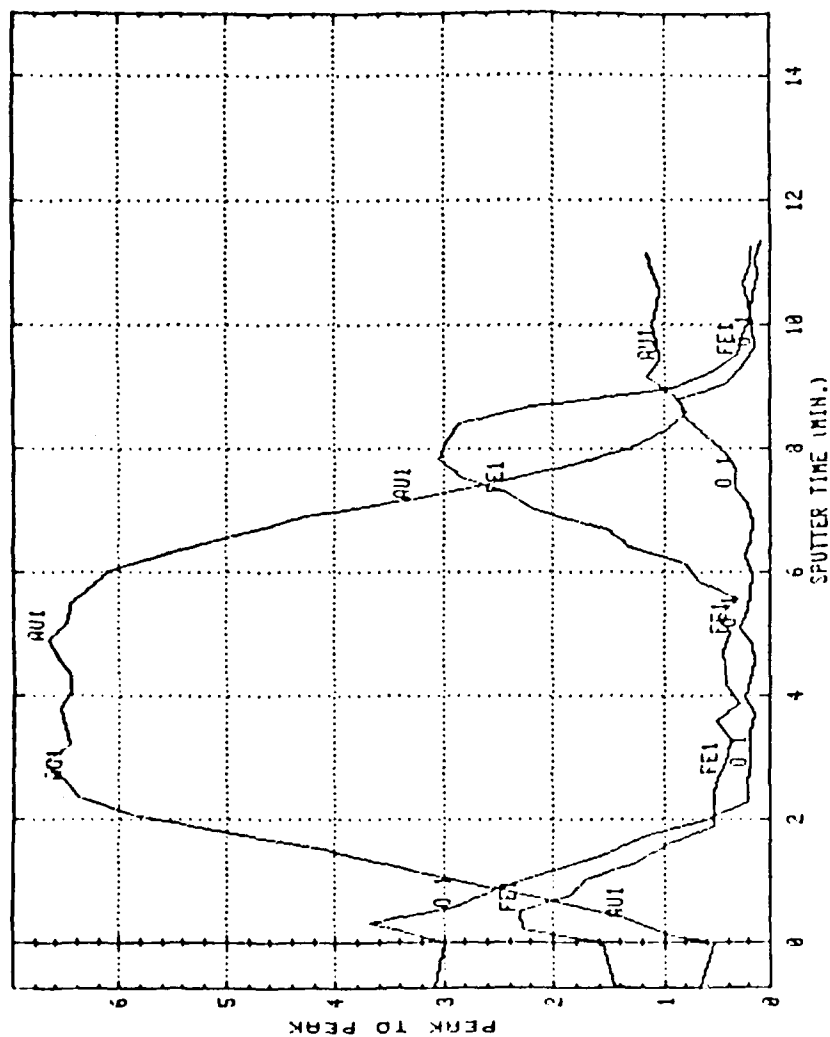


Figure 3.8. Gold, Iron, And Oxygen Concentration Depth Profiles Obtained By AFS Of a Au/Fe Bilayer Film After Heating To 200°C.

the iron intensity rises. It should also be noted that, since the initial iron film was not exposed to air, there is no oxygen at the Au-Fe interface. Oxygen is first observed as the Fe-SiO₂ interface is reached. After heating, as expected, the depth profile (Figure. 3.8) changes drastically. The dominant species at the surface are now oxygen and iron. In addition, the iron is now uniformly distributed throughout the gold layer in trace amounts while the oxygen intensity is essentially zero within the bulk of the gold film. In Figure 3.7 the oscillations at sputter times $t > 23$ min result from sample charging. In Figure 3.8 the tail on the gold profile is likely to be due to interdiffusion of the gold and iron at the interface. In addition, it should be noted that the sputtering rate in Figure 3.8 is greater than that in Figure 3.7.

Nickel and cobalt bilayer film structures identical with that for iron were prepared and studied via an identical protocol. In each case, the nickel and cobalt diffuse to the surface via an oxidation process. The diffusion profiles are similar to that for iron shown in Figure 3.3. The Auger depth profiles are qualitatively similar to that for the Au/Fe bilayer structure. The rates for the low temperature diffusion of nickel and cobalt through gold are tabulated in Table 3.1 and the activation energies and diffusion coefficients are in Table 3.2.

The activation energies in the present study are about 25 kcal mol^{-1} and would therefore be typical of grain boundary diffusion (14-18). Hall and Morabito (11) have emphasized the importance of grain boundaries in theoretical studies concerned with diffusion phenomena in microelectronic packaging.

Additional work with Au/Cr thin film yielded an activation energy of 25 kcal mol^{-1} and a diffusion coefficient pre-exponential of $0.5 \times 10^{-3} \text{ cm}^2 \text{ s}^{-1}$.

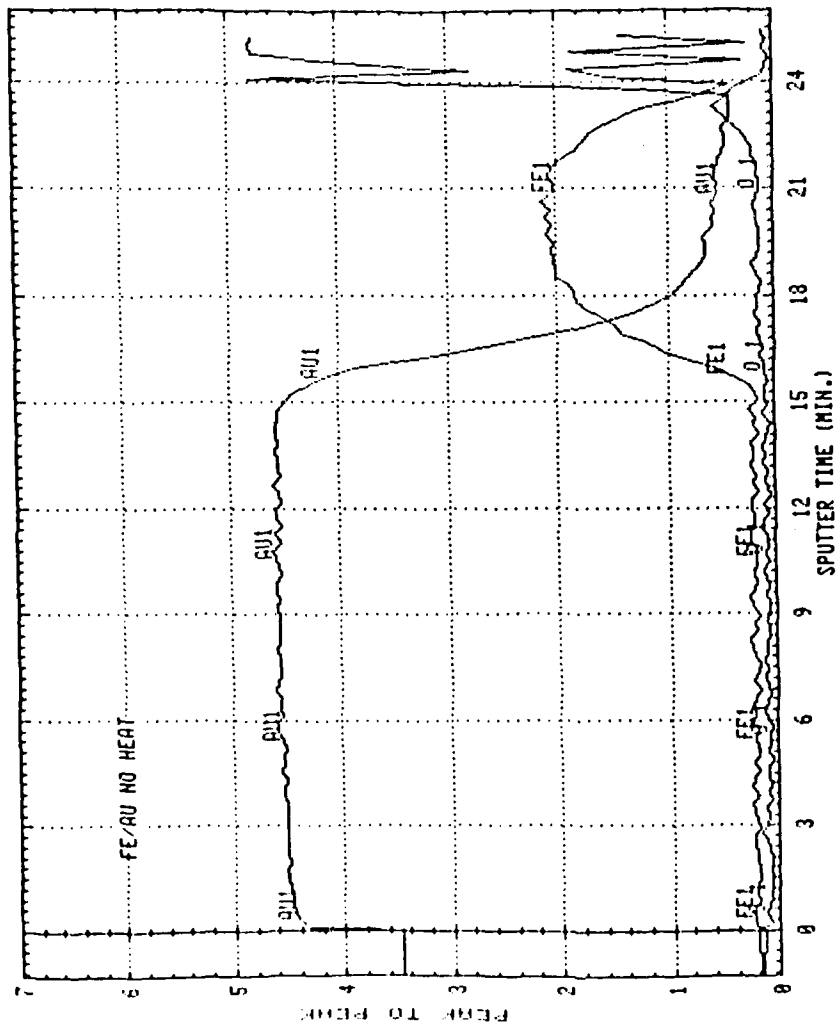


Figure 3.7. Gold, Iron And Oxygen Concentration Depth Profiles Obtained By AES Of An Unheated Au/Fe Bilayer Film.

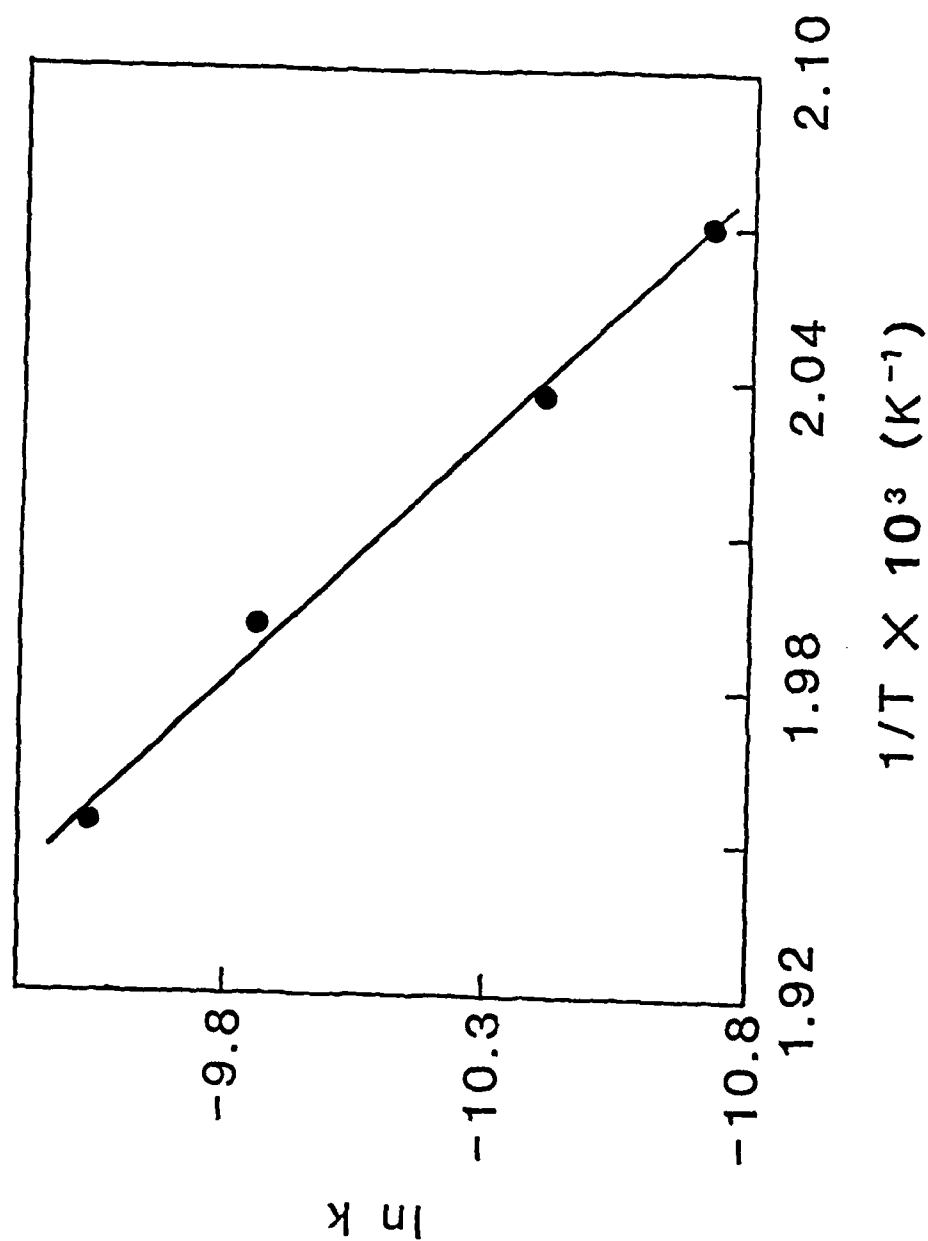


Figure 3.6. Arrhenius Plot For The Oxidative Thermal Diffusion Of Iron Through Gold.

Table 3.2

Diffusion Parameters

<u>Metal</u>	<u>Arrhenius Slope</u>	<u>R*_{corr}</u>	<u>E_a (kcal/mole)</u>	<u>D₀ (cm²/s)</u>
Iron	-10,200	0.997	20	2.7 x 10 ⁻⁵
Nickel	-13,700	0.999	27	3.0 x 10 ⁻³
Cobalt	-13,300	0.998	26	4.8 x 10 ⁻⁴

*Linear correlation coefficient for Arrhenius plot of $\ln k$ vs $1/T$.

where A is the frequency or pre-exponential rate factor, E_a is the activation energy and R is the gas constant. The diffusion coefficient D can be obtained from the equation

$$D = D_0 \exp \left(- \frac{E_a}{RT} \right)$$

where D_0 is the diffusion coefficient pre-exponential factor. From equation (3.1)

$$A = k' D_0 \quad (3.3)$$

where k' (cm^{-2}) is a constant determined by the structure of the gold film. Scanning electron micrographs at magnifications of 47,000 x indicated that the films were continuous. Grain boundaries could not be detected at this magnification. Therefore, it is assumed that the grain boundaries remain constant and k' can be taken as $1/l^2$ where l is the gold film thickness. Thus, the activation energy E_a and the diffusion coefficient pre-exponential factor D_0 for the diffusion of iron through gold can be obtained via a plot in $\ln k$ versus $1/T$. (Figure 3.6). The activation energy for the diffusion of iron through gold is 20 kcal mol^{-1} while the diffusion coefficient pre-exponential factor is $2.7 \times 10^{-5} \text{ cm}^2 \text{ s}^{-1}$ (Table 3.2).

It is possible to study the bilayer structures as a function of depth with Auger electron spectroscopy (AES) and inert ion sputtering. Figure 3.7 is the AES profile of an unheated Au/Fe bilayer film. It should be noted that gold is the only signal observed initially. At the Au-Fe interface,

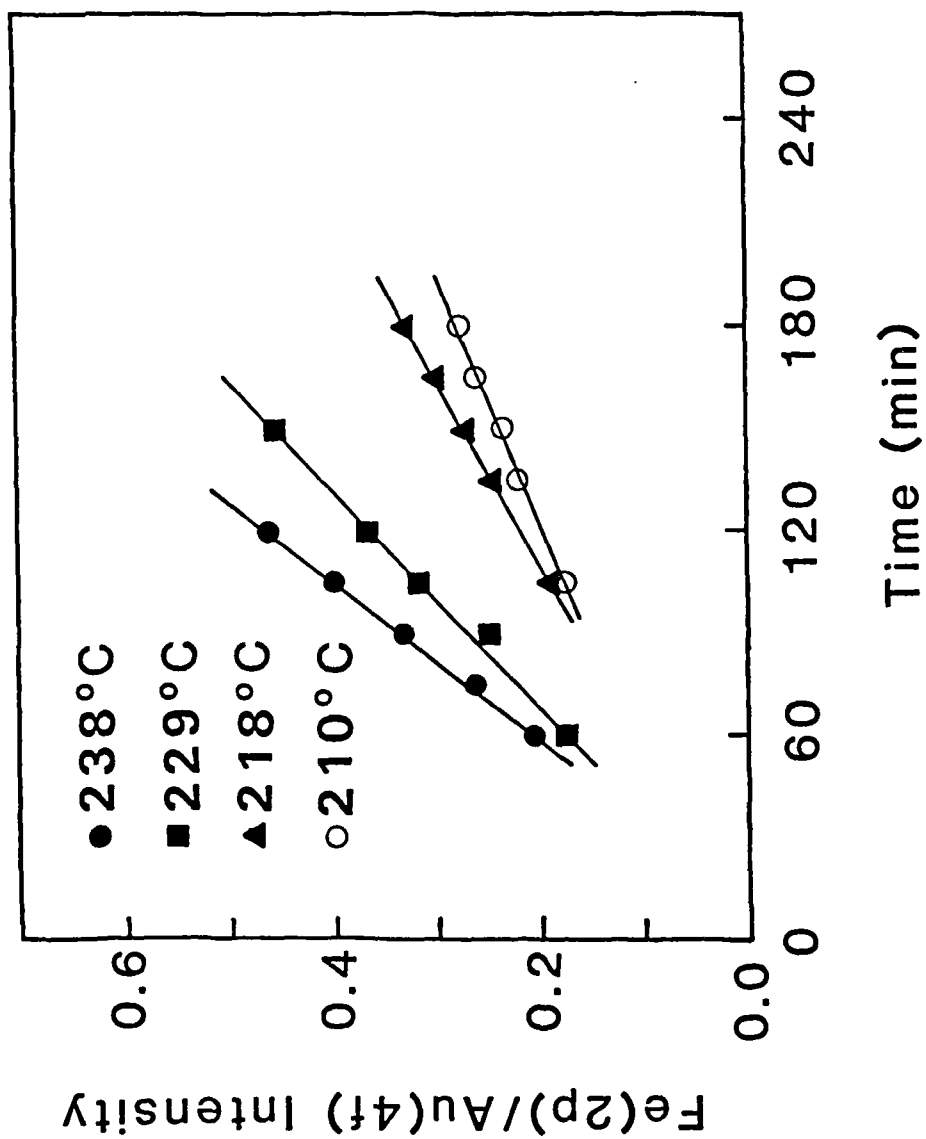


Figure 3.5. Intensity Ratios Of The Fe (2P)_{3/2} Signal To The Au (4f)_{7/2} Signal As A Function Of Time At Constant Temperature.

Table 3.1.

Diffusion Rates

<u>Metal</u>	<u>T C)</u>	<u>k(sec⁻¹)</u>	<u>R_{corr}*</u>
Iron	210	2.24×10^{-5}	0.992
	218	3.03×10^{05}	0.999
	229	5.24×10^{-5}	0.996
	238	7.18×10^{-5}	0.999
Nickel	221	3.34×10^{-6}	0.999
	233	6.62×10^{-6}	0.997
	242	1.03×10^{-5}	0.994
	250	1.56×10^{-5}	0.997
Cobalt	217	8.82×10^{-7}	0.999
	225	1.45×10^{-6}	0.999
	234	2.35×10^{-6}	0.997
	239	2.83×10^{-6}	0.999

* Linear correlation coefficient

The binding energies and peak shape for the diffused iron specimen clearly identify it as an iron oxide. This is consistent with the appearance of the intense O (1s) signal in Figure 3.2. Nelson and Holloway (7) have reported that the primary driving force for the diffusion of chromium through gold films is the oxidation of chromium to Cr_2O_3 at the surface. If the Au/Fe specimen is heated in vacuum or under an N_2 or H_2 environment, no surface accumulation of iron is observed. Heating the bilayer structure in an inert environment would be expected to accelerate the intermixing of the iron and gold at the interface. The intermixing would be expected to be most evident at the grain boundaries. Attempts to measure the extent of intermixing via XPS depth profiles were unsuccessful. It is likely that the amount of intermixing was below the detection limit of the technique. These observations are consistent with the fact that the oxidation of iron to Fe_2O_3 at the surface of the bilayer structure is the primary driving force for the iron diffusion.

In order to determine the initial rates of diffusion, the intensity ratio of the Fe(2p) signal to the Au(4f) signal can be monitored as a function of time over the linear portion of the diffusion profile (Figure 3.3). Figure 3.5 contains the linear diffusion profiles for iron through gold as a function of temperature. The slopes of the lines yield the initial rates of diffusion which are tabulated in Table 3.1.

The Arrhenius relationship between the diffusion rate k and the temperature T is

$$k = A \exp \left(- \frac{E_a}{RT} \right) \quad (3.1)$$

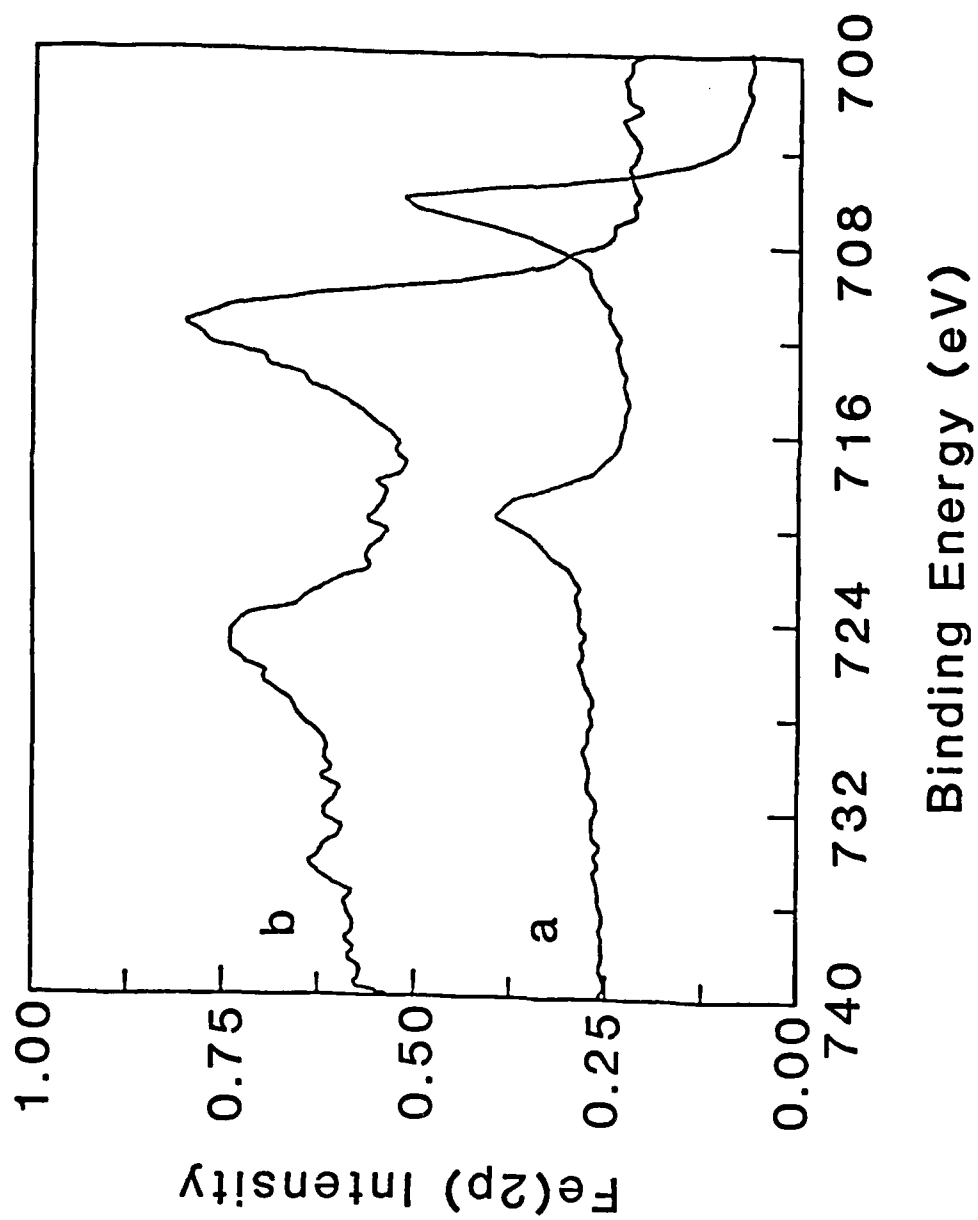


Figure 3.4. Fe(2p) Spectra For A Pure Fe Film (a) And Fe Diffused Through Gold (b) In An Oxidizing Ambient.

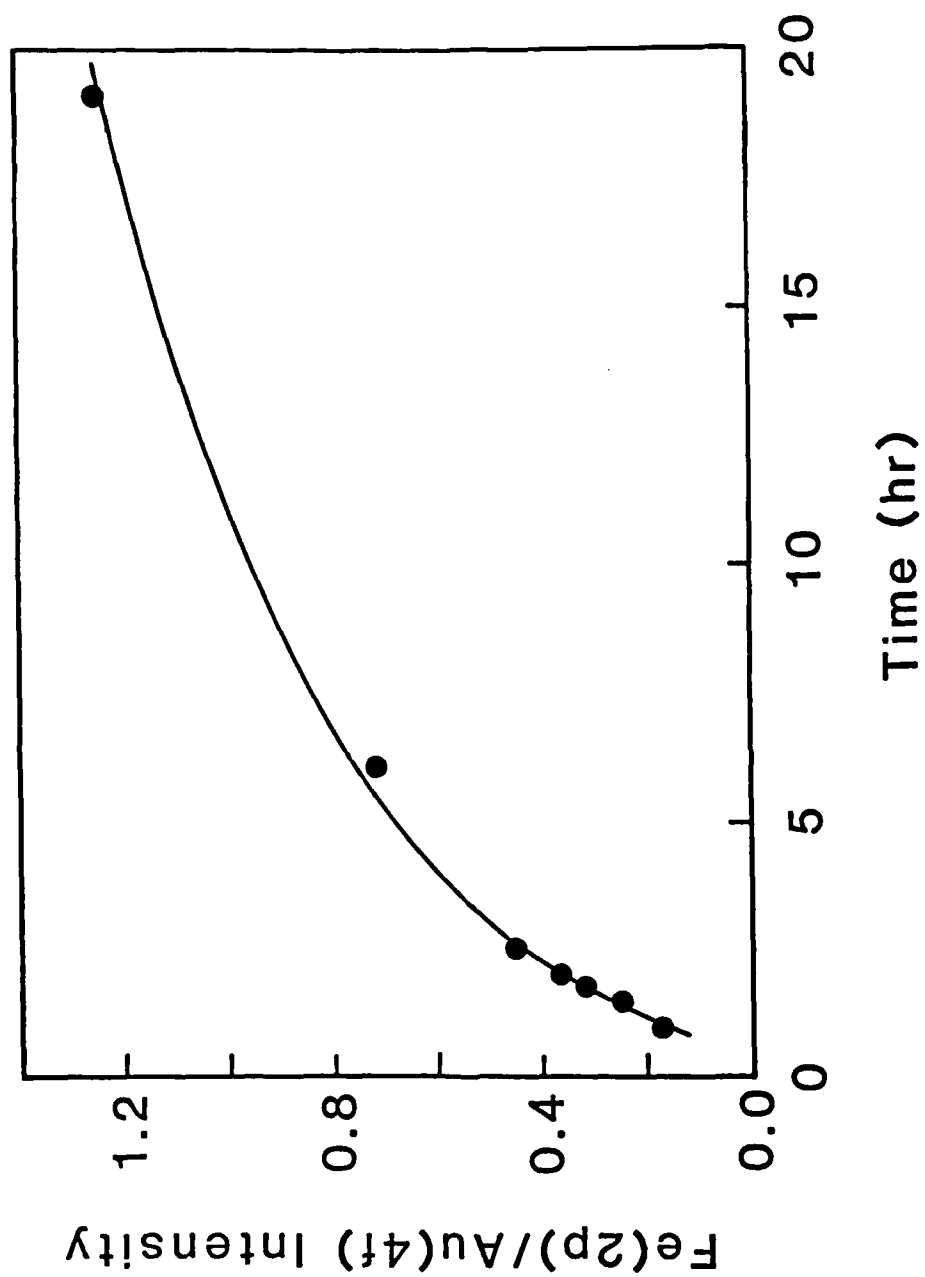


Figure 3.3. Diffusion Profile For Au/Fe Bilayer Film at 229°C.

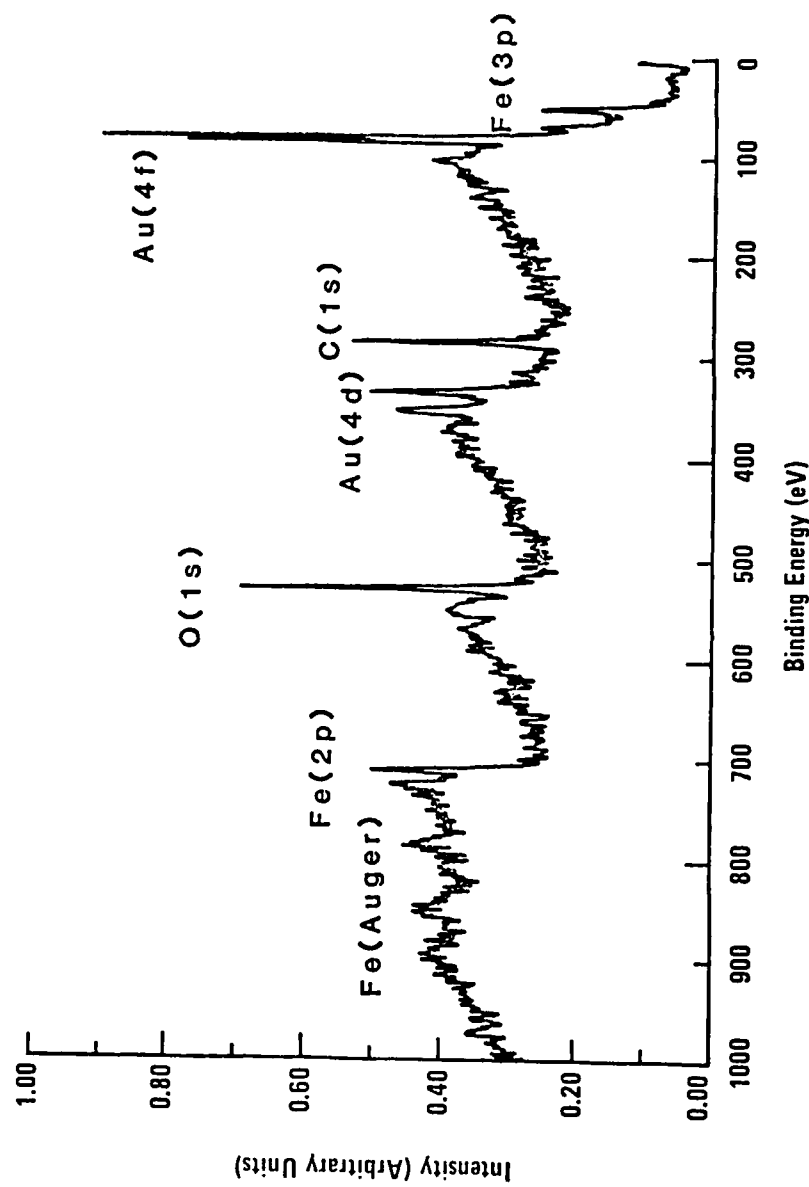


Figure 3.2. Elemental Spectrum Of Au/Fe Bilayer Film After Heat Soak At 229°C For 1.5 Hr.

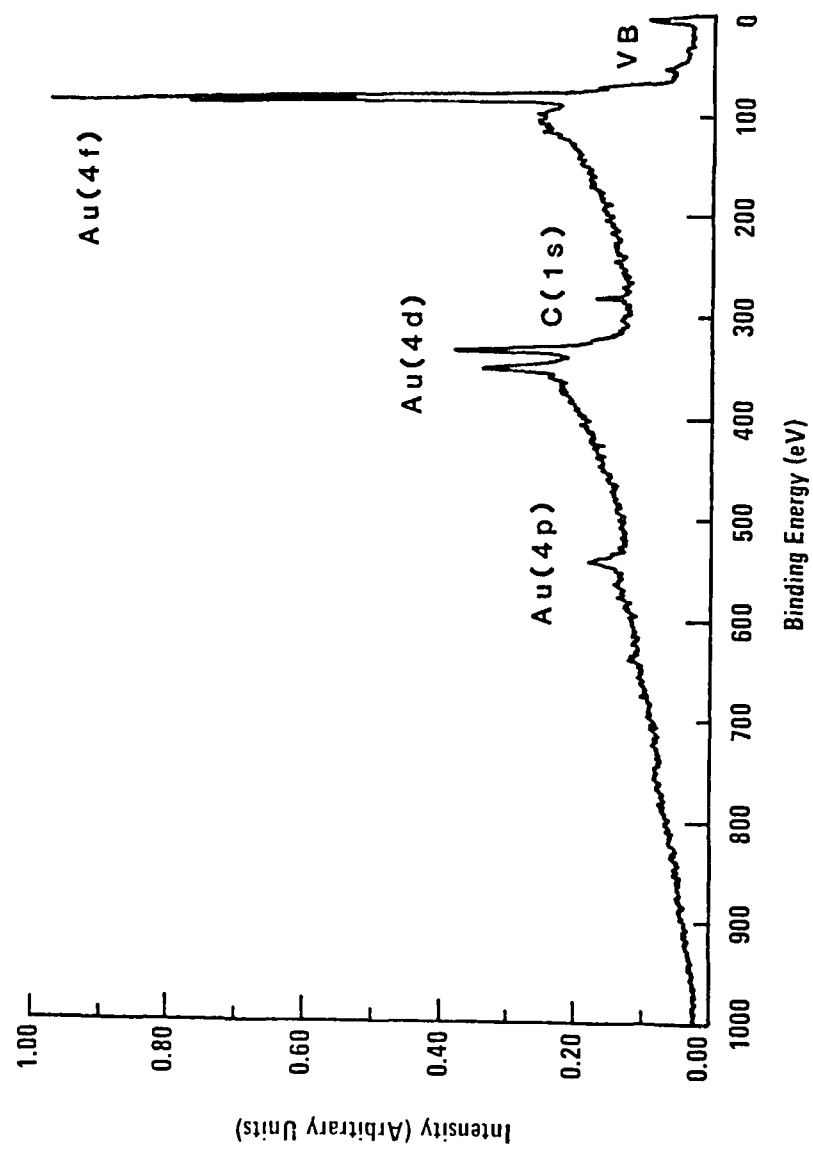


Figure 3.1. Elemental Spectrum Of An Unheated Au/Fe Bilayer Film.

Table 3.2

Diffusion Parameters

<u>Metal</u>	<u>Arrhenius Slope</u>	<u>R*_{corr}</u>	<u>E_a (kcal/mole)</u>	<u>D₀ (cm²/s)</u>
Iron	-10,200	0.997	20	2.7 x 10 ⁻⁵
Nickel	-13,700	0.999	27	3.0 x 10 ⁻³
Cobalt	-13,300	0.998	26	4.8 x 10 ⁻⁴

*Linear correlation coefficient for Arrhenius plot of $\ln k$ vs $1/T$.

This and the other diffusion coefficients calculated in this study are consistent with those determined for similar systems using a variety of experimental techniques (Table 3.3) including resistivity (20,21) radioisotopic tracers (22) and ion scattering spectrometry (7), thus demonstrating the validity of this method.

3.4 CONCLUSIONS

(1) Iron, nickel and cobalt have been shown to diffuse readily through gold at temperatures of about 200°C.

(2) The primary driving force for the diffusion is the oxidation of the transition metal at the surface.

(3) XPS can be employed to determine the kinetic parameters for the diffusion process.

(4) The activation energies and diffusion coefficient pre-exponential factors are consistent with a grain boundary diffusion mechanism.

(5) As temperatures of about 200°C are routinely attained in processing protocols in the microelectronics industry, care must be taken to prevent intermetallic diffusion during device fabrication. Such diffusion could readily influence the reliability of specific devices. The present data suggest that low temperature diffusion can be minimized by processing protocols which avoid oxidizing environments during thermal treatments.

3.5 ACKNOWLEDGMENTS

Appreciation is expressed to Al Gregg, Neutron Devices Department, General Electric Company, for the AES depth profiles.

Table 3.3. Reported Activation energies and pre-exponential factors
for thin film diffusion.

<u>Investigator</u>	<u>Q, kcalmol⁻¹</u>	<u>D₀ cm²s⁻¹</u>	<u>Remark</u>
Rairden et al (20)	25	1.1×10^{-5}	Au/Cr thin films (resistivity)
Schnable and Keen (21)	25	. . .	Au/Cr thin films (resistivity)
Thomas and Haas (23)	27.6	3.5×10^{-6} 3.2×10^{-7}	Au/Cr single crystal thin films (work function)
Gupta and Asai (22)	23	1.8×10^{-2}	self diffusion of Au in grain boundaries (radioactive tracer)
Nelson & Holloway (7)	26	3.8×10^{-3}	Au/Cr thin films (ISS/AES)
Linn and Swartz (24)	25	1.5×10^{-3}	Au/Cr thin films (XPS)

4.0 THE PHYSISORPTION OF WATER ON SURFACES

The physisorption of water onto various substances commonly encountered in integrated circuits has been studied. Data were obtained for iron, nickel, gold, SiO_2 and polyimide using a commercially available quartz crystal thickness monitor. Test gas mixtures containing 100 to 23000 ppmV water were prepared using nitrogen, hydrogen or helium. It was found that adsorption isotherms for most of the materials were similar to BET curves. Exceptions were those obtained for materials such as polyimide, which absorbs as well as adsorbs water. The quartz crystal oscillator technique is a powerful tool for characterizing the physisorption/desorption of water to package component materials. Since the technique can be employed at atmospheric pressure and does not require high vacuum as do other surface techniques, it is possible to study materials under conditions which they may experience during processing and use.

4.1 INTRODUCTION

It is well known that moisture inside a microelectronic package can reside at a number of different locations. At any given time the location of the water is determined by the local temperature differential between competing surfaces and their adsorption/desorption properties as defined by their chemical and physical nature (25). This study was aimed at elucidating the intrinsic moisture uptake properties of materials commonly employed in component parts of microelectronic packages. These include gold, iron, nickel (10), silicon dioxide, silicon nitride, polyimide and others.

Previous work (10) has demonstrated that it was possible to study the physisorption of water onto various substances via a quartz crystal thickness monitor operated at atmospheric pressure. After coating with the substance of interest, the test crystal was exposed to a controlled test gas containing known amounts of moisture. Water adsorption onto the various substrates was monitored by noting the resultant deviation of the frequency of the crystal. Most materials characterized appear to exhibit Brunauer, Emmett, and Teller (BET) (26) type adsorption curves.

4.2 EXPERIMENTAL

4.2.1. Equipment. Quartz crystal oscillator data were obtained using equipment described previously (10). This system consists of a Kronos QM 311 thickness monitor and FTT 350 detection head. The detector head was modified so as to allow unrestricted gas flow to both sides of the crystal and was housed in a stainless steel test chamber measuring 2" wide x 4" long x 1" deep. The analog output of the QM 311 was fed to a Hewlett-Packard 3465S strip chart recorder.

Controlled test gas mixtures containing 200 to 23000 ppmV water were prepared by dilution of water saturated carrier gas. Nitrogen (N_2) (boil off from liquid), dry compressed hydrogen (H_2) or helium (He) served as the carrier gas. The water content of the test gas stream was monitored via a General Eastern National Bureau of Standards (NBS) traceable optical dew-point hygrometer.

4.2.2. Materials. Quartz crystals were obtained in plano-plano configuration from Phelps Electronics. These crystals were supplied with a nominal 1000Å layer of gold over a 1000Å chromium, both thermally evaporated. The base oscillating frequency was 4.72 MHz.

Nickel and iron were obtained with a minimum purity of 99.99% from Research Organics/Research Inorganics. Silicon monoxide was obtained from a commercial coating firm. DuPont Pyralin PI 2550 polyimide was obtained from Honeywell.

4.2.3 Quartz Crystal Preparation. Water adsorption studies on gold were performed both on "as received" crystals and crystals which had been rinsed in isopropanol or trichloroethylene under a blanket of dry nitrogen. Extreme care was exercised in removing all traces of isopropanol since, as was determined during the experiments, the presence of even traces of a polar solvent causes greatly enhanced water uptake. Nickel and iron surfaces were prepared by thermal evaporation of the metal onto the existing gold/chrome surface of crystals which had been previously characterized for moisture uptake properties. Thicknesses ranged from 800Å to 1500Å. Silicon dioxide surfaces were prepared by thermal evaporation of silicon monoxide in a Drumheller (27) style source. Polyimide surfaces were prepared by spin coating the crystals and curing the material according to the procedures given by the manufacturer. All surfaces were analyzed via X-ray photoelectron spectroscopy for purity and composition. Nickel and iron were found to be present as a partially hydrated oxide. Evaporation of silicon monoxide yielded a surface which analyzed as silicon dioxide.

4.2.4 Water Adsorption Testing. Preliminary data were obtained by switching the moisture generation system to "drydown", waiting for the system to reach dry conditions as determined by the dewpoint hygrometer, zeroing the thickness monitor, and then stepping to a preselected moisture value of from 200 to approximately 24,000 parts per million by volume (ppmV). After equilibration (15 min.) and subsequent data recording, the system was switched back to dry conditions. It was found that more rapid equilibration occurred and equivalent data could be obtained if the system were first brought to dry conditions and then stepped sequentially from low to high moisture values. At the conclusion of the data gathering, the system was stepped dry. Drift in the instrumentation was found to be negligible over the time span of an experiment (3 hours). The latter procedure was used in the majority of the work reported herein. Crystals were also stepped from wet to dry in order to demonstrate that the same equilibrium points were obtained. Generally, each crystal was allowed to sit in "drydown" overnight before testing in order to ensure that equilibration with the dry carrier gas was achieved.

4.3 RESULTS AND DISCUSSION

4.3.1. Water Adsorption on Gold. Figure 4.1 presents data obtained for a typical gold coated crystal using nitrogen, hydrogen, and helium carrier gases containing up to approximately 23,000 ppmV water. The data have been corrected to account for only one side of the crystal. As can be seen, the

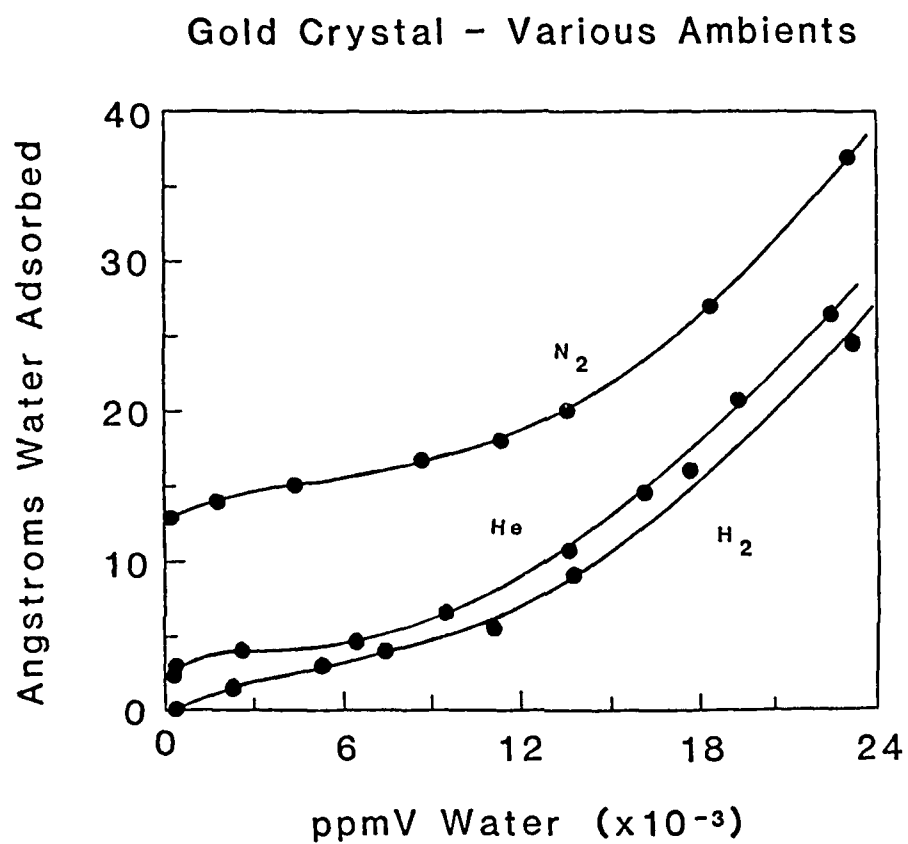


Figure 4.1. Water adsorption on Gold.

shapes of the adsorption isotherms are quite similar for the three carrier gases and appear to be characteristically BET in nature. The onset of multilayer formation appears to occur at approximately 6000 ppmV. It would be expected that multilayer formation would start at the completion of one monolayer of water -- about 4.5 \AA in thickness. Examination of the isotherms reveals that the inflection point at 5000-6000 ppmV water occurs at a 4 to 5 \AA increase in thickness referenced to the zero point under dry conditions. The implication from this data is that a monolayer is formed at approximately 5000 ppmV water. It is possible that microcapillary condensation also occurred, and, since this technique measures a change in mass, this water would also be detected. This seems unlikely since examination of the surface via scanning electron microscopy did not confirm the presence of significant numbers of capillaries. Therefore, fractional monolayers of water are probably present at ambient water concentrations less than 5000 ppmV. It should be noted that heating the crystal at 100°C for several hours in H_2 or N_2 had no effect on the shape or position of the isotherms.

The data have not been corrected for the difference in zero observed when changing from one carrier gas to another. This phenomenon is believed to arise from a difference in packing and therefore condensed phase density of the carrier gas and not in water displacement or accumulation. The same relative change was observed no matter which order was used. With H_2 as zero reference, He was observed to have an increase in mass of 4.5 \AA , while N_2 was $22\text{--}24 \text{ \AA}$. The hydrogen carrier was found to have slightly more trace water contamination than the other two carriers. Repetitive experiments using only dry carriers failed to demonstrate that the differences arose from water adsorption/desorption.

Figure 4.2 shows a comparison between two gold crystals using a H_2 carrier. Similar curves were obtained with N_2 and He. As can be seen, there is a significant difference in moisture uptake between the two crystals. Scanning electron micrographs of the two crystals revealed that crystal 2, with the larger uptake, had an obvious and significantly rougher surface than crystal 1. Therefore, it is believed that the difference observed between these two crystals arises from a difference in surface areas. The crystal with the larger surface area exhibited greater water adsorption. While results from crystal to crystal varied, it was found that adsorption for a given crystal could be well characterized and was quite reproducible.

Figure 4.3 is a plot of water adsorption on iron (iron oxide) using H_2 and N_2 . The plots have been corrected for a zero offset between the two carrier gases of approximately 24\AA . As can be seen, there is a significant enhancement in water adsorption especially in the area of less than 3000 ppmV relative to the gold. This is undoubtedly due to the presence of the oxide. It was found during the course of this study, that oxide on a surface always lead to enhanced water adsorption. This confirms earlier observations (10). The shape of these curves is the same as that found in classical multilayer systems (28). The knee of the curve at approximately 2000 ppmV is traditionally taken to be the completion of one monolayer (28). In the present case, this corresponds to approximately $12\text{-}15\text{\AA}$ of equivalent water. Since the instrumentation reading corresponds to mass, and not true thickness, this suggests that the oxide structure has significantly greater surface area than the gold.

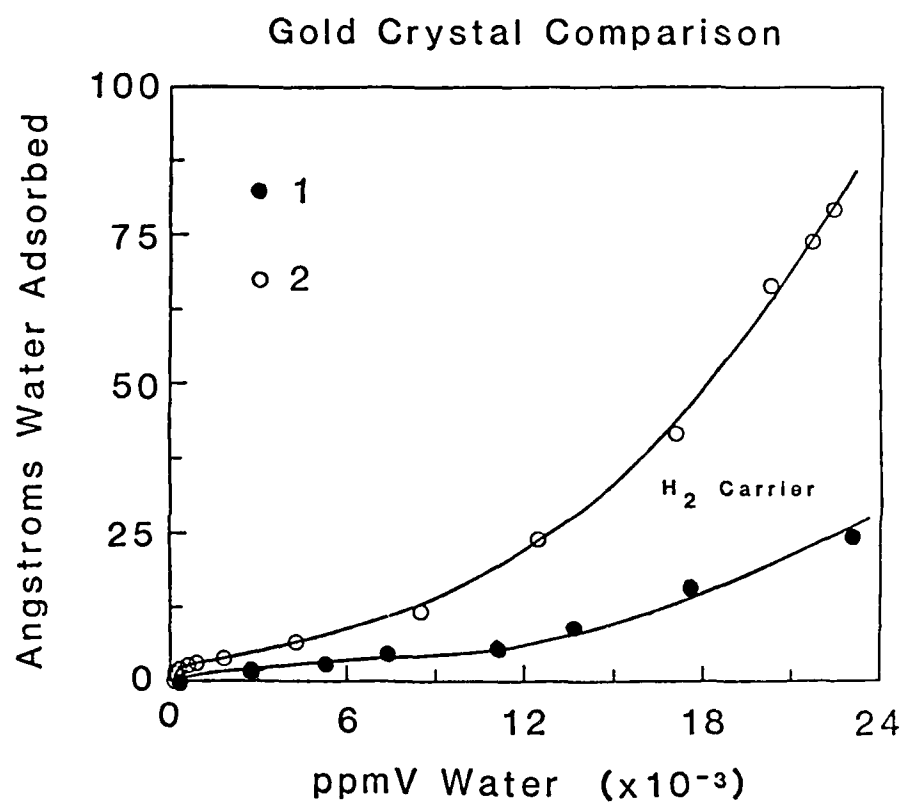


Figure 4.2. Gold Crystal Comparison.

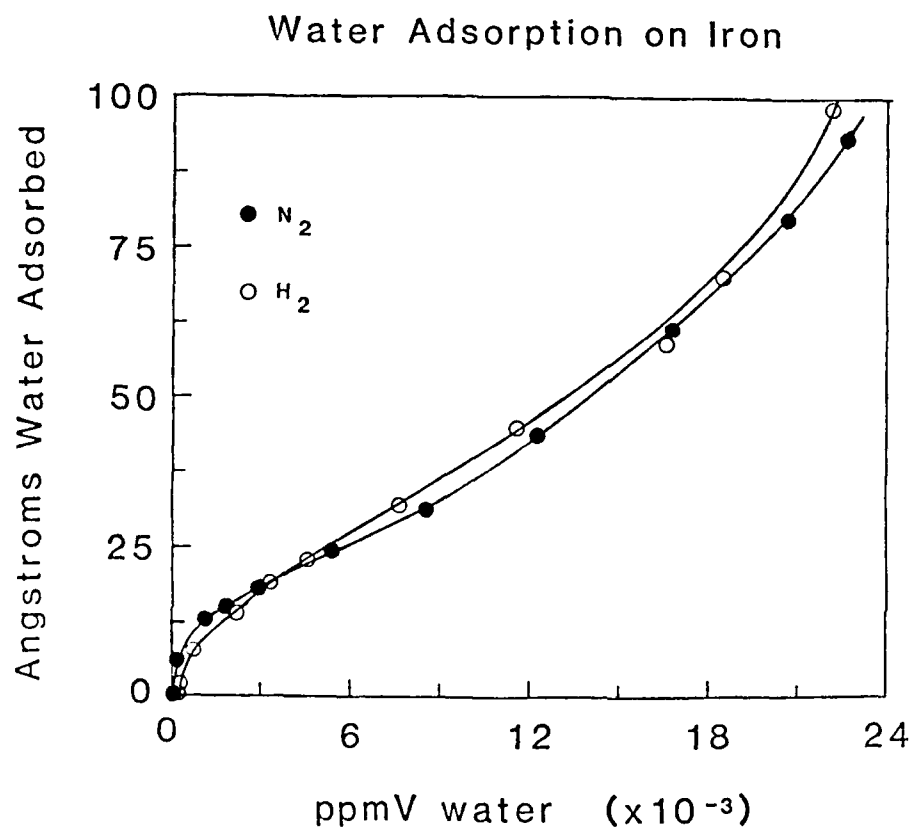


Figure 4.3. Adsorption Isotherms For Iron.

An enlargement of the region of these curves from 0 to 6000 ppmV is shown in Figure 4.4. The displacement of the isotherm obtained in H_2 towards higher water content was reproducible on iron. A similar effect was found in the case of gold or nickel. For iron, it appears that H_2 can cause a suppression of water adsorption at low moisture values. At values less than 3000 ppmV, the partial pressure of water does not seem to be sufficient to cause a full displacement of hydrogen.

Figure 4.5 shows the difference in water adsorption for two different iron crystals. The crystal termed "light oxide" was prepared by exposing a freshly evaporated iron film to air at room temperature, and is the same as that presented in Figure 4.4. The "heavy oxide" crystal was prepared by exposing a freshly deposited iron film to air for 10 minutes while the crystal was at approximately $50^\circ C$. The latter treatment resulted in a visible layer of oxide, which analyzed as an iron oxy-hydroxide by XPS. This is an extreme example of a trend noted repeatedly -- the more oxide present, the more water there is adsorbed, and the longer the time that is required for the surface to release the water and reach equilibrium with a dry carrier gas.

Figure 4.6 shows the results obtained for a nickel (oxide) surface. Again the nitrogen zero has been adjusted by 23° . Both curves are classical multilayer formation curves. The similarity to the iron curves can be explained on the basis of the presence of an oxide surface. It should be noted that this crystal, like the iron crystal in Figure 4.3 was exposed only to air at room temperature. XPS analysis of this surface indicated that nickel is present as a mixture of oxide and water as was the case for

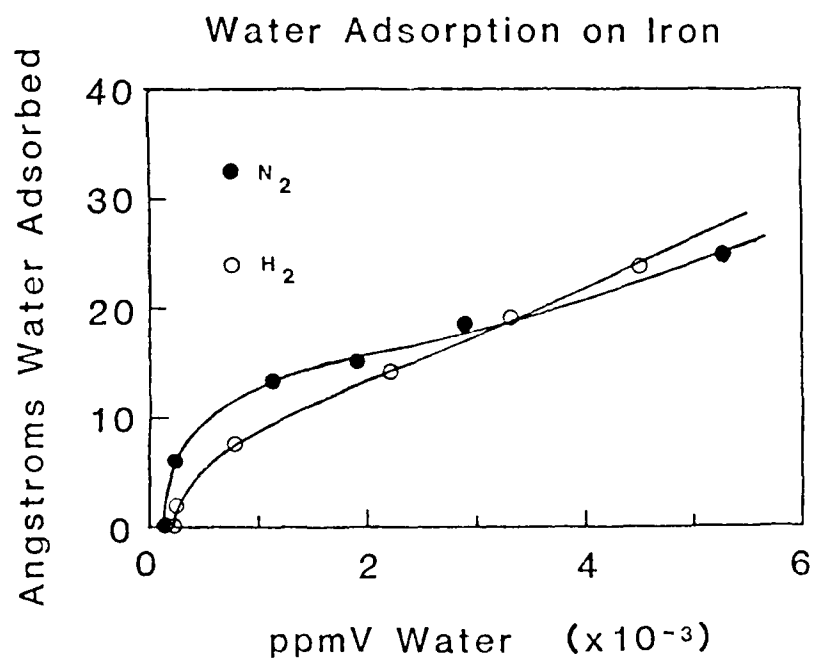


Figure 4.4. Low ppmV Water Adsorption On Iron.

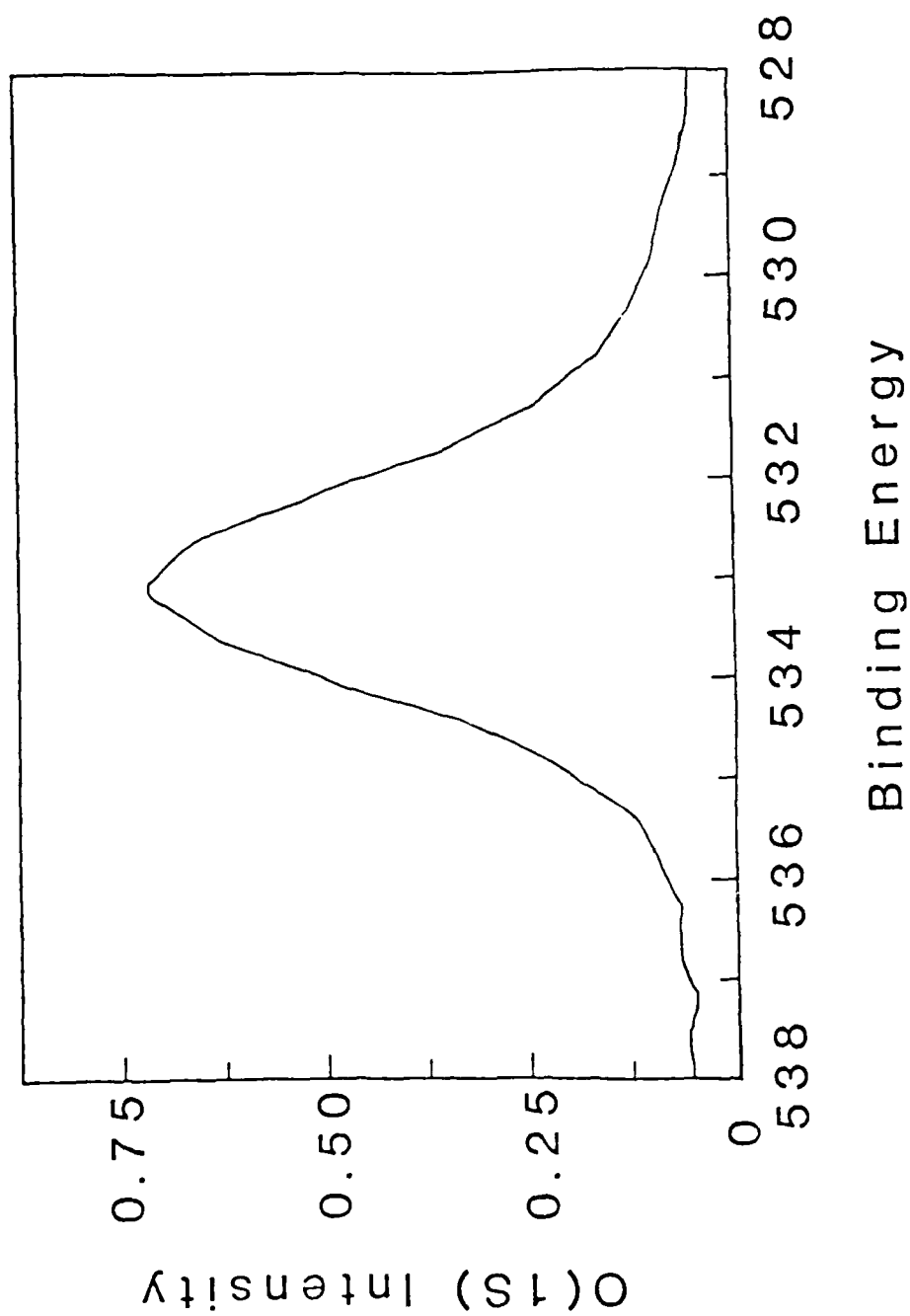


Figure 5.5. O(1s) Spectrum of H₂O Condensed On Gold At 77 K.

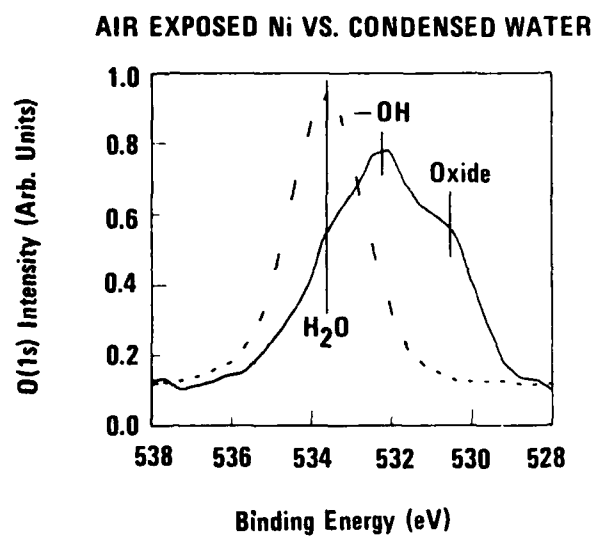


Figure 5.4. O(1s) Spectrum For NiO Exposed To Air (Solid Line) And Condensed Water At -100°C (dashed line).

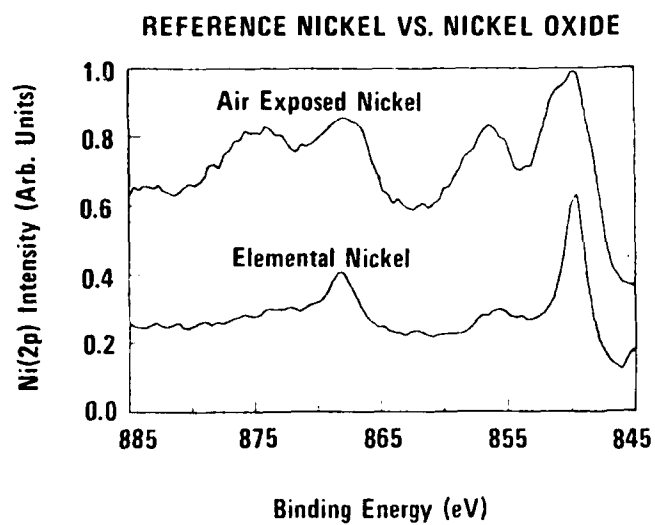


Figure 5.3. Reference Nickel (freshly deposited film) vs. Air Exposed Nickel Film.

laboratory air, the film is oxidized (Figure 5.3). Comparison of Figures 2 and 5.3 clearly demonstrates that the nickel in both cases is present as nickel oxide. Further tests of the nickel were performed on the nickel film, since the O(1s) spectra associated with it was simpler than the one obtained from the lid.

The high resolution O(1s) XPS spectrum for the nickel oxide film in Figure 5.3 after exposure to ambient laboratory air is shown in Figure 5.4. Note that a multi-faceted spectrum results which contains contributions due to adsorbed water, -OH and oxide. Qualitatively these data are identical to those discussed by Roberts (31). Figure 5.5 is a spectrum for water condensed on a nickel film at -120°C and is overlaid as the dashed line on Figure 5.4.

If adsorbed water is to pose a significant reliability problem, it must desorb at temperatures expected for the device. Investigations of the thermal desorption of water from active (i.e. oxidized) transition metal films were conducted by heating the air exposed films in the sample chamber of the XPS spectrometer. Desorption would be reflected in changes in the O(1s) spectra as a function of temperature.

Representative spectra for NiO at 23°C and at 200°C are shown in Figures 5.6 and 5.7. These spectra have been subjected to a Gaussian-Lorentzian line fit in order to deconvolute the spectra and extract representative area contributions for water, hydroxide and oxygen. Note that the water (533eV) and hydroxide (531.5 eV) are drastically reduced at

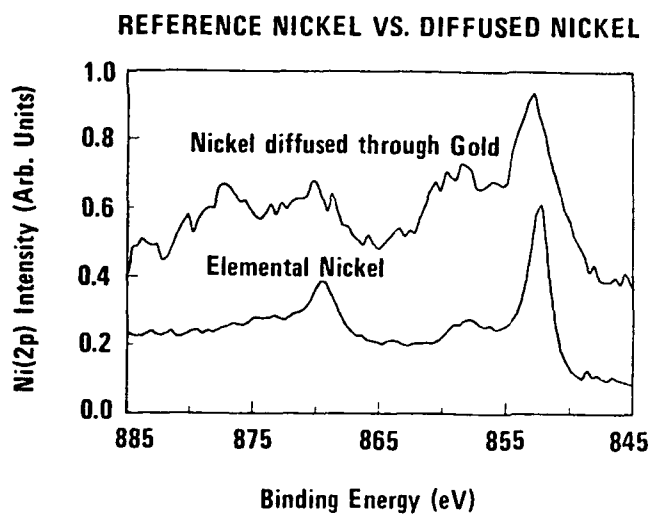


Figure 5.2. Reference Nickel (freshly deposited film) vs. Nickel Diffused Through Gold (Au/Kovar Lid).

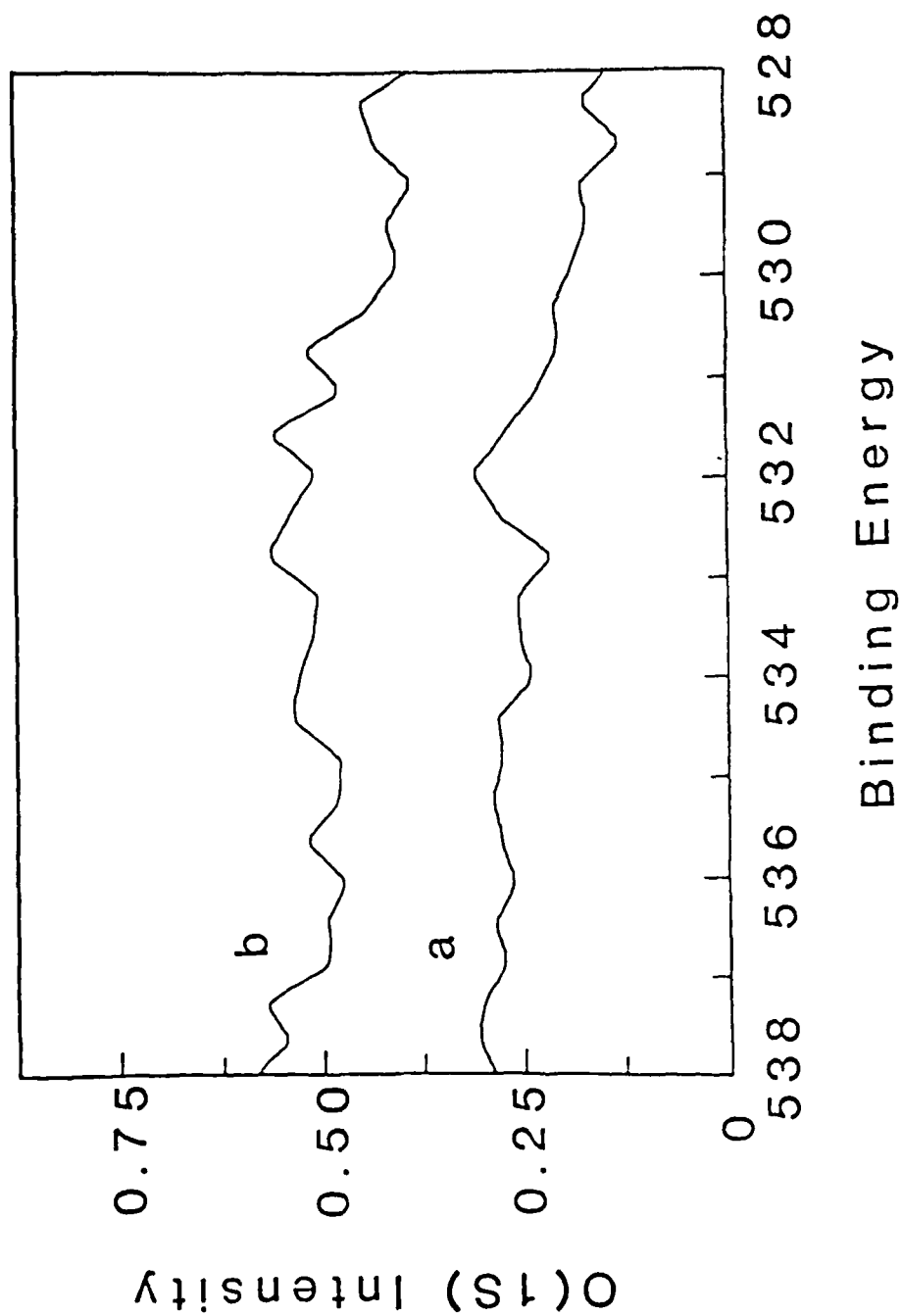


Figure 5.1. O(1s) REGION OF A GOLD SURFACE (a) BEFORE EXPOSURE TO H₂O AND (b) AFTER EXPOSURE TO H₂O.

5.3 RESULTS AND DISCUSSIONS

To monitor the adsorption/desorption of water to and from a metallic surface, one typically follows the O(1s) XPS spectrum as a function of exposure to water (25). Figure 5.1 contains the O(1s) spectra for a freshly deposited gold film before and after exposure to approximately 1×10^{-2} torr of ambient laboratory air for several minutes. Neither spectrum contains any signal above the background noise. This is consistent with the fact that a fresh gold film will not chemisorb water under these experimental conditions. Any physisorption of water would not be observed due to the vacuum environment existing in the sample chamber the XPS spectrometer. Physisorption of water is discussed in section 3 of this report.

Roberts (31) has clearly shown that when a chemically active transition metal surface is exposed to water, a multi-faceted O(1s) XPS spectrum results. Oxygen features due to chemisorbed water and chemically produced hydroxyl (-OH) and oxide species were identified on an active surface after exposure to moisture. In the present studies, freshly deposited nickel and iron films have been exposed to moist laboratory ambient atmospheres. Examples of the results of these exposures are discussed below.

Figure 5.2 shows the Ni(2p) spectra for a metallic nickel film and for the nickel which has diffused through the gold layer of a Au/Kovar lid. The spectra clearly indicate that after diffusion, the nickel is present in an oxidized state. If a freshly deposited nickel film is exposed to ambient

5.0 THE CHEMISORPTION OF WATER ON SURFACES

5.1 INTRODUCTION

As a complement to the study of the physisorption of water on various package materials the chemisorption of water to similar materials was investigated via XPS. Physisorbed water, because of its weak associative bond with surfaces, is released under the experimental conditions prevailing during XPS analysis. Therefore the type of water detected by XPS is chemisorbed onto the substrates or else is waters of hydration.

5.2 EXPERIMENTAL

The X-ray photoelectron spectrometer employed was a GCA/McPherson ESCA 36 equipped with an aluminum X-ray tube ($E_x = 1486.6$ eV). This excitation energy allows sampling depths of 0-20 Å. Pressure in the sample chamber was maintained at or below 5×10^{-7} torr thus allowing the routine study of only chemisorption phenomena.

Single and multiple layer thin films were prepared and treated according to procedures detailed in Section 3. Heating and diffusion were carried out using procedures identical to those reported previously in section 3. Special films such as pure gold and nickel were prepared in the XPS sample chamber by evaporation and analyzed prior to test gas exposure in order to prevent contamination of the film by the laboratory ambient.

4.4 SUMMARY AND CONCLUSION

It has been demonstrated that a quartz crystal thickness monitor may be adapted to measure the adsorption/desorption properties of various materials. It was found that materials which adsorb moisture through interaction with the surface atomic layer only (i.e., gold), exhibit a characteristic BET style adsorption isotherm. Materials which interact through the uppermost atomic layers, such as oxides, exhibit enhanced BET type isotherms. It has been demonstrated that the amount of moisture adsorbed in this case is proportional to the amount of oxide present. Materials which absorb water as well as adsorb water (polyimide) are capable of retaining large amounts of water even under relatively dry conditions. In all cases studied, the adsorption process was found to be freely reversible in as much as desorption readily occurred.

Water Adsorption on Polyimide

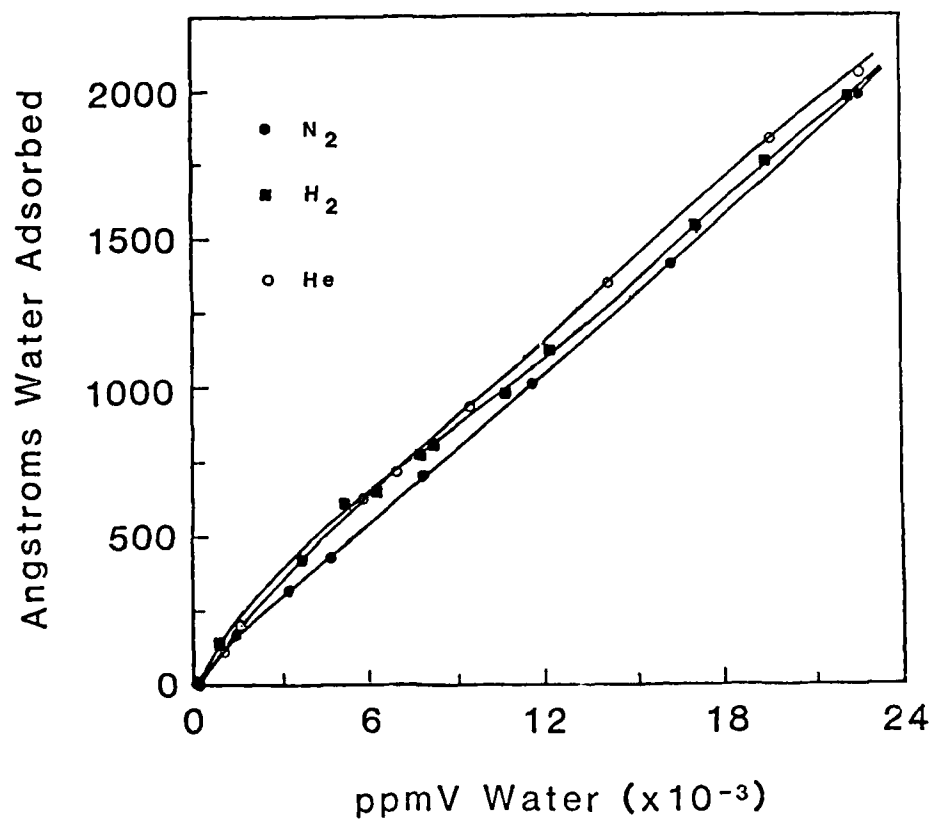


Figure 4.8. Adsorption Isotherms For Polyimide In Various Water/Gas Ambients.

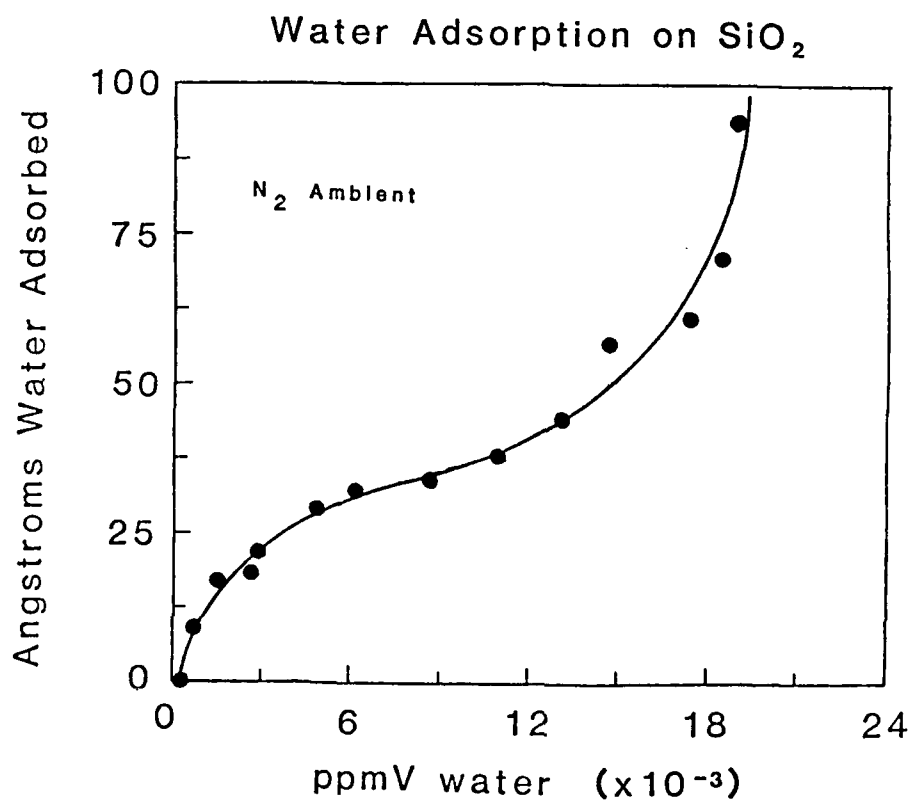


Figure 4.7. Adsorption Isotherm For Thermal SiO_2 .

iron. It has been shown previously (10) that this water is probably water of hydration and is therefore not physically adsorbed. Its presence, however, undoubtedly influences the physisorptive properties of both the nickel and iron surfaces. Oxides and water both are capable of forming associative bonds with water. Both the nickel and iron isotherms may be interpreted in terms of the BET equation or a modification (29).

The results obtained for SiO_2 are shown in Figure 4.7. The large amount of equivalent angstroms of water adsorbed illustrates the well known hygroscopicity of SiO_2 and glass in general. Undoubtedly the water significantly penetrated the upper layers of SiO_2 and formed an hydrated SiO_2 structure (30). Hydrated gel layers are known to exist and vary in depth from 50\AA to 1000\AA depending on the glass. As can be seen from the figure, relatively high levels of moisture (10000ppmV) are required to initiate multilayer formation.

Figure 4.8 presents data obtained for polyimide. As can be seen, this material exhibits an enormous tendency to absorb and adsorb moisture. There is probably a multilayer structure formed on the surface but the amount of water required is insignificant compared to the amount of water absorbed by the polymer. Therefore the characteristically shaped BET curve is not readily seen overlaid onto the bulk absorption curve. The time required for equilibration this material was approximately the same as for the other materials examined. This is probably due to the thickness of the material - a few thousand angstroms.

Water Adsorption on Nickel

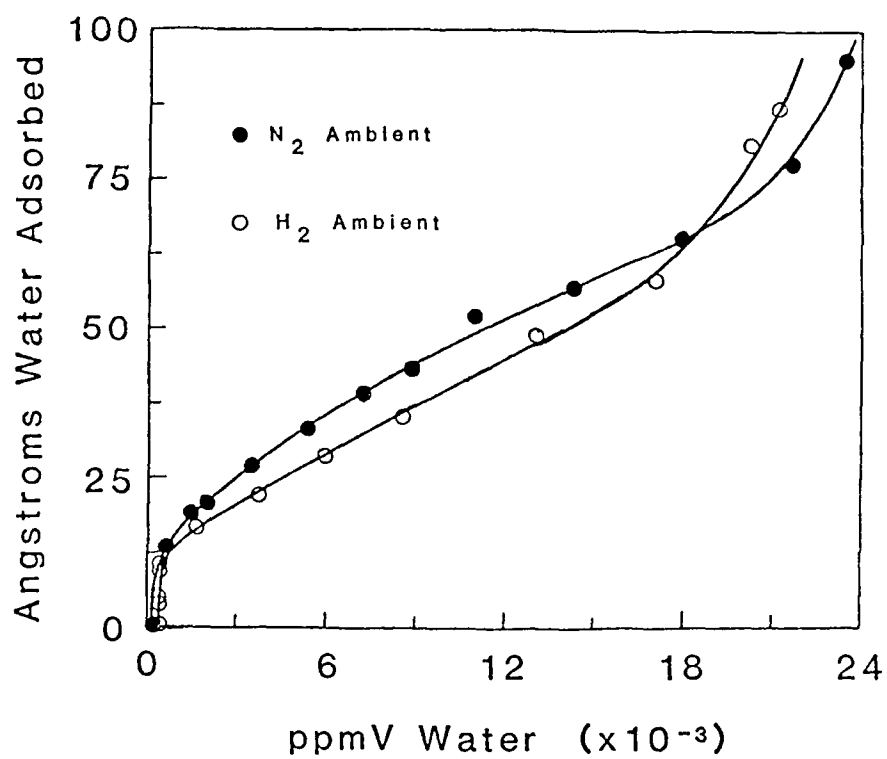


Figure 4.6. Adsorption Isotherms For Nickel.

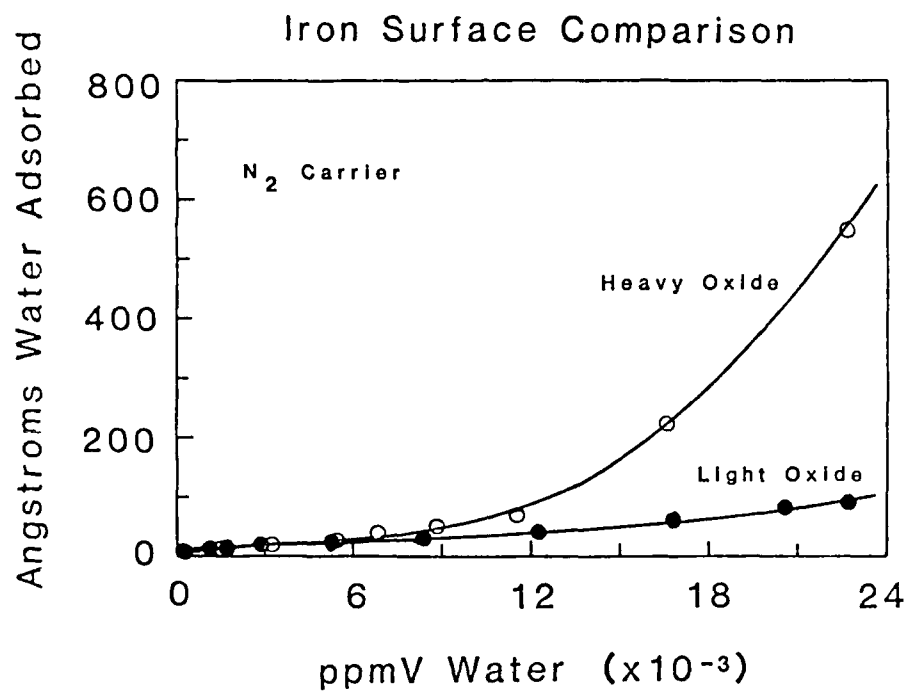


Figure 4.5. Influence Of Amount Of Surface Oxide On Water Adsorption For Iron.

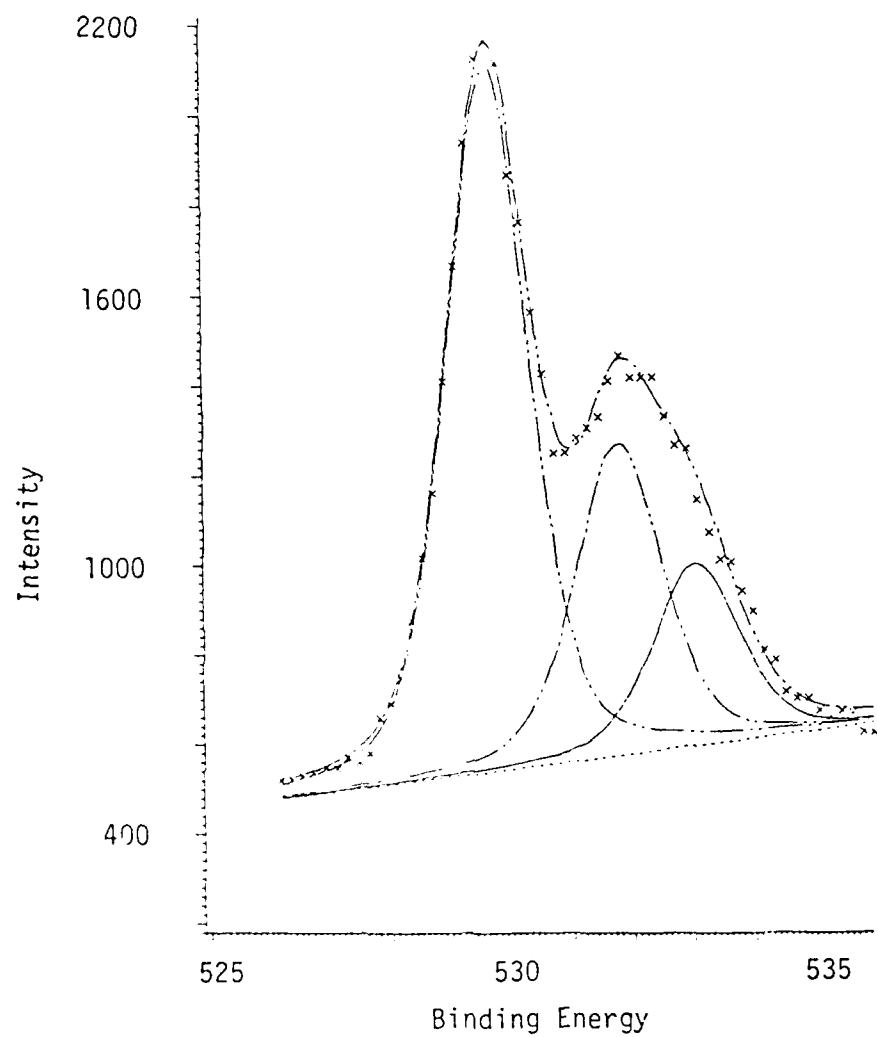


Figure 5.6. O(1S) SPECTRUM OF NiO AT 23°C.

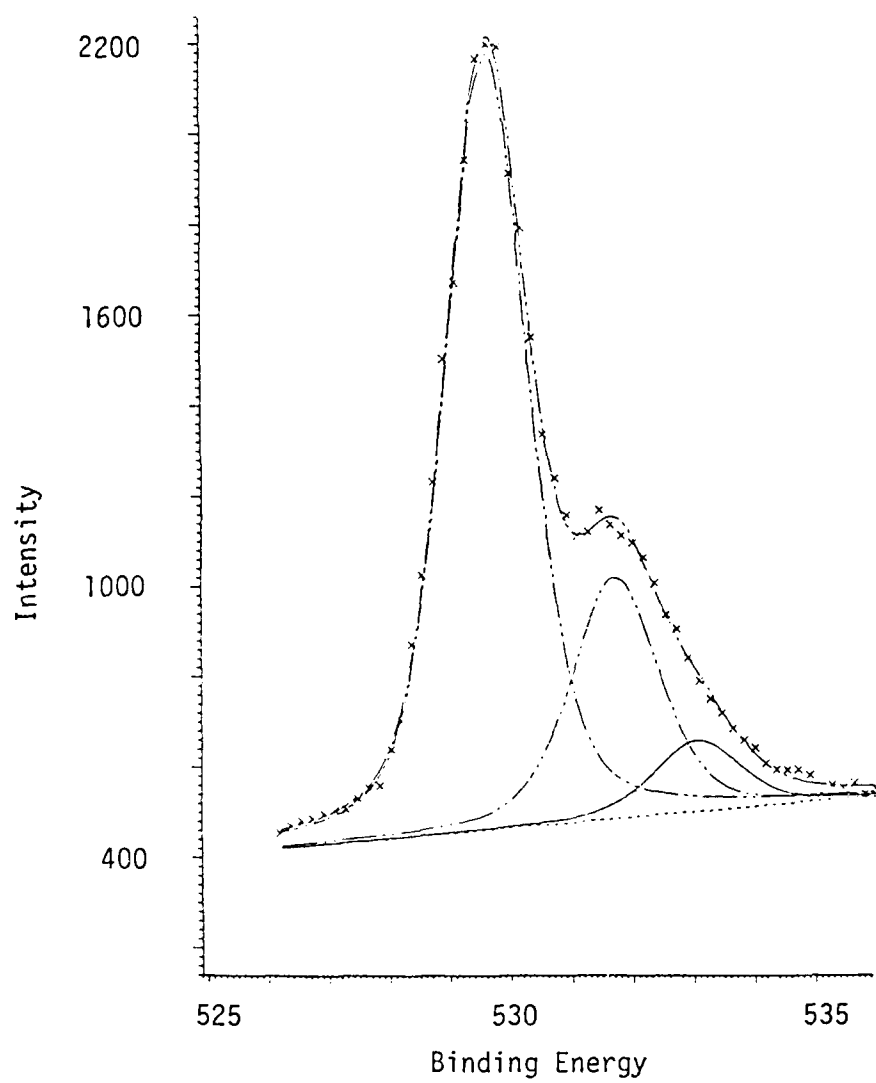


Figure 5.7. O(1S) SPECTRUM OF NiO AT 200°C.

200°C versus 23°C while oxide remains essentially constant in intensity. This suggests that water is desorbing from the oxide and that some hydroxide may be converting to water.

The desorption profile for water and hydroxide from this experiment is plotted in figure 5.8. Note that there is some water desorption even at room temperature under vacuum conditions but that it is not significant until approximately 100-120°C. In this case the area of water plus hydroxide is plotted since water and hydroxide appear to be interrelated.

Similar results have been obtained for iron and cobalt oxide films. The details are to be published soon.

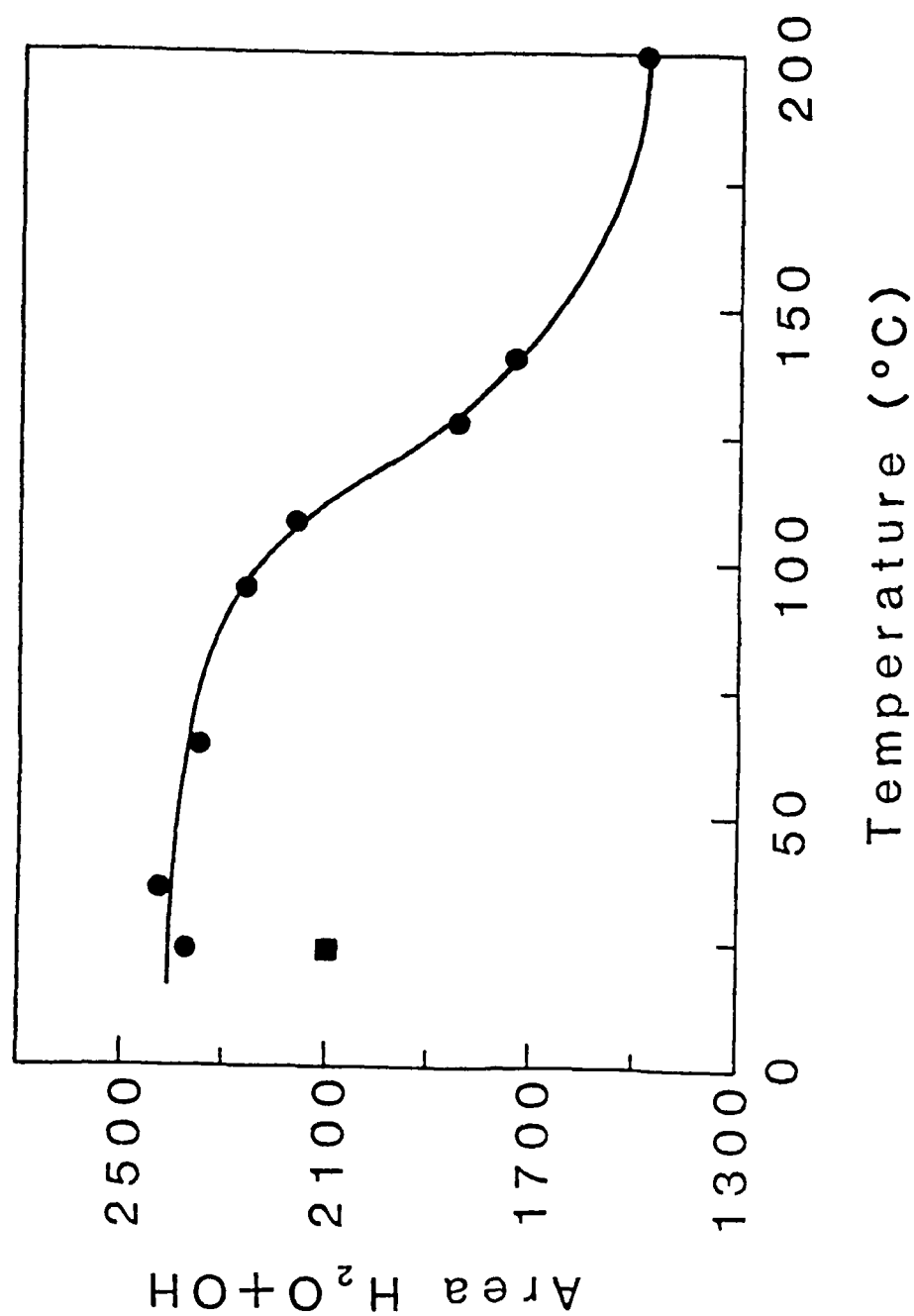


Figure 5.8. Temperature Profile of NiO.

6.0 MOISTURE FAILURE THRESHOLDS

The objective of this series of experiments was to determine the lower threshold for moisture related failures in various packages. The applicable theory is that there should be a concentration of water below which corrosion related failure should not occur. This threshold level has been taken to be 5000 ppmV since this concentration represents a dew/frost point below zero degrees celsius. Therefore water could not exist in the liquid state and hence would not be available to act as a participant or support for aqueous corrosion systems. Recently however, corrosion failures have been reported in ambients of 2000 ppmV or below. Undoubtedly, there are many kinds of water in microelectronic packages and head gas analysis may not accurately reflect moisture content.

6.1 EXPERIMENTAL

6.1.1 Test Fixture. The test fixture used in this series of experiments was a modified Cajon VCR fitting. The gland was machined so as to allow mounting of a delidded package to the compression side with the leads passing through the fitting to external connections. Each circuit was delidded by cutting dry on a metal lathe, visually examined for contamination resulting from the opening operation, and then mounted via low temperature indium solder to the modified gland. The gland was then assembled into a blank VCR cap and a known amount of moisture was sealed in. All parts of the microtest chamber were gold plated to a depth of 50 microinches including the sealing gaskets (both aluminum and stainless were used). This was done since it had been determined (see section 4) that gold

physisorbed the least amount of water of any material tested. A cross-sectional view of the test chamber is shown in Figure 6.1. These chambers were found to be hermetic.

Known amounts of moisture were sealed into the microtest chamber via introduction with a syringe needle through the outgassing port of the fitting. The output of the moisture standard generator (Figure 2.5) was allowed to flush the chamber for 5 minutes prior to sealing. The experimental plan called for starting with gross moisture (circa 20000 ppmV) and then as devices failed, reducing the moisture content until a threshold was established.

In order to maximize the residence time of moisture on the chip surface and therefore enhance the probability of corrosive failure, the test fixtures were temperature cycled. This was accomplished via an "Air-Jet" (registered T.M.) This is a device capable of producing a moving air stream with temperatures ranging from -60°C to $+200^{\circ}\text{C}$. The output of this machine was coupled to a copper multiport tube for multicircuit testing. Most circuits used were mounted on a header equipped with a beryllium oxide die attach reflow heat conductor. This heating pad was pushed into a piece of Teflon tubing which in turn was pressed into a test port. Tests with calibrated diodes showed that a chip temperature of -24°C may be reached in five minutes or less with the Air Jet operated -30°C , and $+35-37^{\circ}\text{C}$ in five minutes with the Air Jet at $+40^{\circ}\text{C}$. The entire assemblage of test fixtures and circuits was housed in a piece of 6" PVC pipe and continuously blanketed with dry nitrogen to prevent moisture/frost condensation on test leads resulting in possible current leakage. The assembly is shown in Figure 6.2.

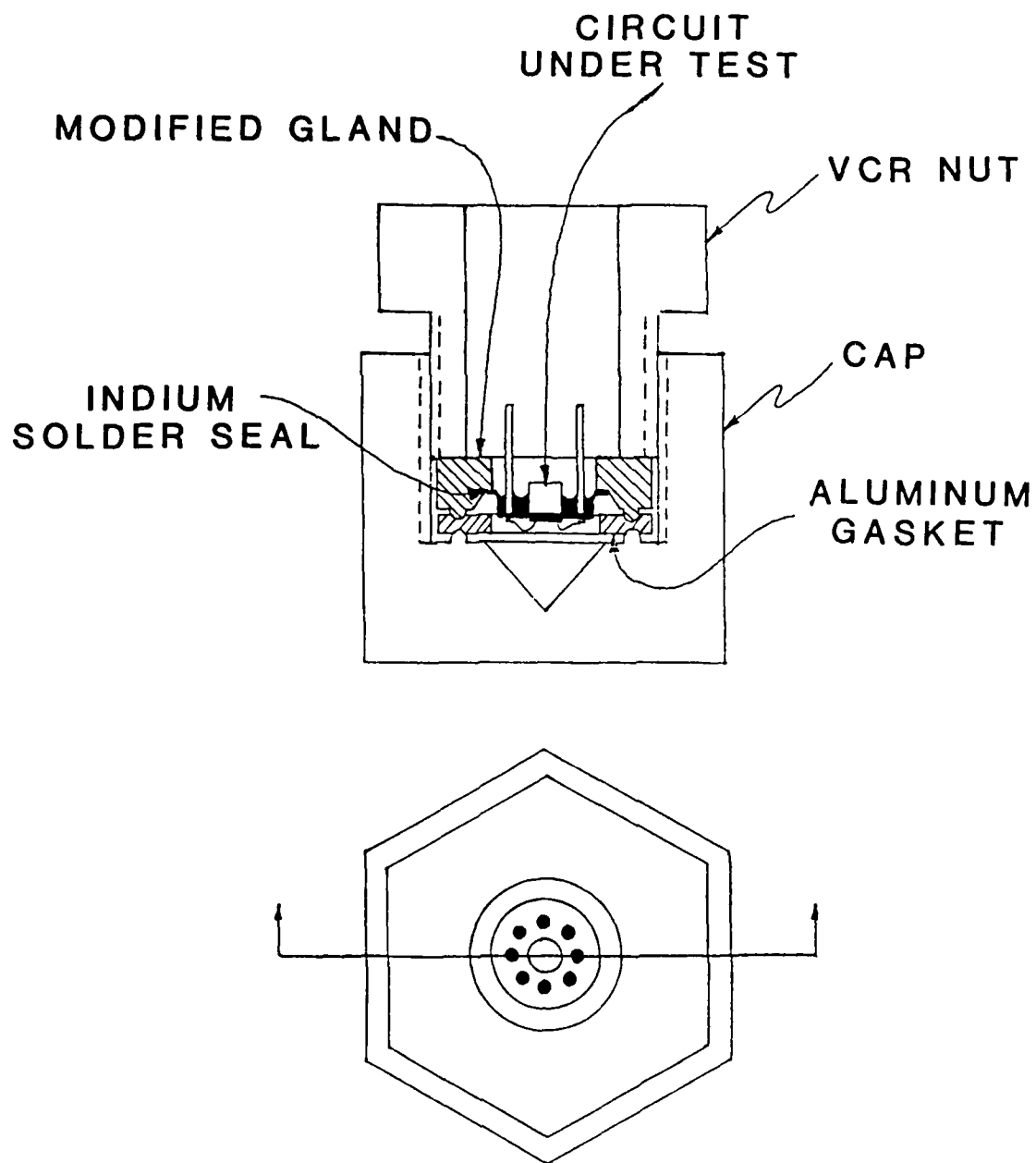


Figure 6.1. Test Fixture For Moisture Failure Threshold Testing.

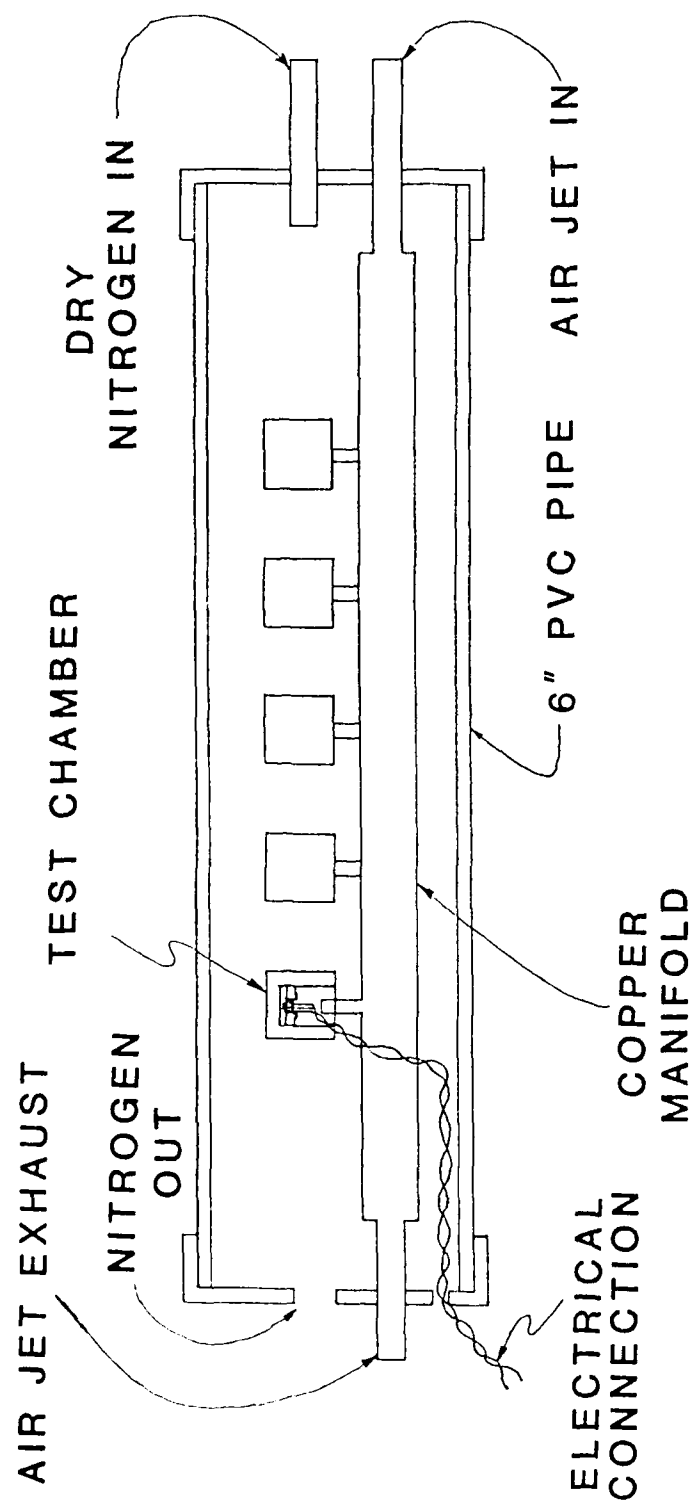


Figure 6.2. Test Fixture Housing For Thermal Cycling.

.1.2 Device Failure Criteria and Experimental Protocol. The 741

operational amplifier as manufactured by supplier A was chosen as a circuit representative of linear bipolar technology. Monitoring of the input offset voltage of the amplifier was selected as a convenient means to track device failure. The test circuit is the gain of 100 arrangement shown in Figure .3.

Stressing and testing of the circuit was as follows. The V^+ and V^- power inputs are removed from the circuit and then +15V is applied to the noninverting input via the 500 Ω resistor shown. The purpose of this resistor is to limit the current through switch S1 to a safe value in the event of a failure. Since power was removed from the circuit and only single bias applied, the temperature of the die did not rise above ambient. The circuit was then temperature stressed between +40°C and -5°C (20000 ppmV/year) with 75% of the time spent at the lower temperature. A high/low cycle is completed in 30 minutes; 20 minutes is spent at low temperature and 10 minutes at high. The temperature was monitored via a calibrated diode and the effective time at low temperature (under dew point) is approximately 5 minutes and at high temperature approximately 5 minutes. After 10 cycles the bias was removed and the circuit was allowed to stabilize at room temperature. This was accomplished by switching the air jet to 23°C and holding for 10 minutes prior to and during testing. The circuits (up to 5) were tested sequentially. Power was applied to a circuit and the die allowed to equilibrate for 10 minutes prior to taking data. The input offset voltage was measured 5 times with a 2 second wait between measurements. The average of the measurements was then computed and the data stored as a string matrix consisting of the time of the test, the 5

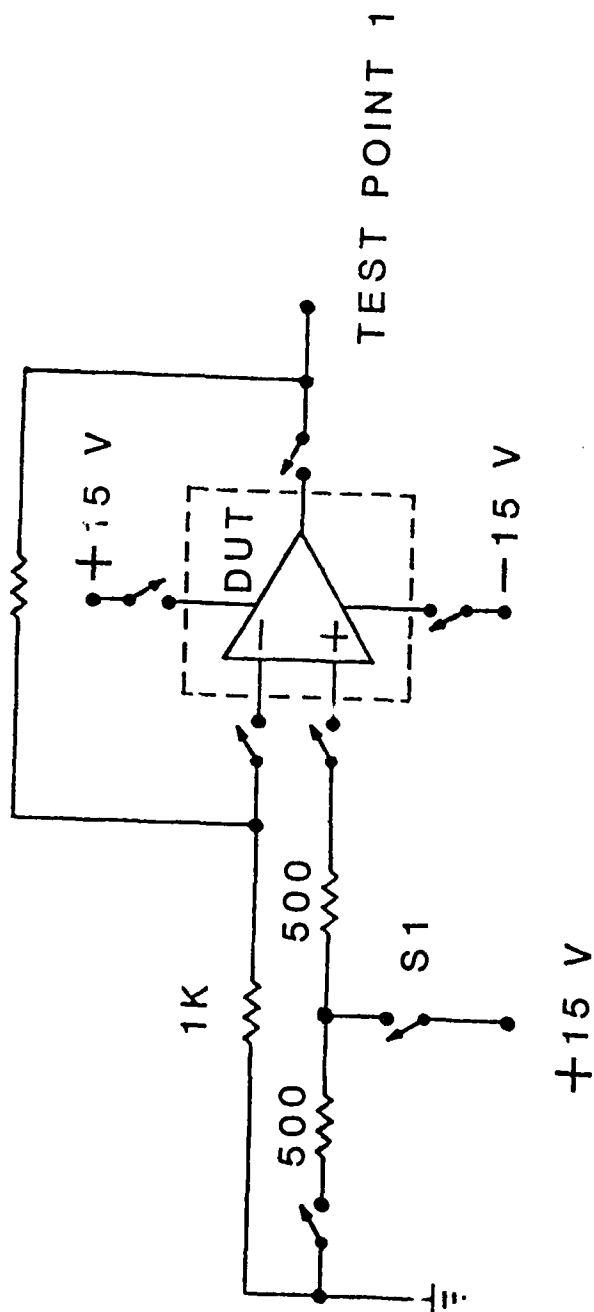


Figure 6.3. Test Circuit For Monitoring The Input Offset Voltage Of The Device Under Test.

measurements, and the average. At the conclusion of testing, the temperature cycling is reinitiated.

The entire testing and stressing sequence was placed under HP85 computer control. For isolation purposes a break before make switching system was used. Addressable relays (via a Keithley 703 mainframe) were used to make and break contact points at the inverting input, noninverting input, power inputs, and bias input (see figure 6.3). The output (test point 1) was permanently connected to an addressable Keithley 619 electrometer. During the bias/temperature stressing period the circuits were isolated from the test structure except for the bias on the inverting input and ground connections. Since the testing was to yield information on production circuits, the glass passivation over the circuit was not removed.

A break on either input conductor leads causes the normal input offset voltage of 0.1 to 2 mV to swing to full power supply voltage; therefore catastrophic failure is easily recognized. The voltage resolution of the Keithley electrometer is 1 microvolt or less. Therefore, any variation in offset voltage was easily recognizable.

RESULTS AND DISCUSSION

A random sample of 4 LM 741 op amps was mounted as described. Three were found to have positive offset voltages and two were negative. These circuits were stressed and tested as described. The range in input offset voltages was +3 microvolts in all cases and was random in nature. No failures were recorded over a 3 month continuous stress period. Since these circuits were operated in 20,000 ppmV worst case moisture conditions, no

tempt was made to reduce the water content for further testing. In the
se of the LM 741 op amp this test/stress scheme does not appear capable of
roducing viable results.

EFFECTS OF HYDROGEN ON METAL WALL SURFACES AS DETERMINED BY XPS.

INTRODUCTION

Recently, Rossiter (32) reported that small amounts of hydrogen in a chromatometer can drastically affect the pumping speed for water. The study shows that small amounts of hydrogen effect the sticking coefficient of metal surfaces. In IC packages, this is important since the sticking coefficient would effect the ratio of "total water" to "adsorbed water" on the IC package wall.

EXPERIMENTAL

The hydrogen-water interaction on gold surfaces has been investigated. To facilitate the experiment, a specially designed probe was used in conjunction with a load-lock reaction chamber. The probe shown in Figure 7.1 is constructed of 0.75" diameter 316 stainless steel tubing and is fitted with an aluminum insert which houses a cartridge heater and a chromel-platinum thermocouple to monitor temperature. The insert is coated with a thermal transfer compound to ensure good heat conduction to the probe tip. The sample is mounted via a stainless steel clamp. The load-lock reaction chamber is shown in Figure 7.2. The device allows the sample probe to be inserted into the XPS sample chamber for analysis or to be withdrawn to another chamber where the sample can be treated with various gases, H_2 , or argon combinations without exposure of the sample to the dry atmosphere. Immediately after treatment, the sample can be moved into the analysis chamber and analyzed.

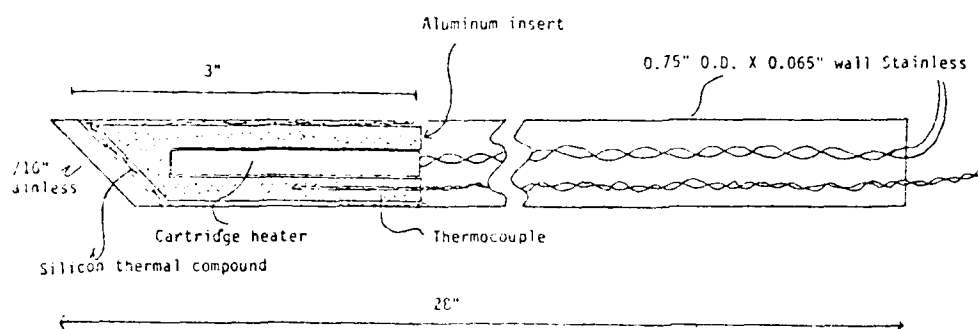


Figure 7.1. Variable temperature sample probe.

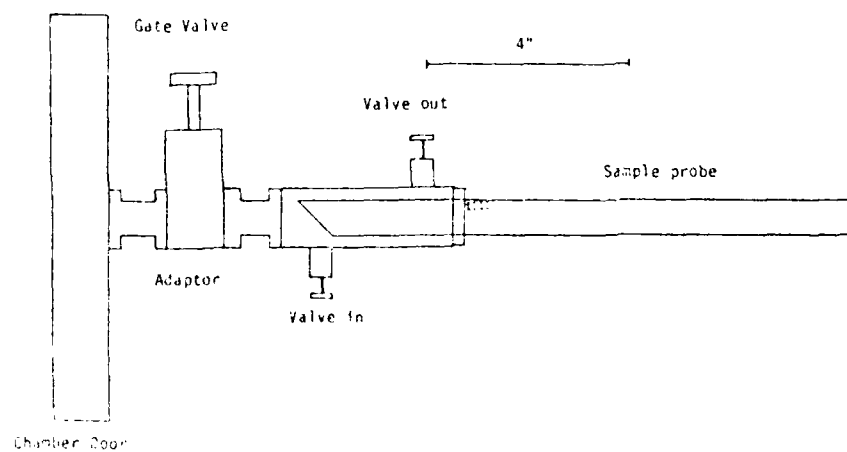


Figure 7.2. Load-lock reaction chamber.

AD-A157 059

MICROENVIRONMENTAL MOISTURE RESEARCH(U) UNIVERSITY OF
SOUTH FLORIDA TAMPA DEPT OF ELECTRICAL ENGINEERING
J M AMMONS ET AL. APR 85 RADC-TR-85-58 F30602-80-C-0169

2/2

UNCLASSIFIED

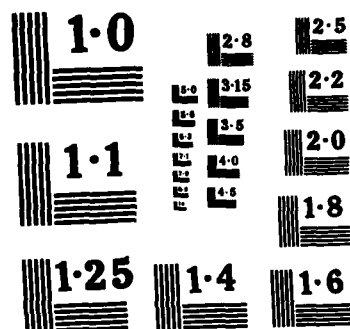
F/G 9/5

NL

END

FORMED

BTB



NATIONAL BUREAU OF STANDARDS
MICROCOPY RESOLUTION TEST CHART

The experimental protocol followed to study the water/surface interaction was as follows. The surface was cleaned by an appropriate method, e.g., ultrasonic rinse in 100% ethanol or Ar^+ etching with 10KeV Ar^+ at 40 μA beam current prior to mounting. After recording a blank $\text{O}(1s)$ spectrum the sample was withdrawn into the reaction chamber and exposed to test conditions and then the $\text{O}(1s)$ signal was recorded again. Any changes in the $\text{O}(1s)$ signal provided information about oxygen containing surface species formed during the treatment.

7.3 RESULTS AND DISCUSSION

7.3.1 Water Uptake on Gold. Standard mil-spec Au/Kovar package lids were etched with 10 KeV Ar^+ at a beam current of 10 μA for 20 minutes. This provided a gold surface free of any extraneous contamination. The lids were then exposed to argon saturated with water at a flow rate of 800 ml/min in the reaction chamber. XPS analysis yielded no significant change in the $\text{O}(1s)$ signal. In some instances a blank $\text{O}(1s)$ signal of unknown origin was present which could only be removed after extensive Ar^+ sputtering. The lids were then exposed to dry H_2 and reanalyzed. No conclusive evidence was found in any of the experiments to suggest that there was water uptake or release by the lid surface as the result of the H_2 treatments.

It was found in later experiments that H_2 does influence the physisorptive properties of gold and various other surfaces. A discussion of this is found in Section 4.

7.3.2 The Source of Residual $\text{O}(1s)$ Signal on Gold. In the experiments described in 7.3.1, note was made of the fact that unheated Au/Kovar package lids often contained a residual $\text{O}(1s)$ signal which could only be removed

with extended Ar^+ sputtering. An attempt was made to determine the source of this troublesome signal.

A piece of 99.9% pure gold foil was chosen for study in place of Au/Kovar lids in order to avoid any complications in data interpretation due to surface contamination via diffusion or other extraneous processes. The foil was mounted onto the probe in the laboratory atmosphere with no special precautions. The $\text{Au}(4p_{3/2})$ and $\text{O}(1s)$ spectra from the foil are shown in Figure 7.3. The intense feature is the $\text{Au}(4p_{3/2})$ line and the weaker feature is the $\text{O}(1s)$ line. The $\text{Au}(4p_{3/2})$ line excited by the $\text{AlK}\alpha_{3,4}$ X-ray satellite would coincide with the $\text{O}(1s)$ from the nonmonochromatic X-ray line, therefore, it was necessary to employ the satellite subtraction routine of the XPS software to remove the satellite. All relevant spectra to be discussed have had the $\text{K}\alpha_{3,4}$ satellite removed.

The gold foil was then sputtered with 10 KeV Ar^+ at 40 μA beam current for 60 minutes until the $\text{O}(1s)$ component was negligible. Negligible is defined as a peak response which is no more than 3X the average peak-to-peak noise or less than 3% of the $\text{Au}(4p_{3,4})$ signal. A typical spectrum is shown in Figure 7.4.

After Ar^+ etching, the gold foil was typically exposed to 10^{-5} torr of oxygen for 30 minutes in the XPS sample chamber. The resulting spectrum (Figure 7.5) indicates no oxygen uptake under the experimental conditions. The data support the conclusion that the $\text{O}(1s)$ signal routinely observed (Figure 7.3) is not due to adsorbed oxygen.

Upon exposure of the clean foil to as little as 5 minutes of laboratory air, an $\text{O}(1s)$ signal reappears (Figure 7.6) with essentially the same intensity as that observed for the unetched gold. This signal does not increase even after exposure to laboratory air for 60 hours. This suggests

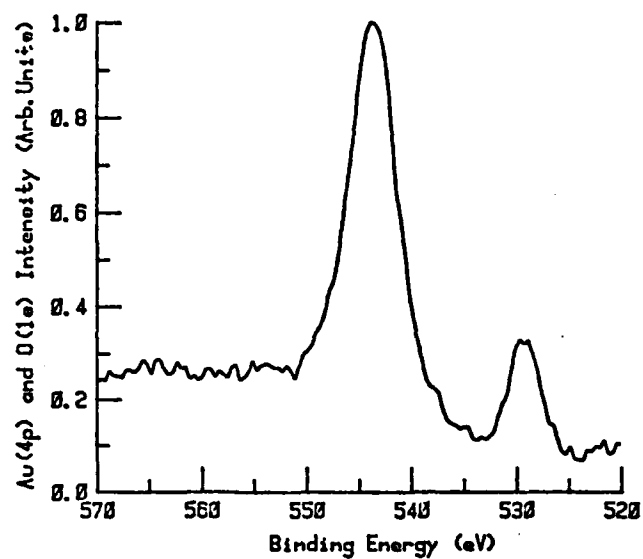


Figure 7.3. Au(4p_{3/2}) and O(1s) spectra for gold foil.

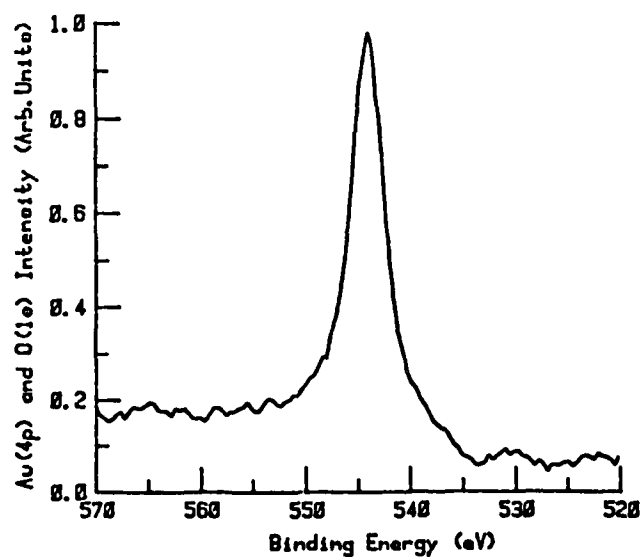


Figure 7.4. Au(4p_{3/2}) spectrum for Ar⁺ sputtered gold foil with AlK_{α3,4} satellite subtracted.

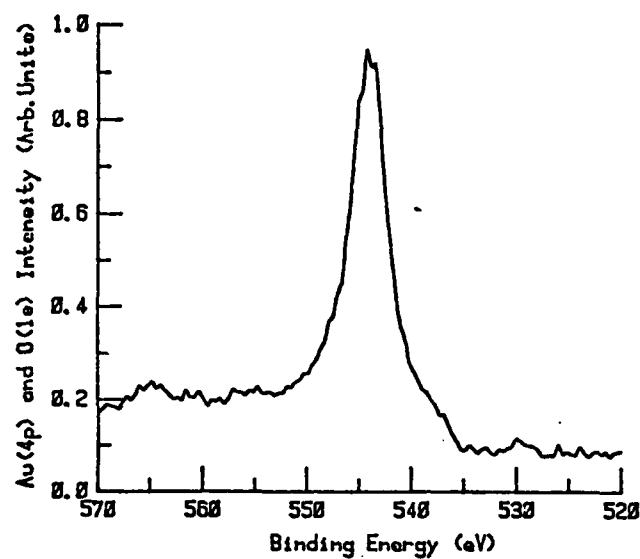


Figure 7.5. Au(4p_{3/2}) for sputtered gold foil after exposure to 10⁻⁵ torr of O₂ for 30 minutes.

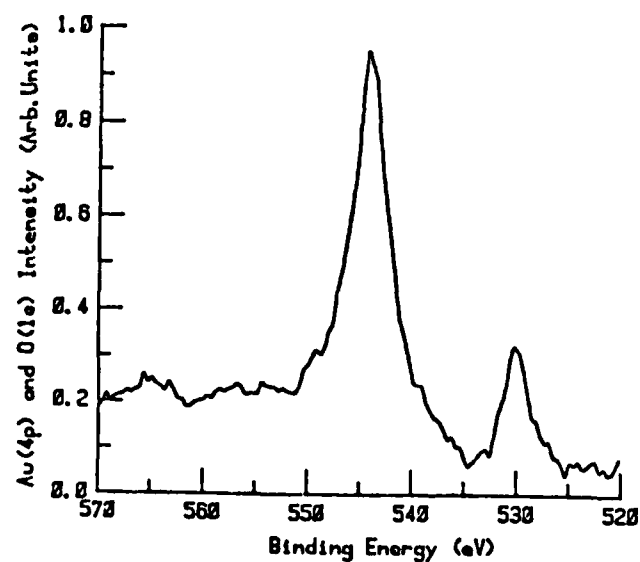


Figure 7.6. Au(4p_{3/2}) and O(1s) spectra for gold foil exposed to laboratory air.

that saturation of the surface is essentially instantaneous. If the foil is heated to 205°C at a pressure of 3×10^{-7} torr for up to 90 minutes, no desorption occurs. (See Figure 7.7) The oxygen species is tightly bound to the gold surface.

Braman and Ammons (33) have shown that gold will effectively adsorb microgram quantities of sulfur from the atmosphere. XPS analyses have shown the presence of SO_4^{2-} species on a gold surface which has been treated with various sulfur containing gases (34). Therefore, S(2p) XPS spectra of the gold foil with the significant O(1s) signal present after atmospheric exposure were obtained. Figures 7.8 and 7.9 are the S(2p) spectra of a clean and ambient air exposed gold foil, respectively. The feature at a binding energy of 169eV indicates the presence of sulfur as sulfate or sulfite. This could easily result from adsorption of SO_2 , H_2SO_4 or $(\text{NH}_4)_2\text{SO}_4$ gas or aerosol from the ambient atmosphere.

Other oxygen contaminants found in minute quantities in ambient air are species such as NO_2 gas or HNO_3 particulate (35). Therefore, N(1s) spectra were determined for the exposed gold surface. Figures 7.10 and 7.11 are the N(1s) spectra for the clean and exposed surface. Note the distinct presence of a nitrogen containing species on the surface. The binding energy suggests that this species is in a NO-like chemical environment.

Atomic sensitivity factors (ASF) for the photoelectric process are routinely employed for semi-quantitative analysis of surfaces (36). Use of ASF data indicates that a significant fraction of the O(1s) signal typically observed on the gold foil may be attributed to sulfur and nitrogen containing species which have been adsorbed from the atmosphere.

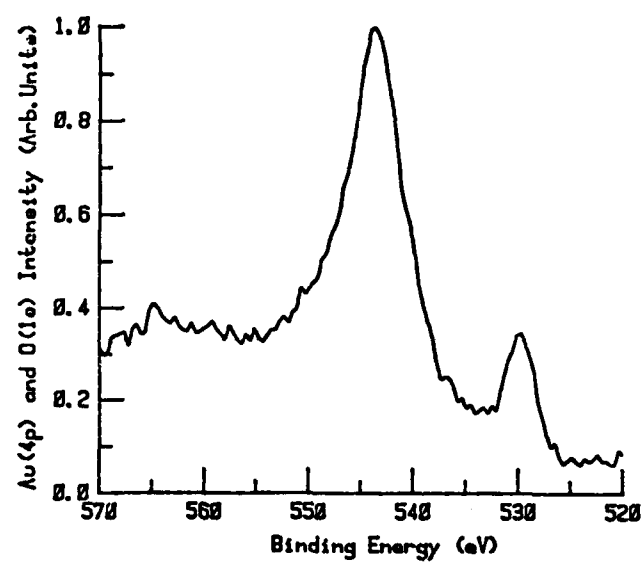


Figure 7.7. Au(4p_{3/2}) and O(1s) spectra of gold foil heated to 205°C.

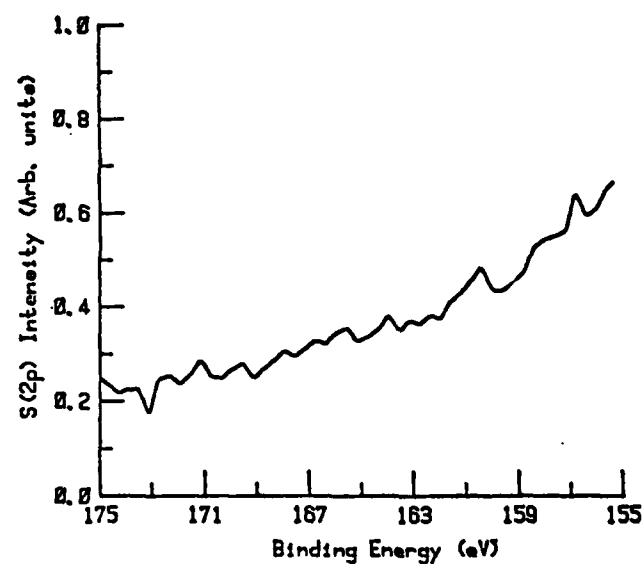


Figure 7.8. S(2p) spectrum of gold foil prior to atmospheric exposure.

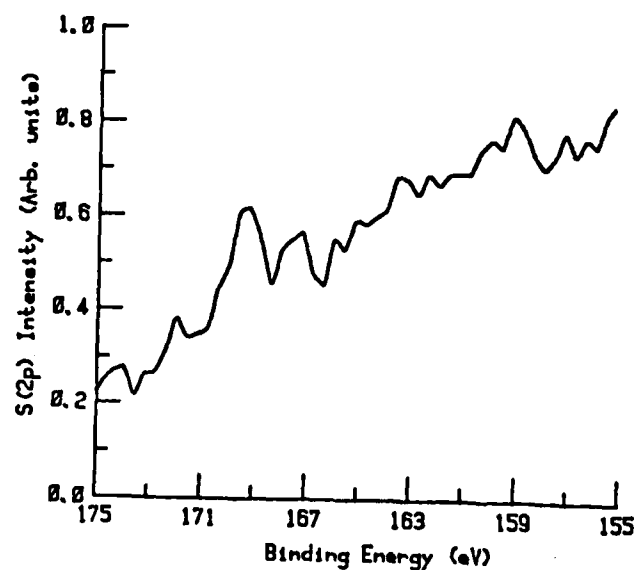


Figure 7.9. S(2p) spectrum of gold foil after atmospheric exposure.

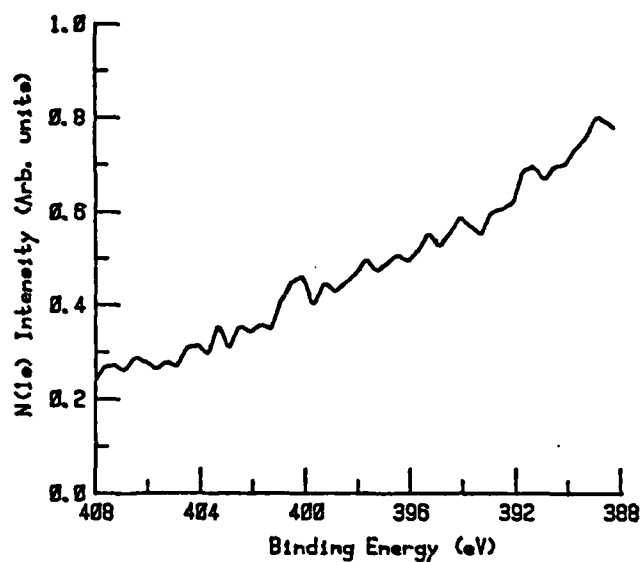


Figure 7.10. N(1s) spectrum prior to exposure to atmosphere.

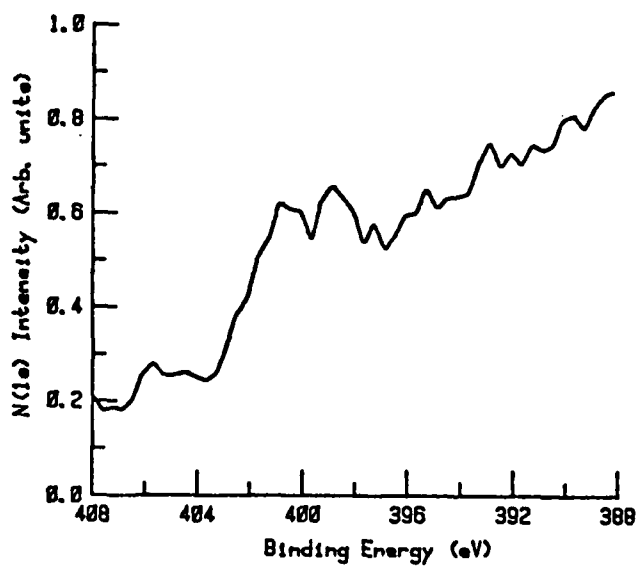


Figure 7.11. N(1s) spectrum after exposure to atmosphere.

8.0 EFFECTS OF PLASMA CLEANING ON SURFACES

8.1 INTRODUCTION

Plasma cleaning is used routinely in many phases of microelectronic manufacturing. This study addressed the problem of surface modification as a result of plasma etching.

8.2 EXPERIMENTAL

Plasma etching was accomplished with a Tegal 1000 barrel style reactor operated at approximately 0.6 torr pressure and 100 to 200 watts of input power. Etching of metallic samples was accomplished by suspending the specimen above the normal wafer carrier. Etching gases used were CF_4/O_2 mixtures.

8.3 RESULTS AND DISCUSSION

"As received" Au/Kovar package lids were subjected to moderately high power CF_4 plasmas to determine the effect of etching on a gold surface. Figure 8.1 is a typical Au(4f) spectrum of an "as received" Au/Kovar lid. Figure 8.2 is the Au(4f) spectrum of the same Au/Kovar lid after exposure for three minutes to a 200W CF_4 plasma. Note the distinct splitting into a doublet of doublets and the overall shift to higher binding energy. Figure 8.3, the elemental spectrum of the lid, contains a strong F(1s) line. The surface has been fluorided during the etching process. Fluorine, the most

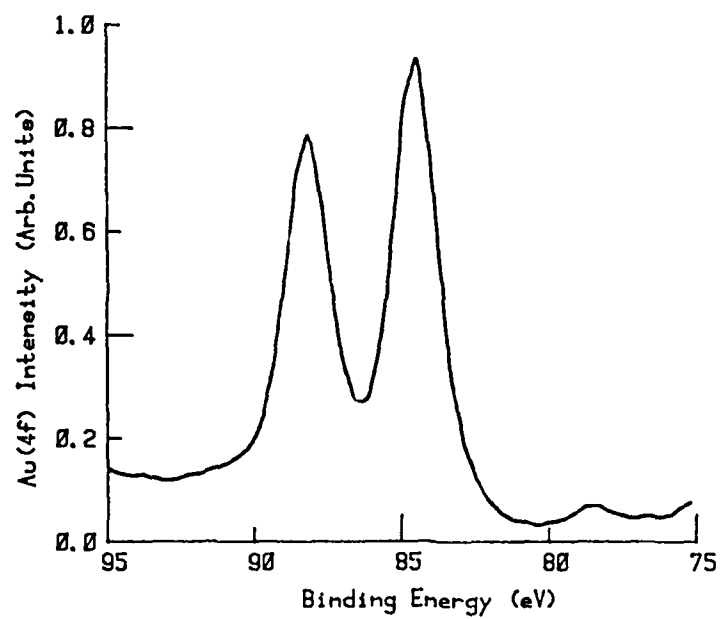


Figure 8.1. Au(4f) Spectrum For An "As Received" Au/Kovar Lid.

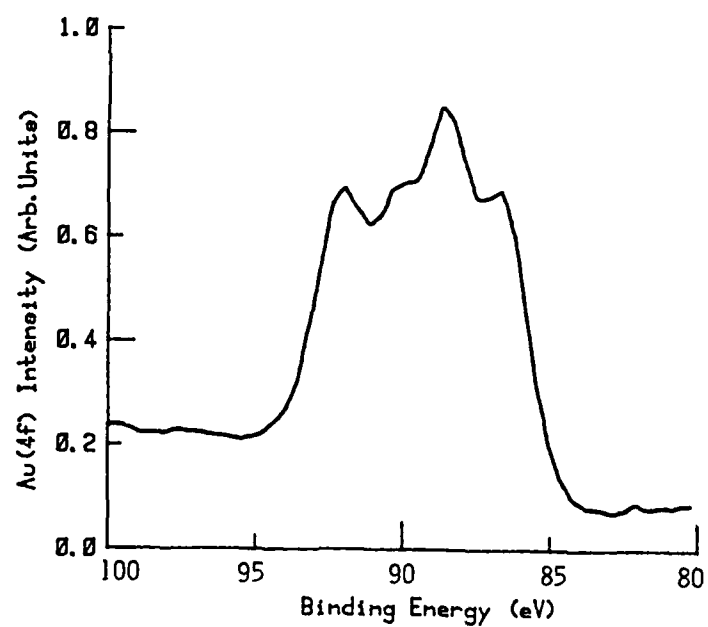


Figure 8.2. Au(4f) Spectrum Of Au/Kovar Lid After Exposure To Three Minutes Of 200W CF_4 Plasma.

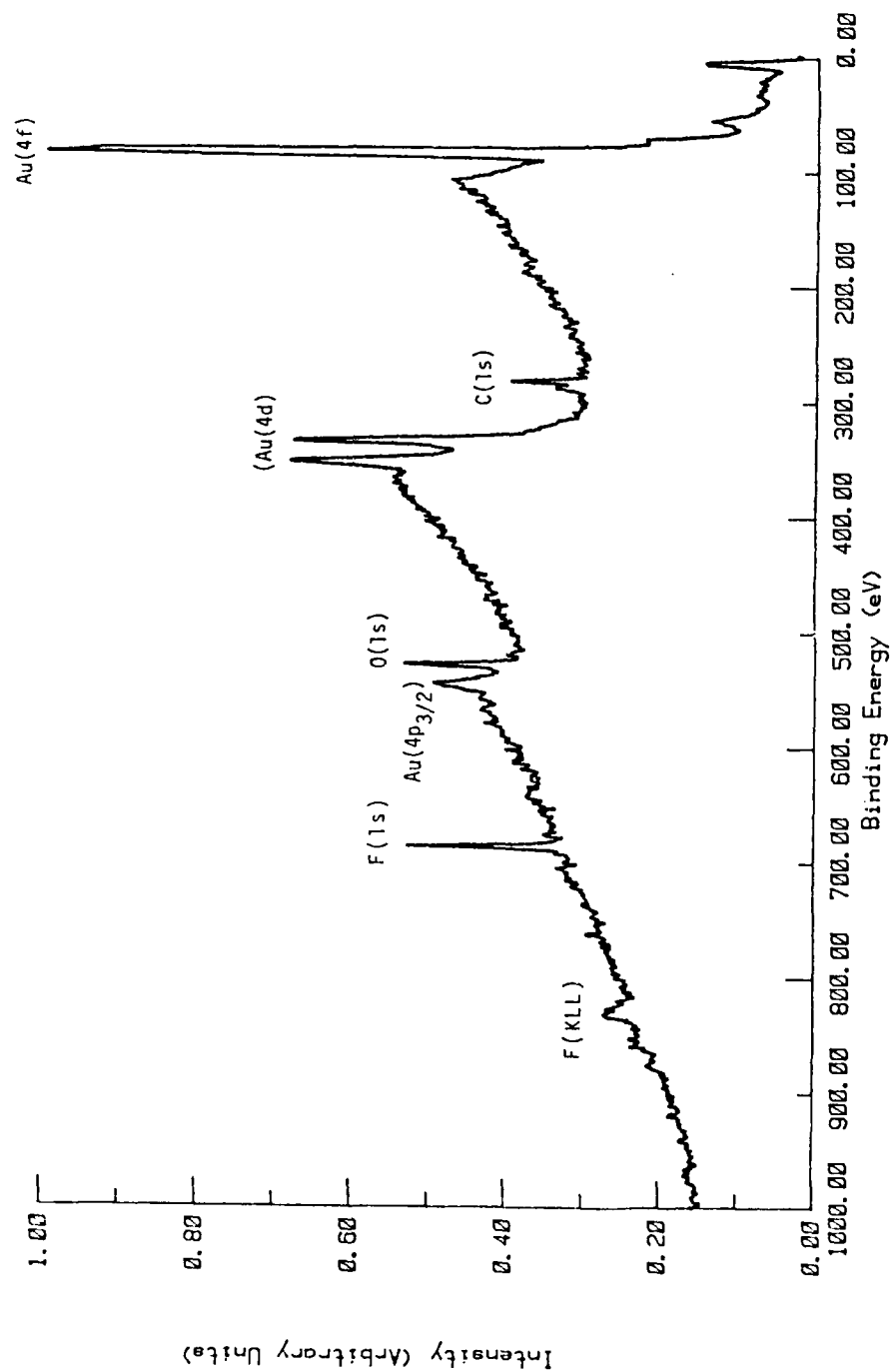


Figure 8.3. Survey Spectrum Of CF_4 Plasma Treated Au/Kovar Lid.

Schnable, G.L., and R.S. Keen, "Study of Contact Failures in Semiconductor Devices", Technical Report RADC-TR-66-165, Rome Air Development Center Research and Technology Division Air Force Systems Command, Griffiss AFB, N.Y., 1966.

Gupta, D.G. and K.W. Asai, Thin Solid Films, 1974, 22, 121.

Thomas, R.E. and G.A. Hars, J. Appl. Phys., 1972, 43, 5900.

Linn, J.H. and W. E. Swartz, Jr., unpublished data, University of South Florida, Tampa, FL 33620.

Samorjai, G.A., Chemistry in Two Dimensions: Surfaces, Cornell University Press, Ithaca/London, 1981.

Brunauer, S., P.H. Emmett and Teller, T. Amer. Chem. Soc., 1938, 60, 309.

Drumheller, C.E., Trans. 7th AVS Symp., Pergamon Press, New York, 1960, p. 306.

Adamson, A.W., Physical Chemistry of Surfaces, 4th Ed., Wiley Interscience, New York, 1982, Chapter 26.

Drain, L.E., and J. A. Morrison, Trans. Faraday Soc., 1953, 49, 654.

Willard, H.H., L.L. Merritt and J. A. Dean, Instrumental Methods of Analysis, 5th Ed., D. Van Nostrand Co., New York, 1974, Chapter 20.

Roberts, M.W., Chem. Br., 1981, 17 (11), 510.

Rossiter, T.J., Presentation at Workshop on Moisture Related Effects in Hybrids, 1979 ISHM Symposium, Nov. 13-15, 1979, Los Angeles, CA.

Braman, R.S., J.M. Ammons and J.L. Bricker, Anal. Chem. 1978, 50 (2), 339.

Ammons, J.M., "Preconcentration Methods for the Determination of Gaseous Sulfur Compounds in Air", Ph.D. Dissertation, University of South Florida, Tampa, FL, 1980.

Braman, R.S., T.J. Shelley and W.A. McLeanny, Anal. Chem. 1982, 54 (3) 358.

Wagner, C.D., et al., Handbook of X-Ray Photoelectron Spectroscopy, Perkin Elmer Corp., 1979.

BIBLIOGRAPHY

- Penn, D.R., J. Electron Spectros. Related Phenon. 1976, 9, 29.
- Holloway, P.H. and D. Harris, private communication 1981.
- Ohkawa, S., O. Akanuma and H. Ishikawa, Japan. J. Appl. Phys. 1975, 14, 1589.
- Tompkins, H.G. and M.R. Pinnel, J. Appl. Phys. 1976, 47, 3804.
- Chang, C., J. Electrochem. Soc. 1980, 127, 1331.
- Hiraki, A., E. Lugujo, M.A. Nicolet and J.W. Mayer, Phys. Stat. Sol. 1971, 7, 401.
- Nelson, G.C. and P.H. Holloway, " Surface Analysis Techniques for Metallurgical Applications", ASTM STP 596, 1976, pp. 68-78.
- Lofton, C.P. and W.E. Swartz, Jr., Appl. Spectrosc. 1978, 32, 177.
- Smith, T., J. Electrochem. Soc. 1972, 119, 1398.
- Swartz, W.E., Jr., J.H. Linn, J.M. Ammons, M.G. Kovac and K. Wilson, Annu. Proc., Reliab. Phys. Symp. 1983, 21, 52.
- Hall, P.M. and J.M. Morabito, Thin Solid Films 1978, 53, 175.
- Czanderna, A.W., Methods of Surface Analysis, Elsevier, New York (1975)
- Schofield, J.H., J. Electron Spectrosc. Relat. Phenom. 1976, 8, 129.
- Duhl, D., K. Hirano and M. Cohen, Acta. Metall. 1963, 11, 1.
- Jenkins, L.H., and M.F. Chung, Surf. Sci. 1971, 24, 125.
- Kunimori, K., T. Kawa, T. Kondow, T. Onishi and T. Tanaru, Surf. Sci. 1974, 46, 576.
- Swartz, W.E., Jr., and D.M. Holloway, Appl. Spectrosc., 1977, 31, 210.
- Lofton, C.P., and W.E. Swartz, Jr., Appl. Spectrosc., 1978, 32, 177.
- Haufte, K., Oxidation of Metals, Plenum, New York, 1965, p. 45.
- Rairden, J.R., C.A. Neugebauer, and R.A. Sigsbee, Metallurgical Transactions 1971, 2, 179.

exposure to the X-rays. Photoelectron reduction of silver halides to elemental silver has been reported.

8.4 CONCLUSION

The three metals studied appear to react differently with CF_4 plasmas. The gold forms Au_xF_y and minimal polymer while aluminum forms a fluoride with maximal polymer. The silver forms several types of fluorine species but these may be sensitive to photoreduction and thus rigorous interpretation of the data is difficult. The studies will be expanded to include other metals such as tin, nickel, and copper and the results will be reported at a later date.

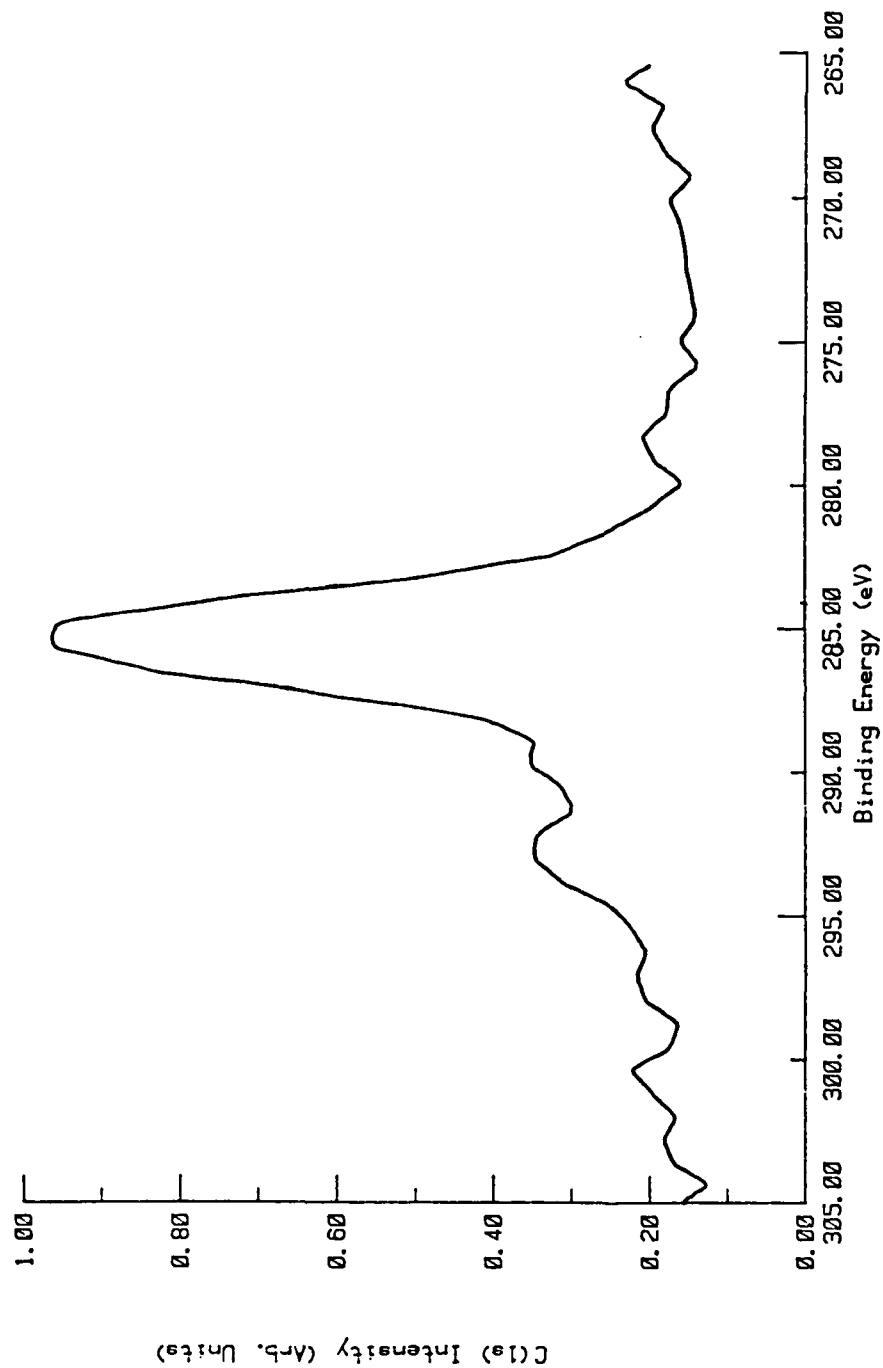


Figure 8.12. C(1s) Spectrum of Silver film Following CF_4 Plasma Treatment

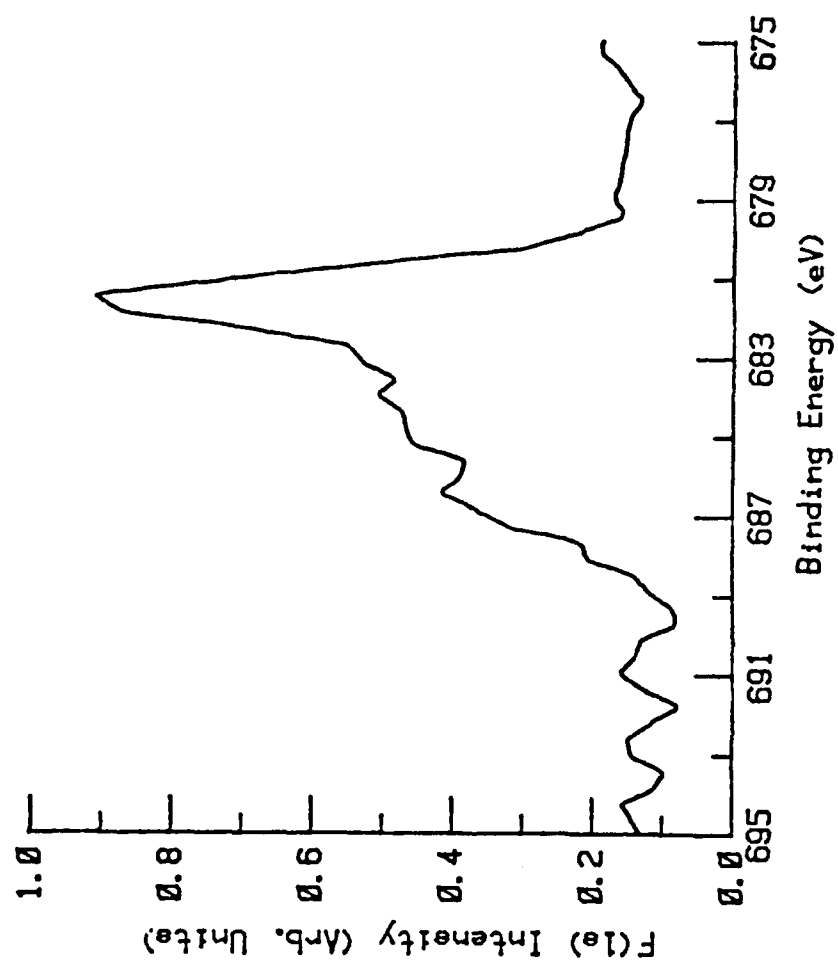


Figure 8.11. F(1s) Spectrum Of Silver Film After Exposure To 200W CF_4 Plasma For Three Minutes.

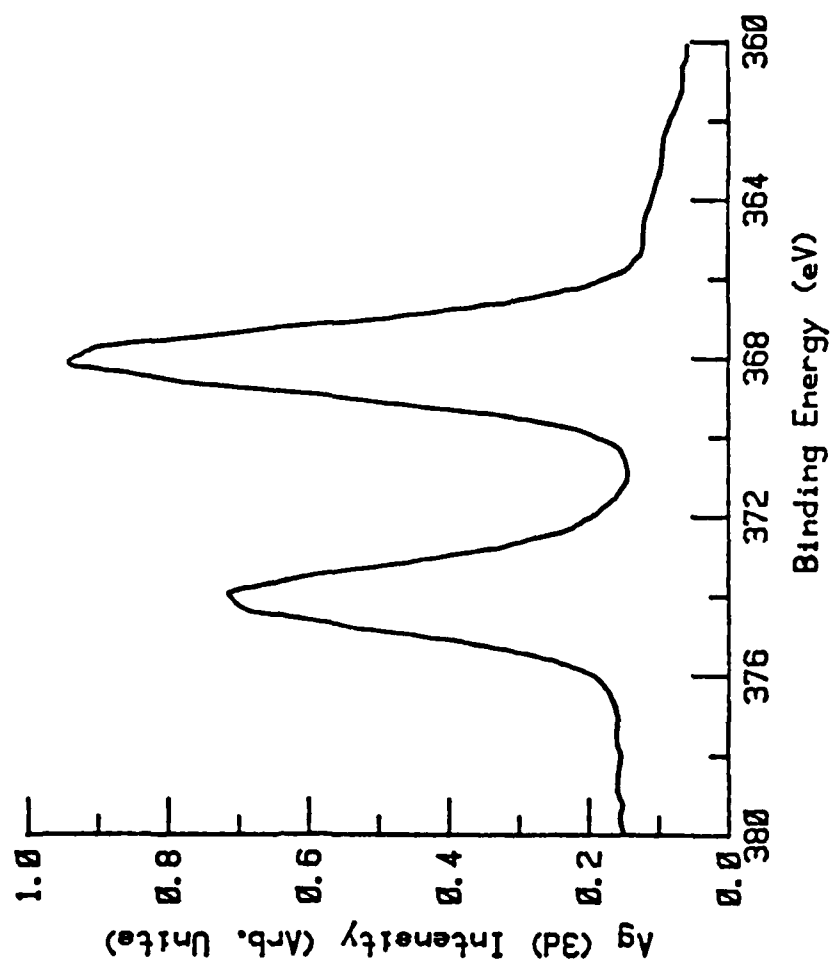


Figure 8.10. Ag(3d) Spectrum Of Silver Film After Exposure To 200W CF_4 Plasma For Three Minutes.

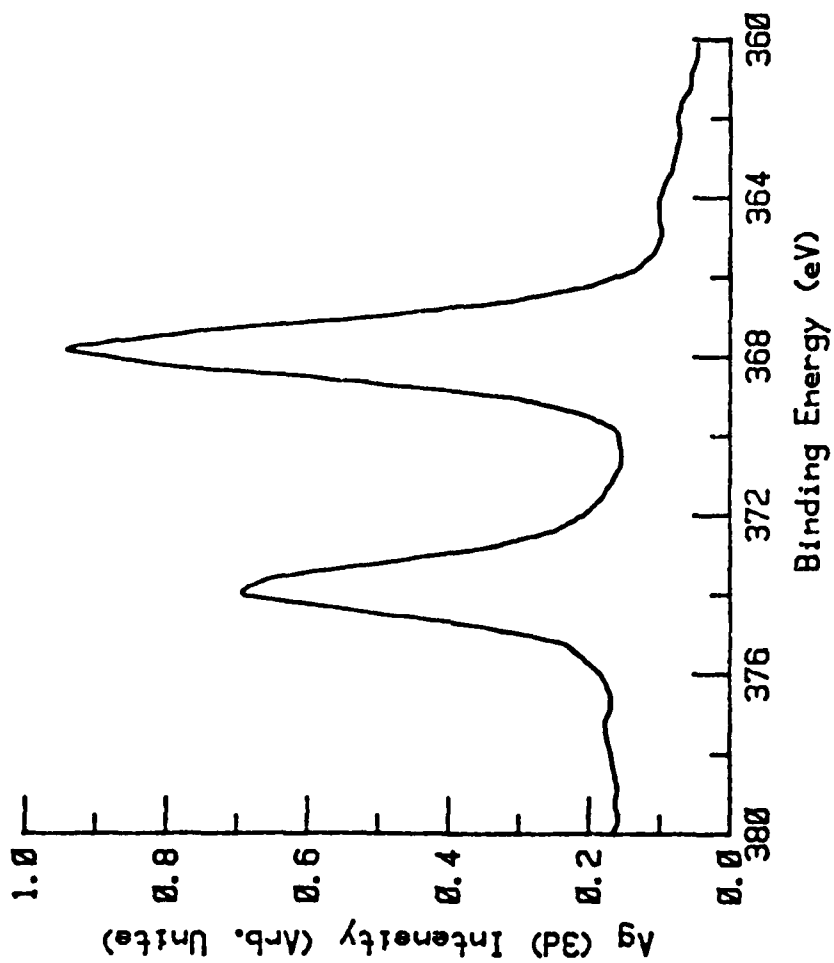


Figure 8.9. Ag(3d) Spectrum For Freshly Deposited Silver Film.

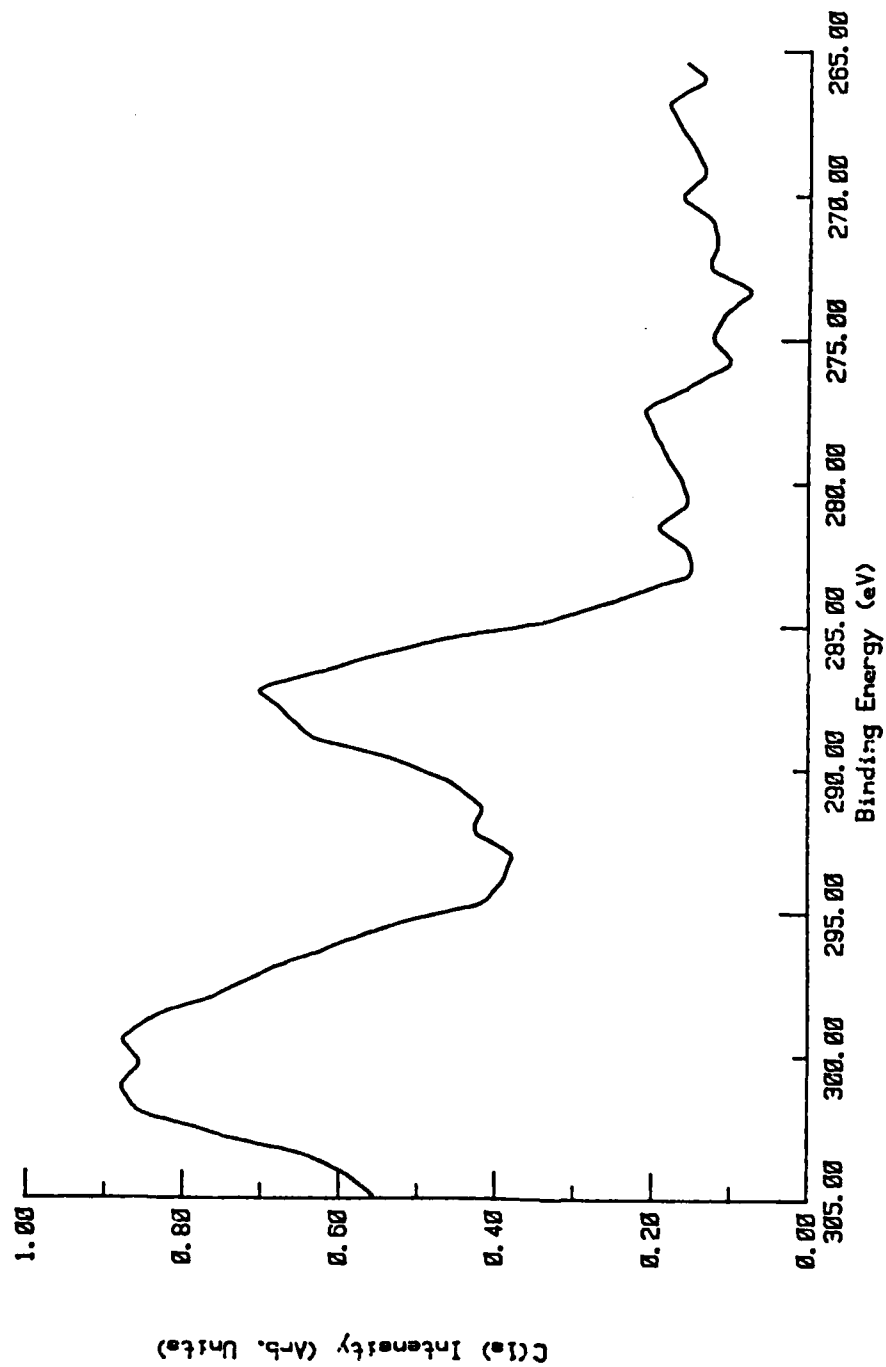


Figure 8.8. C (1s) Spectrum of Aluminum Film After CF_4 Plasma Treatment

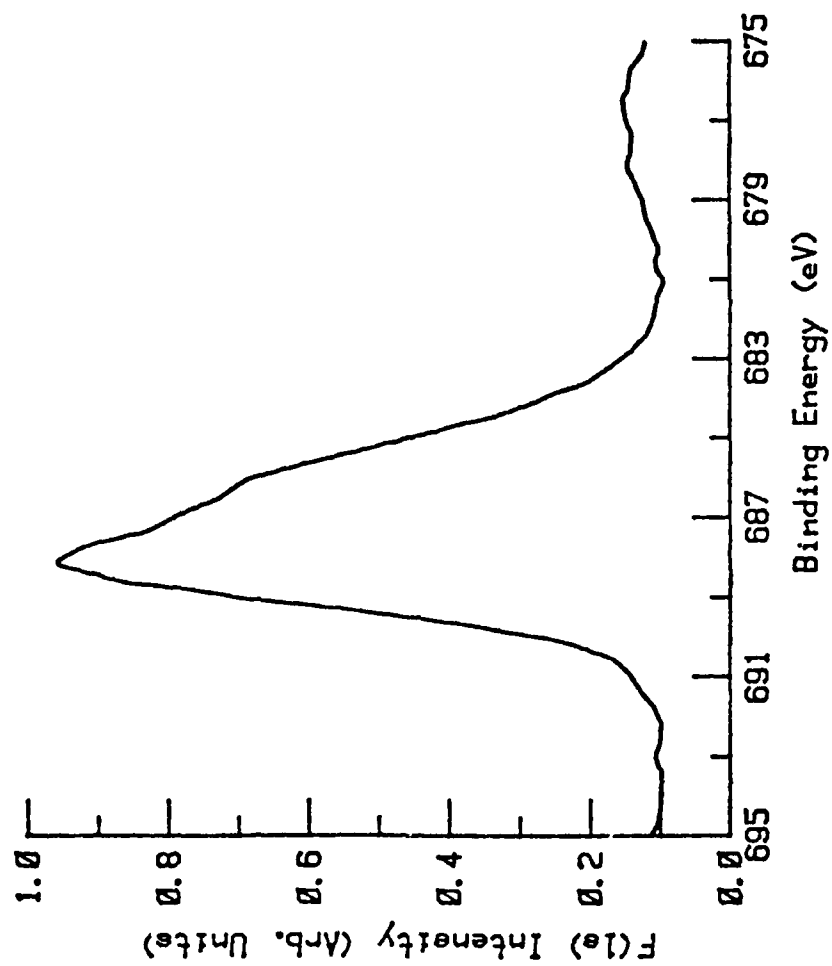


Figure 8.7. F(1s) Spectrum On Aluminum Film After CF_4 Plasma Treatment.

the film has been exposed to a 200W CF_4 plasma for three minutes. The data indicate a shift to higher binding energy and an increase in peak intensity. This supports the transformation of the Al to Al_xF_y with no change in the Al_2O_3 . This is supported by the F(1s) data in Figure 8.7 which indicates the presence of at least two different types of fluorine (Al_xF_y and C_xF_y ??) on the surface. The C_xF_y would be a fluorocarbon polymer as indicated by the high binding energy feature in the C(1s) spectrum (Figure 8.8). The polymer content on the aluminum film is much larger than that of gold films similarly exposed.

Silver was the third metal chosen for study. The Ag (3d) spectrum of a fresh Ag film is shown in Figure 8.9. Figure 8.10 is the Ag (3d) film after exposure to a 200W CF_4 plasma for three minutes. No splitting or shift of the Ag (3d) lines has occurred. This suggests that the CF_4 plasma had no effect on the silver. However, Figure 8.11, the F(1s) spectrum, contains several (at least three) types of fluorine species. The C(1s) spectrum, Figure 8.12, suggests the presence of some C_xF_y , however, not nearly as much as was present on the Al film (Figure 8.8).

The formation of a silver fluoride is suggested from the F(1s) spectrum but not from the Ag (3d) spectrum. It is likely that the chemical shift of the Ag (3d) line ($Ag(3d)_{\text{fluoride}} - Ag(3d)_{\text{silver}}$) is very small and cannot be resolved with the ESCA 36. This is supported by literature data (38). Another possible explanation is that the Ag_xF_y is being reduced to Ag by

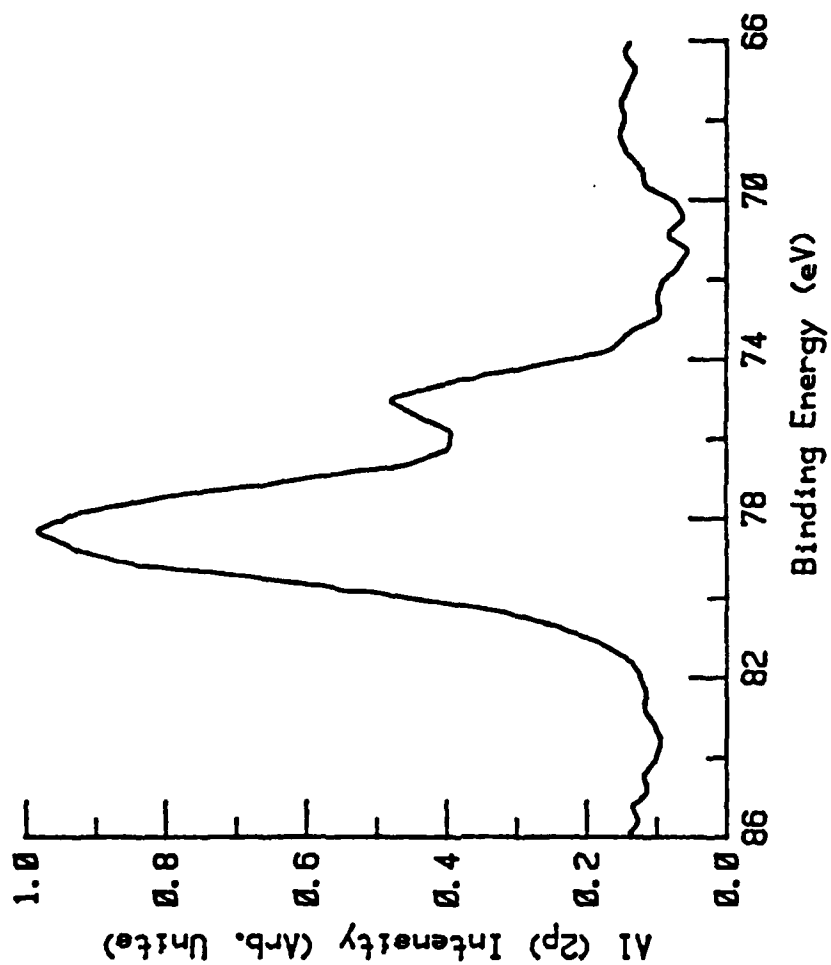


Figure 8.6. Al(2p) Spectrum After Exposure Of Aluminum Film To 200W CF₄ Plasma For Three Minutes

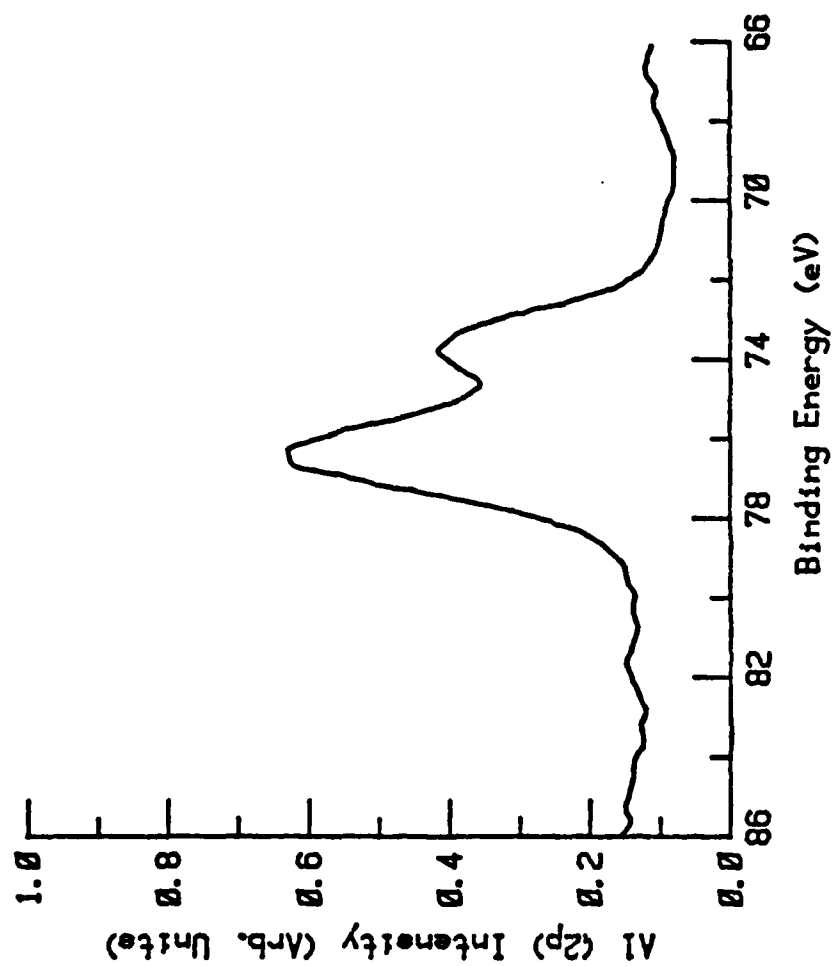


Figure 8.5. Al(2p) Spectrum Of Freshly Deposited Aluminum Film.

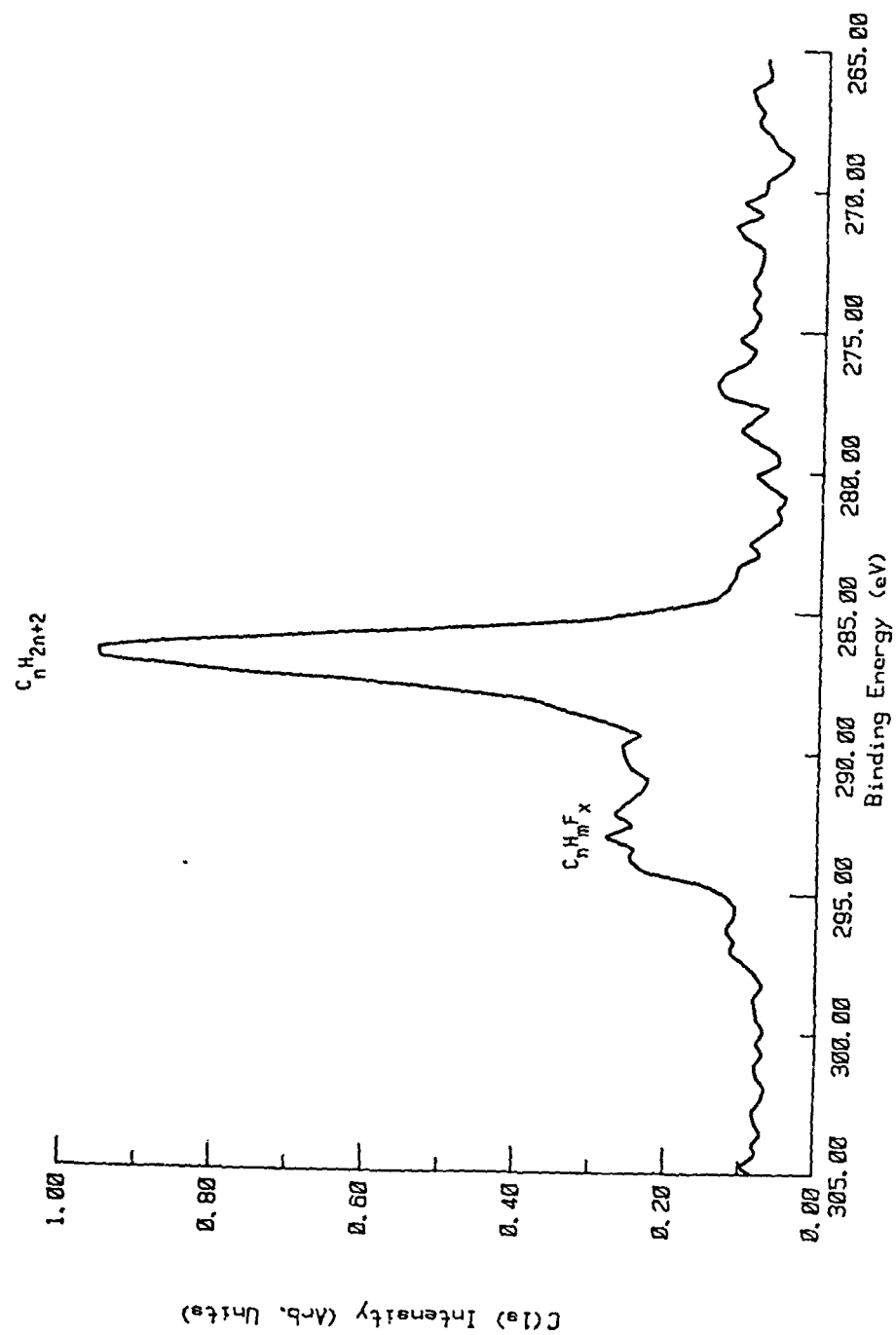


Figure 8.4. C(1s) Spectrum Of CF_4 Plasma Treated Au/Kovar Ltd.

electronegative element is known to cause the longest chemical shifts in electron binding energy. The data seem to indicate that a gold fluoride of unknown stoichiometry (Au_xF_y) has been formed on the lid. This fluoride would account for the higher binding energy component in the Au(4f) spectrum (Figure 8.2). Several other "as received" lids have been exposed to an identical CF_4 plasma with similar results.

A second interesting observation is the formation of a high binding energy component of the carbon spectrum. This is easily detected in the elemental scan (Figure 8.3) and more notably in the high resolution C(1s) spectrum (Figure 8.4). The data suggest the formation of fluorocarbon polymers on the gold surface in addition to the ubiquitous hydrocarbon component. The broadness of the features from the fluorocarbons suggests the presence of several species.

Oxygen is also present on the surface. Even though the RF cavity was evacuated prior to exciting the plasma and minimal amounts of oxygen would be expected to be present, significant amounts of oxygen have been incorporated into the surface. It seems likely that the oxygen is present in the polymers.

Figure 8.5 is the Al (2p) spectrum of a fresh aluminum film deposited onto a glass substrate. The data indicate the presence of elemental aluminum and Al_2O_3 . The presence of Al_2O_3 is not surprising since the oxide forms easily under the conditions of deposition ($P = 2 \times 10^{-7}$ torr; mostly all residual gas is water and CO). Figure 8.6 is the Al (2p) spectrum after

APPENDIX A

Publications and Presentations

Publications

1. Swartz, W.E., Jr., J. H. Linn, J.M. Ammons, M. G. Kovac and K. Wilson, "The Adsorption of Water on Metallic Packages", 21st Annual Proc. Reliability Physics 1983, 21, 52-59.
2. Ammons, J.M., G. R. Hoff, M. G. Kovac, J. H. Linn and W. E. Swartz, Jr., "The Physisorption of Water onto Integrated Circuit Package Components", NBS Special Publication on Moisture Measurement and Control for Semiconductor Devices III, 1984, NBSIR 84-2852, pg. 226-231.
3. Swartz, W.E. Jr., J.H. Linn, J.M. Ammons and M.G. Kovac, "An XPS study of the Diffusion of Iron, Nickel, and Cobalt Through Gold Films", Thin Solid Films 1984, 114(4), 349-356.

Presentations

1. Swartz, W.E. Jr., J. H. Linn, J.M. Ammons, M. Kovac, and K. Wilson, "The Adsorption of Water on Metallic Packages", 21st Annual Meeting of International Reliability Physics Symposium, Phoenix, AZ, April 5-7, 1983.
2. Linn, J.H., W. E. Swartz, Jr., J. M. Ammons and M. Kovac, "An XPS Study of the Diffusion of Nickel and Iron through Gold in Microelectronic Packages", 36th Annual Meeting of the Florida Section of ACS, Jacksonville, FL, May 4-7, 1983.
3. Ammons, J.M., G.R.Hoff, M. Kovac, J. H. Linn, and W.E. Swartz, Jr., "The Physisorption of Water Onto Integrated Circuit Package Components", RADC/NBS Workshop on Moisture Measurement and Control for Semiconductor Devices III, NBS Gaithersburg, MD, November 4-6, 1983.
4. Swartz, W.E., Jr., J.H. Linn, J. M. Ammons, and M. G. Kovac, "The Diffusion of Iron, Nickel, and Cobalt Through Gold in Microelectronic Packages", 35th Annual Southeast Regional Meeting of ACS, Charlotte, NC, November 10-12, 1983.
5. Linn, J.H., W. E. Swartz, Jr., J. M. Ammons and M. G. Kovac, "An XPS Study of the Diffusion of Iron, Nickel, and Cobalt Through Gold Films", 17th Annual Meeting of the American Vacuum Society, Clearwater, FL, February 6-8, 1984.



MISSION of *Rome Air Development Center*

RADC plans and executes research, development, test and selected acquisition programs in support of Command, Control Communications and Intelligence (C³I) activities. Technical and engineering support within areas of technical competence is provided to ESD Program Offices (POs) and other ESD elements. The principal technical mission areas are communications, electromagnetic guidance and control, surveillance of ground and aerospace objects, intelligence data collection and handling, information system technology, ionospheric propagation, solid state sciences, microwave physics and electronic reliability, maintainability and compatibility.

END

FILMED

9-85

DTIC